Application of Hilbert-space coupled-cluster theory to simple $(H_2)_2$ model systems. II. Nonplanar models

Piotr Piecuch[1,2] and Josef Paldus[1,3]
[1]*Department of Applied Mathematics, University of Waterloo, Waterloo, Ontario, Canada N2L 3G1*
[2]*Institute of Chemistry, University of Wrocław, F. Joliot-Curie 14, 50-383 Wrocław, Poland*
[3]*Department of Chemistry and Guelph-Waterloo Center for Graduate Work in Chemistry, Waterloo Campus, University of Waterloo, Waterloo, Ontario, Canada N2L 3G1*
(Received 19 April 1993)

In this series, the recently developed explicit formalism of orthogonally spin-adapted Hilbert space (or state universal), multireference (MR) coupled-cluster (CC) theory, exploiting the model space spanned by two closed-shell-type reference configurations, is applied to a simple minimum-basis-set four-electron model system consisting of two interacting hydrogen molecules in various geometrical arrangements. In this paper, we examine the nonplanar geometries of this system, generally referred to as the T4 models, and their special cases designated as P4 and V4 models. They correspond to different cross sections of the H_4 potential-energy hypersurface, involving the dissociation or simultaneous stretching of two H—H bonds. They involve various quasidegeneracy types, including the orbital and configurational degeneracies, the twofold degeneracy of the ground electronic state and interesting cases of broken-symmetry solutions. We employ the CC with singles and doubles (SD) approximation, so that the cluster operators are approximated by their one- and two-body components. Comparing the resulting CC energies with exact values, which are easily obtained for these models by using the full configuration-interaction method, and performing a cluster analysis of the exact solutions, we assess the performance of various MRCC Hilbert-space approaches at both linear and nonlinear levels of approximation, while a continuous transition is being made between the degenerate and nondegenerate or strongly correlated regimes. We elucidate the sources and the type of singular behavior in both linear and nonlinear versions of MRCC theory, examine the role played by various intruder states, and discuss the potential usefulness of broken-symmetry MRCCSD solutions.

PACS number(s): 31.15.+q, 31.20.Tz, 31.50.+w, 03.65.Ge

I. INTRODUCTION

Recently, we have initiated an exploration of the feasibility and potential of the Hilbert space or state universal multireference (MR) coupled-cluster (CC) formalism [1–14] in describing many-electron correlation effects for a group of low-lying electronic states of a given symmetry species over a wide range of nuclear geometries encompassing both highly quasidegenerate or degenerate and nondegenerate regimes. Following the initial orthogonally spin-adapted formulation of a linear version of this method for the simplest possible case involving two active orbitals of different symmetry, leading to a two-dimensional model space [2], we have extended the method to a fully quadratic version taking into account one- and two-body cluster components relative to each model space configuration [5,9] and applied it to a simple minimum-basis-set (MBS) model consisting of four hydrogen atoms in various nuclear configurations [5,10,14] (see also Refs. [6,7]). This simple model, consisting essentially of two interacting and slightly stretched H_2 molecules in different mutual orientations, was initially used [15] to examine the performance of standard single reference (SR) CC theory in cases when the reference configuration employed becomes (quasi)degenerate with the lowest biexcited configuration. One of the main assets of this model, in addition to its great simplicity that enables one to obtain exact solutions for a large number of geometries using the full configuration-interaction (FCI) procedure, is the ability to continuously vary the degree of quasidegeneracy from the fully degenerate limit to an entirely nondegenerate situation, using a single parameter defining the geometry of the H_4 cluster considered. This is the reason why this model was extensively explored to examine the performance of various SR as well as MR methods [16–22].

In the first part of this series [14], subsequently referred to as paper I, we presented a detailed study of the four planar H_4 models with the nuclei arranged in an isosceles trapezoidal (H4 model), rectangular (P4 model), linear (D4 model), and square (S4 model) configurations (see Fig. 1 of paper I). In this way we were able to examine the performance of various MRCCSD (coupled clus-

ter method involving singly and doubly excited clusters relative to a given reference configuration) methods, including linear approximation (L-MRCCSD), when modeling the dissociation of one, two, or all four single H–H "bonds." Although the linear approximation was found to perform well in degenerate situations, it suffered from a singular behavior due to various intruder states. However, the quadratic version of the MRCCSD theory provided excellent results over the whole range of nuclear configurations explored, except in cases where the two-dimensional model space was clearly lacking the ability to describe the dissociation process under consideration.

In this paper we extend our study to various nonplanar H_4 models that again involve a stretching and/or a dissociation of two H–H bonds. These models represent additional cuts of the H_4 potential-energy hypersurface that can be described—at least in principle—by the same two-reference MRCC theory [2,5,9,10,14] and enable us to explore in greater detail the role of the symmetry breaking not only at the one-electron level of approximation but also at the CC level. We shall explore the performance of various versions of the MRCCSD method, including the linear approximation.

In this work we again systematically exploit the restricted Hartree-Fock (RHF) molecular orbitals (MO's). In fact, all the models investigated in this paper possess a sufficiently high spatial symmetry that completely determines the RHF MO's, as long as we rely on the MBS models. One advantage of this fact is that these MO's represent simultaneously Brueckner (or maximum overlap) orbitals, so that monoexcited T_1 clusters automatically vanish. Moreover, in view of the hole-particle symmetry of the MBS models, the triexcited clusters T_3 vanish as well. We are thus left with the most important pair clusters (T_2) and quadruply excited clusters (T_4). In this way we can extricate the most essential cluster effects in a clean and natural way, although we are well aware of the limitations of our model. Indeed, we intend to explore not only larger basis sets (double zeta plus polarization, etc. [19]) that are essential for a successful modeling of real systems [23], but also other than RHF-type MO's, such as multiconfiguration (MC) self-consistent field (SCF) MO's. Of course, when using the MC SCF MO's, it would be most efficient to start not with individual configurations spanning the model space but, in fact, with the MC SCF N-electron states themselves that already provide an excellent description in most cases of interest. Although some initial steps in this direction were made using the unitary group formalism [24–27], the general procedure of this kind is yet to be developed. We thus restrict ourselves in this work to the RHF MO's.

We first present a very brief outline of the MRCC method employed in Sec. II. The studied models and computational details, including a rather detailed discussion of the role of orbital and configurational degeneracies and of the symmetry breaking, are the subject of Sec. III. The main results and their discussion are presented in Sec. IV, while Sec. V summarizes the main conclusions concerning the performance of various approximations employed.

II. MULTIREFERENCE HILBERT-SPACE COUPLED-CLUSTER THEORY: GENERAL STRUCTURE OF MRCC EQUATIONS AND METHODS EMPLOYED

In any MRCC formalism one first selects a suitable set of configurations $|\Phi_p\rangle$, $p = 1,\ldots,M$, that is capable of providing a reasonable zeroth-order approximation for a group of M exact solutions $|\Psi_\mu\rangle$, $\mu = 1,\ldots,M$, of the electronic Schrödinger equation over the required range of nuclear geometries. This is accomplished by partitioning the employed spin orbital or molecular orbital set into the three disjoint subsets of core, valence (or active), and virtual (or excited) (spin) orbitals. The reference configurations $|\Phi_p\rangle$, $p = 1,\ldots,M$, differ in the occupancies of valence (spin) orbitals, while having core and virtual (spin) orbitals completely occupied and unoccupied, respectively.

The complete model space $\mathcal{M}_0$ [1], $\mathcal{M}_0 = \text{span}\{|\Phi_p\rangle : p = 1,\ldots,M\}$, which we shall employ in this paper, is a subspace of the N-electron Hilbert space $\mathcal{H}_N$ spanned by the reference configurations $|\Phi_p\rangle$, $p = 1,\ldots,M$, which correspond to all possible distributions of valence electrons [electrons occupying valence (spin) orbitals] among valence (spin) orbitals. It is invariant under unitary transformations of valence (spin) orbitals. In the presence of spin and spatial symmetries, $\mathcal{M}_0$ factors into a direct sum of invariant subspaces, each of which may serve as an independent model space that is complete for the symmetry species considered [11] (cf. paper I of this series, Ref. [14]). We thus use $\mathcal{M}_0$ to designate any invariant subspace of the model space that is relevant to a given problem. The completeness requirement is essential for theoretical developments that follow. Indeed, the completeness of $\mathcal{M}_0$ implies the connectivity of cluster operators and of the effective Hamiltonian, so that the resulting MRCC formalism leads to a size extensive description of many-body systems [1]. It should be emphasized, however, that it is possible to obtain a size-extensive MRCC theory that employs incomplete model spaces (cf., e.g., Refs. [4], [13], and [28]).

Once the reference configurations $|\Phi_p\rangle$ have been selected, we define projection operators onto $\mathcal{M}_0$ and its orthogonal complement $\mathcal{M}_0^\perp$ (with respect to the N-electron Hilbert space $\mathcal{H}_N$), which we designate by P and Q, respectively,

$$P = \sum_{q=1}^{M} P_q \equiv \sum_q P_q, \quad P_q = |\Phi_q\rangle\langle\Phi_q|\,, \tag{1}$$

$$Q = 1 - P\,, \tag{2}$$

and introduce the model space projections of the exact states $|\Psi_\mu\rangle$,

$$|\tilde{\Phi}_\mu\rangle = P|\Psi_\mu\rangle\,. \tag{3}$$

We assume that $|\tilde{\Phi}_\mu\rangle$ are linearly independent (even though usually not orthogonal) and span $\mathcal{M}_0$.

The key concept of MRCC theories is a wave operator U (referred to as the Bloch wave operator [29]), which

transforms the model states $|\tilde{\Phi}_\mu\rangle$ into the exact solutions $|\Psi_\mu\rangle$,

$$|\Psi_\mu\rangle = U|\tilde{\Phi}_\mu\rangle\,, \tag{4}$$

and annihilates any state from the subspace $\mathcal{M}_0^\perp$. We find that U, just like the projector P, is idempotent and satisfies the relationships

$$PU = P\,, \tag{5}$$

$$UP = U\,, \tag{6}$$

and

$$U|\Psi_\mu\rangle = |\Psi_\mu\rangle\,. \tag{7}$$

Relationship (5) is equivalent to the condition of intermediate normalization, which in the MR case requires that

$$\langle\Phi_p|\tilde{\Psi}_q\rangle = \delta_{pq} \quad (p,q = 1,\ldots,M)\,, \tag{8}$$

where the ket states

$$|\tilde{\Psi}_p\rangle = U|\Phi_p\rangle \tag{9}$$

span the same subspace of the N-electron Hilbert space $\mathcal{H}_N$ as the exact wave functions $|\Psi_\mu\rangle$, $\mu = 1,\ldots,M$.

The Bloch operator U represents the MR generalization of the wave operator $W = e^T|\Phi_0\rangle\langle\Phi_0|$ of the SRCC theory [11,30–38]. In particular, it satisfies an energy independent equation

$$UHU = HU, \tag{10}$$

usually referred to as the generalized Bloch equation [1,11,29,39–42]. Once this equation is solved, the unknown states $|\tilde{\Phi}_\mu\rangle$, and the corresponding energies E_μ that are associated with the exact wave functions $|\Psi_\mu\rangle$, are determined by diagonalizing the effective Hamiltonian

$$H^{\rm eff} = PHU = PHUP \tag{11}$$

within the model space $\mathcal{M}_0$. Thus the problem of solving the Schrödinger equation for a finite number of eigenstates $|\Psi_\mu\rangle$ reduces to a finite-dimensional secular problem

$$\sum_q \left(H^{\rm eff}_{pq} - \delta_{pq}E_\mu\right) c_{q\mu} = 0\,, \tag{12}$$

where

$$H^{\rm eff}_{pq} = \langle\Phi_p|H^{\rm eff}|\Phi_q\rangle = \langle\Phi_p|HU|\Phi_q\rangle \tag{13}$$

and

$$c_{q\mu} = \langle\Phi_q|\Psi_\mu\rangle = \langle\Phi_q|\tilde{\Phi}_\mu\rangle. \tag{14}$$

The coefficients $c_{q\mu}$ represent linear expansion coefficients of functions $|\tilde{\Phi}_\mu\rangle$ with respect to the model configurations $|\Phi_p\rangle$, $p = 1,\ldots,M$. Throughout the paper we shall assume that the internuclear repulsion term is excluded from the Hamiltonian, so that H represents the pure *electronic* Hamiltonian.

Different *Ansätze* for the wave operator U lead to distinct MRCC methods [1,11,43]. In the present paper we employ the Hilbert-space approach [1], in which U is represented as a superposition of exponential operators corresponding to individual reference configurations $|\Phi_p\rangle$,

$$U = \sum_q e^{T^{(q)}} P_q\,. \tag{15}$$

Thus the exact states $|\Psi_\mu\rangle$, $\mu = 1,\ldots,M$, are expressed in the form

$$|\Psi_\mu\rangle = \sum_q c_{q\mu} e^{T^{(q)}} |\Phi_q\rangle\,. \tag{16}$$

Just as in the SRCC theory, cluster operators $T^{(p)}$ are expanded in terms of a conveniently chosen set of excitation operators ${}^{(p)}G_i$,

$$T^{(p)} = \sum_i {}^{(p)}t_i\, {}^{(p)}G_i\,. \tag{17}$$

Completeness of the model space $\mathcal{M}_0$ implies that both the operators ${}^{(p)}G_i$ and the corresponding cluster amplitudes ${}^{(p)}t_i$ carry at least one nonvalence (i.e., core or virtual-type) label [1]. For every model configuration $|\Phi_p\rangle$ we have a distinct family of operators ${}^{(p)}G_i$ and a distinct family of cluster amplitudes ${}^{(p)}t_i$.

The matrix elements of the effective Hamiltonian that determines the expansion coefficients $c_{q\mu}$ and the energies E_μ, Eqs. (12) and (13), are evaluated as

$$H^{\rm eff}_{pq} = \langle\Phi_p|e^{-T^{(q)}} H e^{T^{(q)}}|\Phi_q\rangle, \tag{18}$$

whereas the generalized Bloch equation (10), which is needed to find the unknown cluster operators $T^{(p)}$, takes the form of a highly nonlinear system of coupled algebraic equations for ${}^{(p)}t_i$,

$$\langle {}^{(p)}G_i\Phi_p|e^{-T^{(p)}} H e^{T^{(p)}}|\Phi_p\rangle = \sum_{q\ (\neq p)} \langle {}^{(p)}G_i\Phi_p|e^{-T^{(p)}} e^{T^{(q)}}|\Phi_q\rangle\, H^{\rm eff}_{qp} \qquad (p = 1,\ldots,M)\,. \tag{19}$$

The left-hand side of the above system, which is essentially identical with that of the SRCC method (with $|\Phi_p\rangle$ as a reference and other reference configurations excluded from the excited-state manifold), is referred to as the *direct term*, whereas the right-hand side of Eq. (19), which has no counterpart in the SR case, represents the so-called *coupling term*.

It was proved (cf. Ref. [1]) that the MRCC method, defined by Eqs. (19) and (12), with the effective Hamiltonian matrix elements given by Eq. (18), leads to connected expansions for the cluster operators $T^{(p)}$, so that the resulting energies E_μ are size extensive. We can thus consider several approximate variants of the MRCC formalism, obtained by neglecting either the higher nonlinear terms in Eqs. (19) and (18), or higher many-body

components in expansion (17) (cf. Refs. [1–11,14,44]), without introducing disconnected terms into the $H^{\rm eff}$, i.e., without losing the size extensivity of the resulting approximate energies.

In the present paper, similarly as in paper I [14], we employ the CCSD approximation, so that the cluster operators $T^{(p)}$ are approximated by their one- and two-body components $T_1^{(p)}$ and $T_2^{(p)}$, respectively. Moreover, we neglect cubic and higher-order nonlinear terms in Eq. (19), while using the full expansion for the effective Hamiltonian matrix, Eq. (18). The only exception is the linear version of the MRCCSD formalism (L-MRCCSD), in which the off-diagonal elements of the effective Hamiltonian matrix $H_{qp}^{\rm eff}$ $(q \neq p)$ that enter linear coupling terms are approximated by matrix elements $H_{qp} = \langle \Phi_q | H | \Phi_p \rangle$ in order to preserve the linearity of the resulting equations.

We restrict ourselves to the simplest possible case of a two-dimensional model space, spanned by closed-shell (CS)-type configurations $|\Phi_1\rangle$ and $|\Phi_2\rangle$ involving two active orbitals $|k\rangle$ and $|\ell\rangle$ that belong to different symmetry species of the spatial symmetry group of the system considered. As explained in Ref. [2] (cf. also paper I of this series), such a model space is complete, assuming that we focus our attention on the totally symmetric singlet states. When cubic and higher-order nonlinear terms are neglected, the corresponding two-reference CCSD equations take the following form [2,5,9,10,45] (see also paper I):

$$\sum_{n=0}^{2} L_n^{(p)}(G_i^\dagger) + \sum_{\substack{n,n'=1 \\ (n \leq n')}}^{2} Q_{nn'}^{(p)}(G_i^\dagger) = \sum_{n=1}^{2} R_n^{(p)}(G_i^\dagger) + \sum_{\substack{n,n'=1 \\ (n \leq n')}}^{2} B_{nn'}^{(p)}(G_i^\dagger) + \tilde{B}_{12}^{(p)}(G_i^\dagger) \qquad (p = 1,2). \quad (20)$$

Here $G_i \equiv {}^{(p)}G_i$ designate at most biexcited operators relative to $|\Phi_p\rangle$ that generate totally symmetric singlet configurations from $\mathcal{M}_0^\perp$. The absolute, linear, and bilinear direct terms $L_0^{(p)}(G_i^\dagger)$, $L_n^{(p)}(G_i^\dagger)$ $(n = 1,2)$, and $Q_{nn'}^{(p)}(G_i^\dagger)$ $(n,n' = 1,2, n \leq n')$, respectively, are given by the well-known SR-like expressions

$$L_0^{(p)}(G_i^\dagger) = \langle \Phi_p | {}^{(p)}G_i^\dagger H | \Phi_p \rangle , \quad (21)$$

$$L_n^{(p)}(G_i^\dagger) = \langle \Phi_p | {}^{(p)}G_i^\dagger [H, T_n^{(p)}] | \Phi_p \rangle , \quad (22)$$

$$Q_{nn'}^{(p)}(G_i^\dagger) = (1+\delta_{nn'})^{-1} \langle \Phi_p | {}^{(p)}G_i^\dagger [[H, T_n^{(p)}], T_{n'}^{(p)}] | \Phi_p \rangle , \quad (23)$$

and the linear and bilinear coupling terms by the formulas

$$R_n^{(p)}(G_i^\dagger) = \langle \Phi_p | {}^{(p)}G_i^\dagger T_n^{(q)} | \Phi_q \rangle H_{qp}^{\rm eff} , \quad (24)$$

$$B_{nn}^{(p)}(G_i^\dagger) = \tfrac{1}{2} \langle \Phi_p | {}^{(p)}G_i^\dagger (T_n^{(q)})^2 | \Phi_q \rangle H_{qp}^{\rm eff} , \quad (25)$$

$$B_{12}^{(p)}(G_i^\dagger) = \langle \Phi_p | {}^{(p)}G_i^\dagger T_2^{(q)} (T_1^{(q)} - T_1^{(p)}) | \Phi_q \rangle H_{qp}^{\rm eff} , \quad (26)$$

$$\tilde{B}_{12}^{(p)}(G_i^\dagger) = \langle \Phi_p | {}^{(p)}G_i^\dagger [T_2^{(q)}, T_1^{(p)}] | \Phi_q \rangle H_{qp}^{\rm eff} , \quad (27)$$

where in the latter four equations $q = 3 - p$. Since in our case $|\Phi_2\rangle$ is a doubly excited configuration relative to $|\Phi_1\rangle$ and vice versa, i.e.,

$$|\Phi_2\rangle = {}^{(1)}G_{kk}^{\ell\ell}(0) |\Phi_1\rangle , \quad |\Phi_1\rangle = {}^{(2)}G_{\ell\ell}^{kk}(0) |\Phi_2\rangle , \quad (28)$$

where, in general, ${}^{(p)}G_{\alpha\beta}^{\rho\sigma}(i)$, $i = 0,1$, designate the particle-particle–hole-hole coupled biexcitation operators of the orthogonally spin-adapted formalism [2,5,9,45] (here and in the following text, α, β, etc. designate orbitals occupied in $|\Phi_p\rangle$, while ρ, σ, etc. label orbitals unoccupied in $|\Phi_p\rangle$), the off-diagonal elements of the effective Hamiltonian, which enter Eqs. (24)–(27), involve at most quartic terms, namely $(T_1^{(p)})^4$. The diagonal elements $H_{pp}^{\rm eff}$, which together with the off-diagonal terms $H_{qp}^{\rm eff}$, $p = 1,2$, $q = 3 - p$, are needed to solve the corresponding 2×2 secular problem, Eq. (12), are identical to corresponding SRCC expressions for the energy and involve at most quadratic terms $(T_1^{(p)})^2$.

Explicit, orthogonally spin-adapted expressions for the quantities given by Eqs. (21)–(27), and for the effective Hamiltonian (18), in terms of cluster amplitudes, are given in Refs. [2,5,9,45]. They were obtained independently by exploiting both the replacement operator technique [46] and the diagrammatic procedure based on graphical methods of spin algebras [32,47].

Formulas (20)–(27), together with Eq. (12) and the pertinent expressions for the effective Hamiltonian matrix elements [2,9,45], represent basic expressions of the fully quadratic MRCCSD formalism, hereafter referred to as the MRCCSD-3 method (see paper I). As in paper I, we also consider two additional approximate variants of the nonlinear MRCCSD approach, designated as MRCCSD-1 and MRCCSD-2 methods, as well as the linear L-MRCCSD method arising by neglecting the nonlinear terms $Q_{nn'}^{(p)}(G_i^\dagger)$, $B_{nn'}^{(p)}(G_i^\dagger)$, and $\tilde{B}_{12}^{(p)}(G_i^\dagger)$ in Eq. (20). We recall that MRCCSD-1 equations are obtained by setting $Q_{11}^{(p)}(G_i^\dagger) = Q_{12}^{(p)}(G_i^\dagger) = B_{nn'}^{(p)}(G_i^\dagger) = \tilde{B}_{12}^{(p)}(G_i^\dagger) = 0$ in system (20). Thus the only nonlinear term considered in the MRCCSD-1 method is the direct $\frac{1}{2}(T_2^{(p)})^2$ term $Q_{22}^{(p)}(G_i^\dagger)$. Finally, the MRCCSD-2 approximation considers pair-cluster interactions in both direct and coupling terms, namely, $Q_{22}^{(p)}(G_i^\dagger)$ and $B_{22}^{(p)}(G_i^\dagger)$, while neglecting the remaining bilinear terms $Q_{11}^{(p)}(G_i^\dagger)$, $Q_{12}^{(p)}(G_i^\dagger)$, $B_{11}^{(p)}(G_i^\dagger)$, $B_{12}^{(p)}(G_i^\dagger)$, and $\tilde{B}_{12}^{(p)}(G_i^\dagger)$ (cf. paper I and Ref. [10]). Thus, the MRCCSD-1 approximation enables us to test the role of disconnected tetraexcited clusters $\frac{1}{2}(T_2^{(p)})^2$ in the direct term, whereas the comparison of the MRCCSD-2 and MRCCSD-3 methods allows us to assess the role played by nonlinear terms involving monoexcited clusters $T_1^{(p)}$. Whenever the monoexcited clusters $T_1^{(p)}$ vanish, there is

no difference between the MRCCSD-2 and MRCCSD-3 approximations and the resulting approach is designated by the acronym MRCCSD-2,3. In fact, this is always the case for the nonplanar models examined in this paper.

In paper I, we applied the above described MRCCSD schemes to several MBS four-electron model systems consisting of two interacting hydrogen molecules in planar geometrical arrangements. In the present paper we concentrate on nonplanar geometries of the same model system. A description of nonplanar models studied in this paper, as well as of computational details associated with the use of the orthogonally spin-adapted two-reference CCSD formalism in this case, are given in the next section.

III. MODELS EMPLOYED AND COMPUTATIONAL DETAILS

A. Model description

As in paper I, we study a prototypical molecular system for which the range of the configurational and orbital quasidegeneracies [48] continuously varies with geometry and which is simple enough to enable numerous computations using different methods including the FCI, providing the exact solution. The model consists of two interacting hydrogen molecules in various geometrical arrangements.

The first model that we investigate, designated as T4, is obtained from the P4 model of paper I (having the rectangular geometry [cf. Fig. 1(a)]) by rotating one of the H_2 molecules with respect to the other about the C_2 axis passing through their centers by angle θ, while keeping the intermolecular separation (designated as α in the P4 model) fixed at a chosen value R, as schematically shown in Fig. 1(b). The H–H bond length of both hydrogen molecules is fixed and equal to a. To enhance the quasidegeneracy effects, and thus to make a comparison of the MRCCSD results with the FCI data more demanding (in view of the increasing role of configurations from $\mathcal{M}_0^{\perp}$), we consider slightly stretched hydrogen molecules with a=2.0 a.u. [5,10] (cf. paper I). We vary the rotation angle θ in the interval $[0, \pi/2]$ and we define the angular parameter $\alpha = \theta/\pi$, so that $\alpha \in [0, \frac{1}{2}]$, as indicated in Fig. 1(b). Thus, for every intermolecular distance R, we have a single parameter α describing the geometry of the model, as for the previously defined planar models in paper I. Proceeding from the planar rectangular conformation ($\alpha = 0$) to the maximally twisted perpendicular one ($\alpha = \frac{1}{2}$), we obtain a cross section of the H_4 potential-energy surface involving a simultaneous stretching of two chemical bonds H(1)–H(4) and H(2)–H(3). Recall that the $\alpha = 0$ geometry of the T4 model corresponds to the P4 model of Jankowski and Paldus [15] with the P4 intermolecular distance α equal to R [cf. Figs. 1(a) and 1(b)], which was employed to study a simultaneous breaking of two chemical bonds H(1)–H(4) and H(2)–H(3) when the P4 parameter $\alpha \gg a$ [cf. Fig. 1(a)]. Moreover, as shown in paper I, it is also instructive to study the highly degenerate compressed case when the P4 parameter $\alpha < a$ (see Secs. III B and III C).

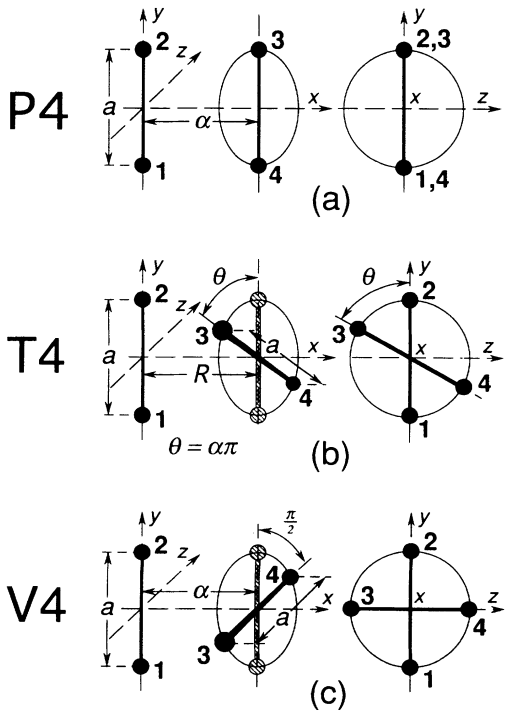

FIG. 1. Nuclear configurations and definition of the parameters R and α for the (a) P4, (b) T4, and (c) V4 models.

Another interesting type of dissociation of the H_4 molecular cluster is achieved when we consider the maximally twisted ($\alpha = \frac{1}{2}$) geometry of the T4 model and vary the intermolecular separation R. The resulting V4 model is illustrated in Fig. 1(c). In analogy to the P4 model, the intermolecular distance R is now designated by α. As we shall explain in Secs. III B and III C, it is again instructive to study the $\alpha \to \infty$ limit and the region of small values of α. Note that for the V4 model with $\alpha = a/\sqrt{2}$, the nuclei form the vertices of a regular tetrahedron (T_d).

As in paper I, we restrict ourselves to MBS models with one 1s-type atomic orbital [49] located on each hydrogen nucleus (the same basis was employed in Refs. [5,6,10,15–18,20,21]). Computations with larger basis sets, including the double zeta plus polarization (DZP) basis [19] (cf. also Refs. [6] and [22]), reveal that the MBS models display all the qualitative features involved [such as the singular behavior of the linear CC (L-CC) approaches [5,10,15,19] and the role of various terms arising in the theory [10,15]] and provide us with a good quantitative estimate of the performance of various approximate procedures when compared with the corresponding FCI results. Nonetheless, in spite of all these useful features of the MBS H_4 models, we must keep in mind their inherent limitations.

B. Reference configurations and orbitals

To define our model spaces we employ restricted Hartree-Fock MO's. Just as in the P4 case, these are

fully determined by the D_2 symmetry group of the T4 model, so that

$$\phi_i = a_i\big(\chi_1 + (-1)^{[\frac{i-1}{2}]}\chi_2 + (-1)^{[\frac{i}{2}]}\chi_3 + (-1)^{i+1}\chi_4\big), \quad (i = 1,\ldots,4), \tag{29}$$

where $[x]$ designates the largest integer not exceeding x (Gauss symbol) and χ_j $(j = 1,\ldots,4)$ represents the $1s$ atomic orbital centered on the H(j) nucleus (cf. Fig. 1). Moreover, for the V4 model, $a_3 = a_4$, so that orbitals ϕ_i, Eq. (29), are adapted to the chain $D_2 \subset D_{2d}$, the latter group being the symmetry group of V4. It is easy to verify that in this case the coefficients $a_3 = a_4$ do not depend on the intermolecular distance α and are only a function of the overlap $\langle\chi_1|\chi_2\rangle = \langle\chi_3|\chi_4\rangle$. For the tetrahedral geometry of V4, arising when $\alpha = a/\sqrt{2}$ [cf. Fig. 1(c)], we have that $a_2 = a_3 = a_4$, so that the orbitals ϕ_i are adapted to the chain $D_2 \subset D_{2d} \subset T_d$. Thus orbitals (29) of the V4 model can be classified either according to the irreducible representations of D_2, which is the symmetry common to all the models studied in this paper, or according to D_{2d}. For the tetrahedral geometry, we can even use T_d. For the P4 model (or T4 with $\alpha = 0$), orbitals (29) can be classified according to the irreducible representations of D_2 or D_{2h}, the latter being the symmetry group of P4. Finally, for the square geometry of the P4 model (the so-called S4 model [14]), $a_2 = a_3$, and the corresponding MO's are adapted to the chain $D_2 \subset D_{2h} \subset D_{4h}$.

The symmetry groups of various models and the symmetry species of the corresponding RHF MO's are summarized in Table I. We note that for the V4 model, ϕ_3 and ϕ_4 span two one-dimensional irreducible representations of D_2, b_3 and b_2, respectively, or a two-dimensional irreducible representation e of D_{2d}, which decomposes into b_3 and b_2 when restricted (or subduced) to D_2,

$$e(D_{2d}) \downarrow D_2 = b_2 \oplus b_3\,. \tag{30}$$

Similarly, for the tetrahedral geometry, orbitals ϕ_2, ϕ_3, and ϕ_4 span three one-dimensional irreducible representations of D_2, b_1, b_3, and b_2, respectively, or b_2 and e irreducible representations of D_{2d}, or, finally, a single three-dimensional irreducible representation t_2 of T_d, in agreement with relations

$$t_2(T_d) \downarrow D_{2d} = b_2 \oplus e\,, \tag{31}$$

$$b_2(D_{2d}) \downarrow D_2 = b_1\,, \tag{32}$$

and Eq. (30). For the square configuration, referred to as the S4 model, ϕ_2 and ϕ_3 span two one-dimensional irreducible representations b_1 and b_3 of D_2 or two one-dimensional irreducible representations b_{2u} and b_{3u} of D_{2h} or, finally, a single two-dimensional irreducible representation e_u of D_{4h}, in agreement with relations (cf. Sec. IV B of paper I)

$$e_u(D_{4h}) \downarrow D_{2h} = b_{2u} \oplus b_{3u}\,, \tag{33}$$

$$b_{2u}(D_{2h}) \downarrow D_2 = b_1,\ b_{3u}(D_{2h}) \downarrow D_2 = b_3\,. \tag{34}$$

For most geometries, the orbital labeling ϕ_i, $i = 1,2,3,4$, corresponds to the increasing orbital energy and the RHF ground-state configuration is $|\Phi_1\rangle = |(\phi_1)^2(\phi_2)^2\rangle$. There are, however, regions of the nuclear configuration space where the RHF ground-state configuration is $|\Phi_2\rangle = {}^{(1)}G^{33}_{22}(0)|\Phi_1\rangle = |(\phi_1)^2(\phi_3)^2\rangle$ or even $|\Phi_3\rangle = {}^{(1)}G^{44}_{22}(0)|\Phi_1\rangle = |(\phi_1)^2(\phi_4)^2\rangle$. This may be easily seen by examining the dependence of the diagonal configuration-interaction (CI) matrix elements $H_{jj} = \langle\Phi_j|H|\Phi_j\rangle$, $j = 1-3$, on the geometry of the nuclear framework or the corresponding dependence of the orbital energies obtained with CS configuration $|\Phi_1\rangle$, $|\Phi_2\rangle$, or $|\Phi_3\rangle$ as a reference. The dependence of the diagonal CI matrix elements pertinent to the FCI $A(D_2)$ problem (see Sec. III E) on the geometry of the nuclear framework is shown in Figs. 2 (few representative T4 models), 3 (P4 model), and 4 (V4 model), and the corresponding dependence of the orbital energies that are associated with references $|\Phi_1\rangle$, $|\Phi_2\rangle$, and $|\Phi_3\rangle$ is displayed in Figs. 5, 6, and 7, respectively (in the case of the P4 model, Fig. 6, orbital energies associated with $|\Phi_3\rangle$ are not shown). For the T4 models (see Figs. 2 and 5), we selected three most representative intermolecular separations R characterizing the short-range $(R \leq a)$ region, namely, $R = 1.1428, \sqrt{2}$, and 2.0 a.u. (recall that $a = 2.0$ a.u.) and three values of R from the long-range $(R > a)$ region $(R = 3.0, 4.0$, and 7.0 a.u.).

Two observations are immediate: For $R > a$, the ground-state RHF configuration is $|\Phi_1\rangle$, whereas for $R < a/\sqrt{2}$ it is $|\Phi_2\rangle$ that becomes the RHF ground state, while $|\Phi_1\rangle$ represents one of the excited configurations [the first or even the second one; cf. the T4 model with $R = 1.1428$ a.u. as an example, Figs. 2(a) and 5(a)]. For $a/\sqrt{2} \leq R \leq a$, either $|\Phi_1\rangle$ or $|\Phi_2\rangle$ will represent the

TABLE I. Symmetry groups of the studied models and their special cases and symmetry species of the corresponding RHF MO's, Eq. (29).

Model	Symmetry group	MO symmetry species			
		ϕ_1	ϕ_2	ϕ_3	ϕ_4
T4 (general)	D_2	a	b_1	b_3	b_2
T4 ($\alpha = 0$), P4	D_{2h}	a_g	b_{2u}	b_{3u}	b_{1g}
T4 ($\alpha = 0, R = a$), S4	D_{4h}	a_{1g}	e_u	e_u	b_{2g}
T4 ($\alpha = \frac{1}{2}$), V4	D_{2d}	a_1	b_2	e	e
T4 ($\alpha = \frac{1}{2}, R = \frac{a}{\sqrt{2}}$)	T_d	a_1	t_2	t_2	t_2

RHF ground state, depending on the relative orientation of hydrogen molecules in space: The energy of $|\Phi_2\rangle$, relative to that of $|\Phi_1\rangle$, increases with the increasing angular parameter α (cf. Fig. 2), so that for small values of α the lowest energy configuration is $|\Phi_2\rangle$, whereas in the vicinity of the perpendicular geometry ($\alpha \approx \frac{1}{2}$), the ground-state RHF wave function is represented by $|\Phi_1\rangle$. For the T4 model with $R = a/\sqrt{2}$ and $\alpha = \frac{1}{2}$ (tetrahedral geometry) and for the T4 model with $R = a$ and $\alpha = 0$ (square geometry), the configurations $|\Phi_1\rangle$ and $|\Phi_2\rangle$ are degenerate, and the orbital energy pictures associated with $|\Phi_1\rangle$ and $|\Phi_2\rangle$ are equivalent [see Figs. 5(b) and 5(c); cf. also Figs. 2(b) and 2(c)]. For the tetrahedral geometry, all three occupation schemes corresponding to

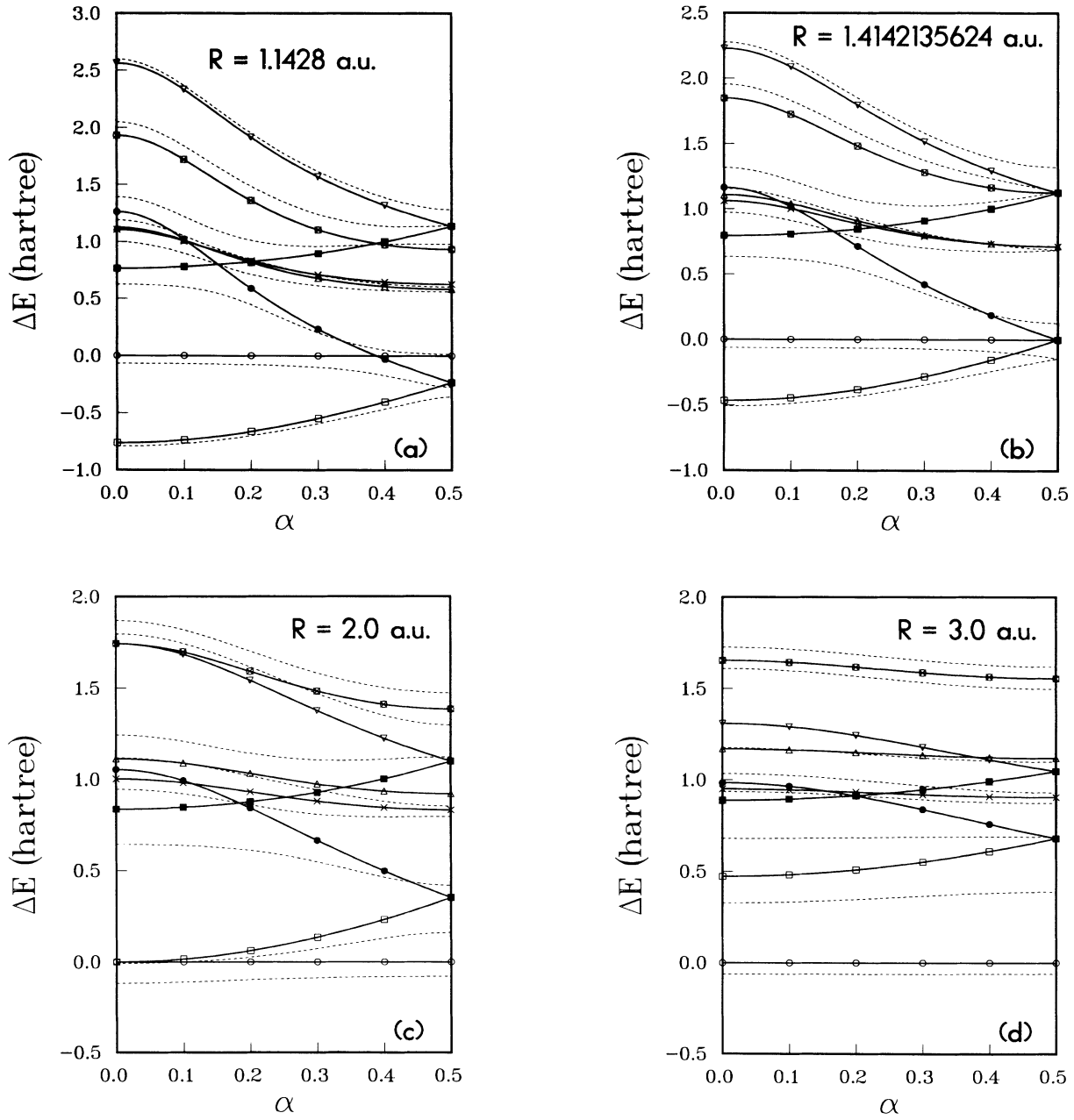

FIG. 2. Dependence of diagonal CI matrix elements $H_{jj} = \langle\Phi_j|H|\Phi_j\rangle$, $j = 1 - 8$, where the configurations $|\Phi_j\rangle$ are defined in Table IV, relative to the RHF energy $H_{11} = \langle\Phi_1|H|\Phi_1\rangle = \langle(\phi_1)^2(\phi_2)^2|H|(\phi_1)^2(\phi_2)^2\rangle$ (except for the T4 models with $R < a$, H_{11} represents the ground-state RHF energy), on the geometry of the nuclear framework, as measured by the angular parameter α (solid lines), for the MBS T4 models with $a = 2.0$ a.u. and $R = 1.1428$ (a), $\sqrt{2}$ (b), 2.0 (c), 3.0 (d), 4.0 (e), and 7.0 (f) a.u. Open circles and squares (○ and □) represent matrix elements H_{11} and H_{22}, respectively, whereas solid circles and squares (• and □) represent H_{33} and H_{44}. The remaining matrix elements H_{jj}, $j = 5 - 8$, are represented by ▽, △, ×, and ⊗, respectively. The dotted lines correspond to successive FCI singlet eigenstates of the $A(D_2)$ symmetry.

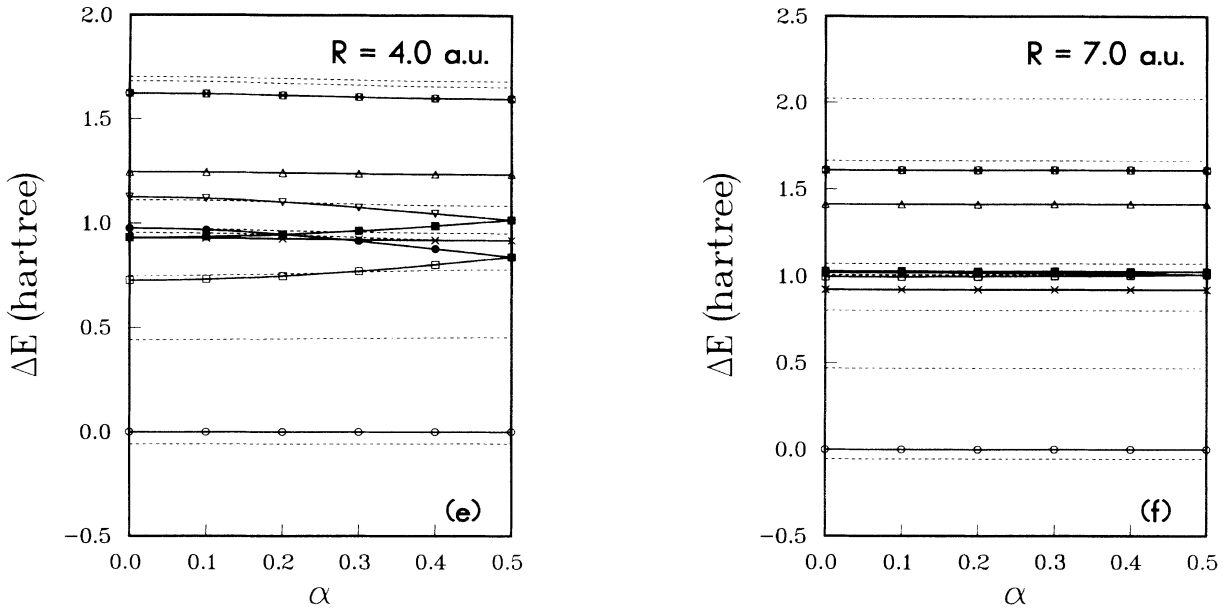

FIG. 2 *(Continued).*

configurations $|\Phi_1\rangle$, $|\Phi_2\rangle$, and $|\Phi_3\rangle$ give equivalent orbital energies, so that $H_{11} = H_{22} = H_{33}$. In fact, $|\Phi_2\rangle$ and $|\Phi_3\rangle$ are degenerate and yield equivalent orbital energies for all V4 geometries (see Figs. 4 and 7).

For the MBS V4 model, described by the single-determinantal function $|\Phi_1\rangle$, orbitals ϕ_3 and ϕ_4 are degenerate (see Fig. 7), since they belong to the same

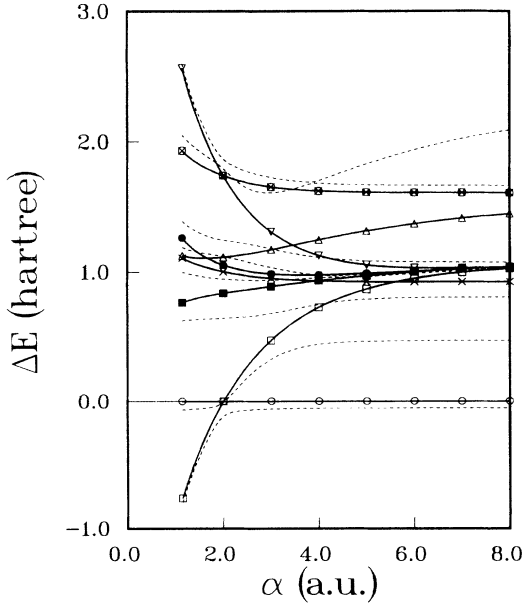

FIG. 3. Same as Fig. 2 for the MBS P4 model with $a =$ 2.0 a.u. and 1.1428 a.u. $\leq \alpha \leq$ 8.0 a.u. In this case, the $A(D_2)$ FCI singlet states become $A_g(D_{2h})$ singlets. For $\alpha \geq a$, matrix element H_{11} represents the ground-state RHF energy.

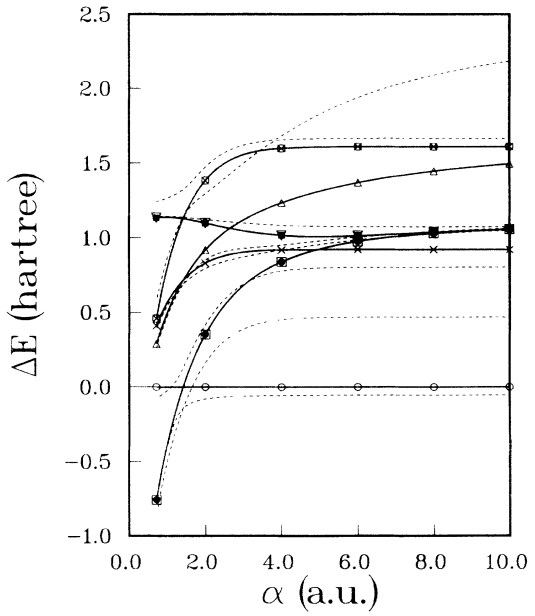

FIG. 4. Same as Figs. 2 and 3 for the MBS V4 model with $a =$ 2.0 a.u. and 0.7117 a.u. $\leq \alpha \leq$ 10.0 a.u. In this case, the $A(D_2)$ FCI singlet states are either $^1A_1(D_{2d})$ or $^1B_1(D_{2d})$ states. We do not distinguish between $A_1(D_{2d})$ and $B_1(D_{2d})$ FCI subproblems, since the two-reference CC theory studied in this paper breaks the D_{2d} symmetry of the V4 model. Note that for $\alpha > a/\sqrt{2}$, the FCI ground state belongs to the $A_1(D_{2d})$ subproblem and the first excited $A(D_2)$ singlet is a $B_1(D_{2d})$ state. For $\alpha < a/\sqrt{2}$, this order is reversed. For tetrahedral geometry ($\alpha = a/\sqrt{2}$), the two states become degenerate and span the two-dimensional irreducible representation $E(T_d)$. For $\alpha \geq a/\sqrt{2}$, the matrix element H_{11} represents the ground-state RHF energy.

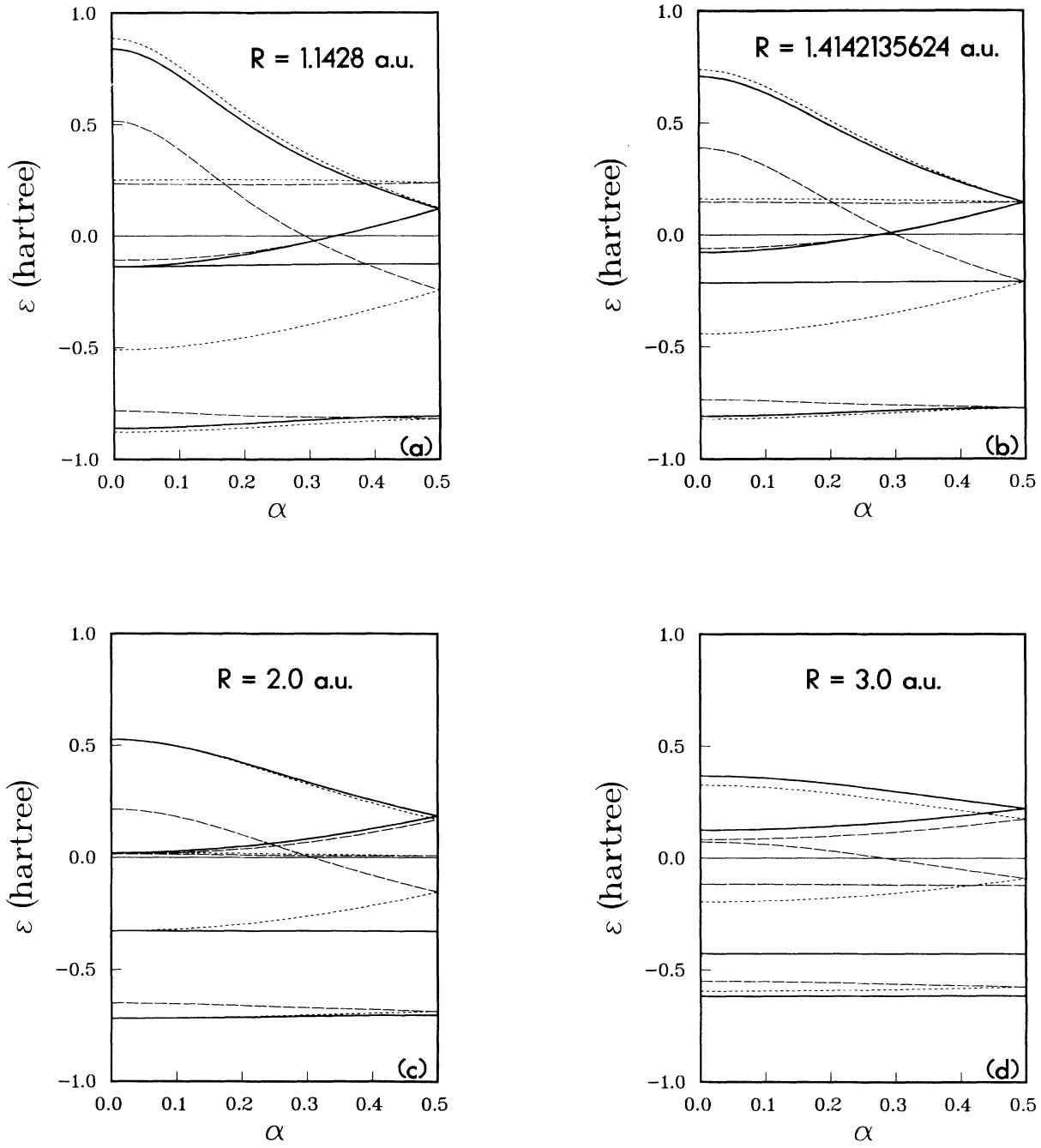

FIG. 5. Dependence of Hartree-Fock orbital energies ϵ_i (in hartrees) of MO's ϕ_i, Eq. (29), associated with three different reference configurations $|\Phi_1\rangle = |(\phi_1)^2(\phi_2)^2\rangle$ (solid lines), $|\Phi_2\rangle = |(\phi_1)^2(\phi_3)^2\rangle$ (dotted lines), and $|\Phi_3\rangle = |(\phi_1)^2(\phi_4)^2\rangle$ (short-dashed lines) on the geometry of the nuclear framework, as measured by the angular parameter α, for the MBS T4 models with $a = 2.0$ a.u. and $R = 1.1428$ (a), $\sqrt{2}$ (b), 2.0 (c), 3.0 (d), 4.0 (e), and 7.0 (f) a.u. For the configuration $|\Phi_1\rangle$, the energies ϵ_i for $\alpha = 0$ increase in the order $\epsilon_1 < \epsilon_2 \leq \epsilon_3 < \epsilon_4$ ($\epsilon_2 = \epsilon_3$ for $R = 1.1428$ a.u.). The same order holds for the configuration $|\Phi_2\rangle$, provided that $R \geq 3.4611$ a.u. (again, for $R = 3.4611$ a.u., ϕ_2 and ϕ_3 are degenerate). For T4 models with $R < 3.4611$ a.u., the orbital energies associated with the configuration $|\Phi_2\rangle$ for $\alpha = 0$ increase in the order $\epsilon_1 < \epsilon_3 < \epsilon_2 < \epsilon_4$. For $R \leq a/\sqrt{2}$ and $\alpha = 0.5$, the orbital energies associated with the configuration $|\Phi_3\rangle$ increase in the order $\epsilon_1 < \epsilon_4 < \epsilon_3 \leq \epsilon_2$ ($\epsilon_3 = \epsilon_2$ for $R = a/\sqrt{2}$). For $a/\sqrt{2} < R \leq R_0$, we obtain $\epsilon_1 < \epsilon_4 \leq \epsilon_2 < \epsilon_3$ (for $R = R_0$, $\epsilon_4 = \epsilon_2$; for $a = 2.0$ a.u., $R_0 \approx 2.8$ a.u.), whereas for $R > R_0$, $\epsilon_1 < \epsilon_2 < \epsilon_4 < \epsilon_3$. Notice that for all T4 models with $\alpha = 0.5$, the orbitals ϕ_3 and ϕ_4 associated with the configuration $|\Phi_1\rangle$ are degenerate and the remaining two configurations $|\Phi_2\rangle$ and $|\Phi_3\rangle$ yield equivalent orbital energy diagrams. For the square geometry ($R = a$ and $\alpha = 0$), $|\Phi_1\rangle$ and $|\Phi_2\rangle$ yield equivalent orbital energy pictures. All three occupation schemes, corresponding to configurations $|\Phi_1\rangle$, $|\Phi_2\rangle$, and $|\Phi_3\rangle$, give equivalent orbital energy spectra for the tetrahedral geometry ($R = a/\sqrt{2}$ and $\alpha = 0.5$). Except for the occupation scheme represented by $|\Phi_3\rangle$, degeneracy of ϕ_2 and ϕ_3 is shifted away from the square geometry.

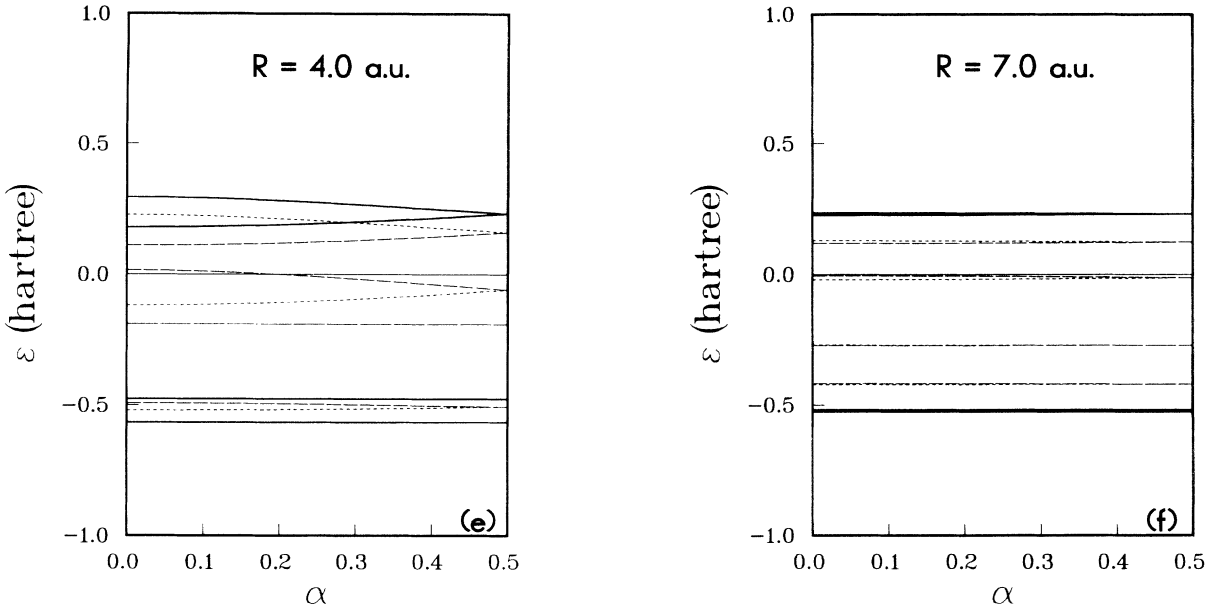

FIG. 5 *(Continued).*

symmetry species e of D_{2d} (cf. Table I) and the configuration $|\Phi_1\rangle \equiv |(\phi_1)^2(\phi_2)^2\rangle$ does not break the D_{2d} symmetry of the V4 model. Indeed, both e orbitals are unoccupied in $|\Phi_1\rangle$, so that the corresponding Fock operator $F((\phi_1)^2(\phi_2)^2)$ commutes with all the symmetry operations of D_{2d}. Symbolically, we can express this fact

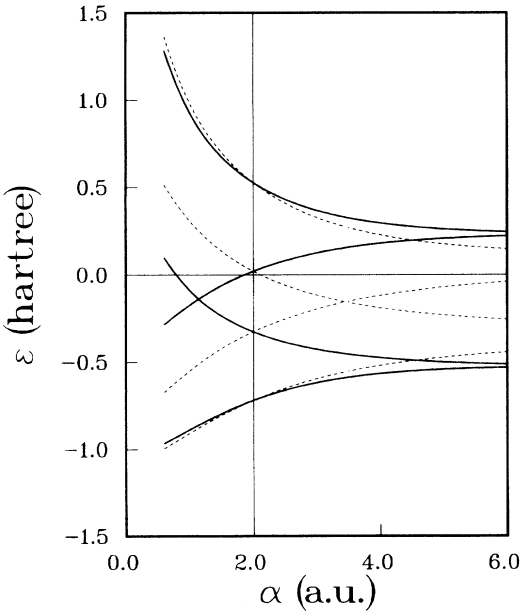

FIG. 6. Same as Fig. 5 for the MBS P4 model with $a = 2.0$ a.u. and 0.6 a.u. $\leq \alpha \leq 6.0$ a.u. Orbital energies associated with the configuration $|\Phi_3\rangle$ are not displayed. For both configurations $|\Phi_1\rangle$ and $|\Phi_2\rangle$, the energies ϵ_i of MO's ϕ_i, Eq. (29), for $\alpha = 6.0$ a.u. increase in the order $\epsilon_1 < \epsilon_2 < \epsilon_3 < \epsilon_4$ and the crossing of HOMO and LUMO energy levels is shifted away from the square ($\alpha = a$) geometry. For the RHF solution $|\Phi_1\rangle$, it occurs at $\alpha_0' = 1.1428$ a.u., while relative to the configuration $|\Phi_2\rangle$ it occurs at the distance $\alpha_0'' = 3.4611$ a.u. For $\alpha = a$, configurations $|\Phi_1\rangle$ and $|\Phi_2\rangle$ yield equivalent orbital energy diagrams.

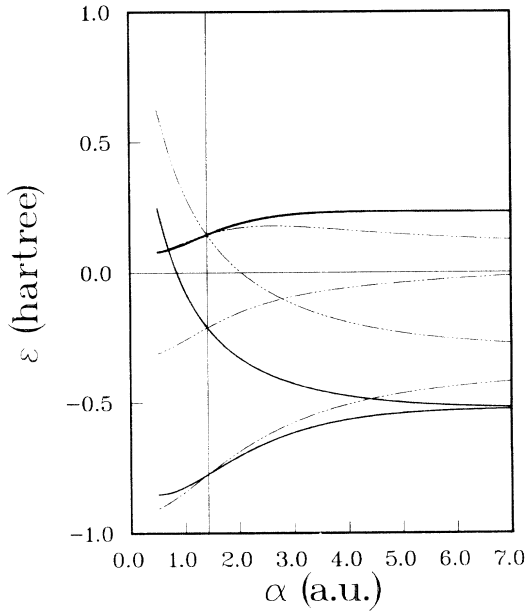

FIG. 7. Same as Figs. 5 and 6 for the MBS V4 model with $a = 2.0$ a.u. and 0.5 a.u. $\leq \alpha \leq 7.0$ a.u. The orbital energy diagrams associated with configurations $|\Phi_2\rangle$ and $|\Phi_3\rangle$ are equivalent, so that we use chain-dashed lines to designate the corresponding orbital energies. For the configuration $|\Phi_2\rangle$, the energies ϵ_i of MO's ϕ_i, Eq. (29), for $\alpha = 7.0$ a.u. increase in the order $\epsilon_1 < \epsilon_2 < \epsilon_3 < \epsilon_4$. For the same geometry, the orbital energies associated with the configuration $|\Phi_3\rangle$ increase in the order $\epsilon_1 < \epsilon_2 < \epsilon_4 < \epsilon_3$. For the configuration $|\Phi_1\rangle$, the energies ϵ_i for $\alpha = 7.0$ a.u. increase in the order $\epsilon_1 < \epsilon_2 < \epsilon_3 = \epsilon_4$. In this case, orbitals ϕ_3 and ϕ_4 remain degenerate over the entire region of α. For the tetrahedral ($\alpha = a/\sqrt{2}$) geometry, indicated by the solid vertical line, all three configurations $|\Phi_1\rangle$, $|\Phi_2\rangle$, and $|\Phi_3\rangle$ yield the same orbital energies. The crossing of ϵ_2, ϵ_3, and ϵ_4 for the configuration $|\Phi_1\rangle$ is shifted away from the tetrahedral geometry towards the $\alpha < a/\sqrt{2}$ region (for $a = 2.0$ a.u., it occurs at $\alpha = 0.7117$ a.u.).

by writing

$$[F((\phi_1)^2(\phi_2)^2),\, D_{2d}] = 0. \tag{35}$$

This, however, no longer holds when we employ $|\Phi_2\rangle$ or $|\Phi_3\rangle$ as a reference. These configurations violate the D_{2d} symmetry of the V4 model since the e orbitals are only partially filled in $|\Phi_2\rangle$ and $|\Phi_3\rangle$ configurations (i.e., either the orbital ϕ_3, or the orbital ϕ_4, is occupied, but never both of them). This implies the following symmetry breaking when $|\Phi_2\rangle$ or $|\Phi_3\rangle$ is employed as a reference:

$$[F((\phi_1)^2(\phi_j)^2),\, D_{2d}\backslash D_2] \neq 0 \quad (j = 3,4)\,, \tag{36}$$

and, in consequence, ϕ_3 and ϕ_4 are no longer degenerate (see Fig. 7). Similar symmetry breaking is observed for the tetrahedral geometry, independently of the reference configuration employed ($|\Phi_1\rangle$, $|\Phi_2\rangle$, or $|\Phi_3\rangle$). In this case, there exists a nonvanishing orbital energy gap between the highest occupied MO (HOMO) (ϕ_2 for $|\Phi_1\rangle$, ϕ_3 for $|\Phi_2\rangle$, and ϕ_4 for $|\Phi_3\rangle$) and the lowest (degenerate) unoccupied MO's (LUMO's) (ϕ_3 and ϕ_4 for $|\Phi_1\rangle$, ϕ_2 and ϕ_4 for $|\Phi_2\rangle$, and ϕ_2 and ϕ_3 for $|\Phi_3\rangle$), in spite of the fact that ϕ_2, ϕ_3, and ϕ_4 span a single three-dimensional irreducible representation t_2 of T_d (see Table I). This means that the Fock operator associated with either one of these configurations does not commute with all the symmetry operations of T_d. Indeed, in the case of $|\Phi_1\rangle$ we have that

$$[F((\phi_1)^2(\phi_2)^2),\, D_{2d}] = 0\,, \tag{37}$$

$$[F((\phi_1)^2(\phi_j)^2),\, T_d\backslash D_{2d}] \neq 0\,, \tag{38}$$

so that ϕ_3 and ϕ_4 remain degenerate (as they do in all other V4 geometries), while $\epsilon_2 < \epsilon_3 = \epsilon_4$ (ϵ_i is the energy of ϕ_i). The crossing (or the degeneracy) of all three orbital energies ϵ_2, ϵ_3, and ϵ_4 in the V4 model will occur for $\alpha = \alpha_0 < a/\sqrt{2}$ (for $a = 2.0$ a.u., $\alpha_0 = 0.7117$ a.u.; cf. Fig. 7). Recall that we encountered a similar situation in the P4 model (see Fig. 6 and Sec. IV B of paper I): Using $|\Phi_1\rangle$ as a reference and proceeding from the long-range $\alpha > a$ region, where $|\Phi_1\rangle$ represents the ground-state RHF solution, the corresponding HOMO and LUMO, ϕ_2 and ϕ_3, respectively, become degenerate at some intermolecular separation $\alpha = \alpha_0' < a$ (for $a = 2.0$ a.u., $\alpha_0' = 1.1428$ a.u.). On the other hand, when $|\Phi_2\rangle$ is employed and we proceed from the short-range $\alpha < a$ region, where $|\Phi_2\rangle$ represents the ground-state RHF configuration, the corresponding HOMO and LUMO energies, ϵ_3 and ϵ_2, respectively, cross one another at the distance $\alpha = \alpha_0'' > a$ (for $a = 2.0$ a.u., $\alpha_0'' = 3.4611$ a.u.). HOMO and LUMO energies do not cross at the square geometry, since Fock operators associated with configurations $|\Phi_1\rangle$ and $|\Phi_2\rangle$ break the D_{4h} symmetry of the S4 model [14]. Consequently, orbitals ϕ_2 and ϕ_3 of the S4 model are not degenerate despite the fact that they belong to the same symmetry species of D_{4h}. We would have to employ $|\Phi_3\rangle$ configuration, in which both e_u orbitals remain unoccupied, to achieve degeneracy of ϕ_2 and ϕ_3 for the square conformation.

The fact that HOMO and LUMO energies do not cross at the square geometry of the P4 model and that the crossing of ϵ_2 with ϵ_3 and ϵ_4 is shifted away from the tetrahedral geometry towards the $\alpha < a/\sqrt{2}$ region of the V4 model when $|\Phi_1\rangle$ is employed as a reference was first documented by Fukutome in his studies of instabilities of RHF solutions describing chemical reactions [50,51]. Fukutome showed that crossings of HOMO and LUMO energy levels, when using $|\Phi_1\rangle$ as a reference, cannot take place at the square or tetrahedral geometries, where they would occur according to simple MO theory, because of the presence of the interelectronic repulsion terms in the Hamiltonian. The size of the HOMO-LUMO gap in square and tetrahedral arrangements of atomic sites is measured by the magnitude of the interelectronic repulsion integral $\langle\chi_1\chi_2|\chi_1\chi_2\rangle \equiv (\chi_1\chi_1|\chi_2\chi_2)$ [50,51] (cf. Sec. IV B of paper I).

The symmetry breaking discussed above has interesting consequences for the MRCC formalism employing $|\Phi_1\rangle$ and $|\Phi_2\rangle$ as references. We address this problem in Sec. III D. Before doing so, however, we discuss various degeneracy types characterizing our models.

C. Orbital and configurational degeneracies

As pointed out in the preceding section, the configuration $|\Phi_1\rangle$ represents the RHF ground state for most geometries considered. There are, however, regions of the nuclear configuration space, where the ground-state RHF wave function is represented by $|\Phi_2\rangle$. As we have seen above, different occupation schemes, represented by $|\Phi_1\rangle$ and $|\Phi_2\rangle$, lead to different orbital energy spectra, even though the MO's themselves are always the same [see Eq. (29)], being determined by the symmetry of the model. When we are employing the ground-state RHF MO's as our one electron states in defining the model space, we should, in principle, switch to the orbitals associated with $|\Phi_2\rangle$, whenever the energy of this configuration becomes lower than that of $|\Phi_1\rangle$. In the present case, however, the same RHF MO's result, irrespective of the reference employed, since they are completely determined by the symmetry of the system. Since, further, both configurations $|\Phi_1\rangle$ and $|\Phi_2\rangle$ are included in our model space, it should be irrelevant which one of them represents the RHF ground state. However, this will no longer be the case when larger bases than a MBS are employed, in which case the role played by the choice of the MO basis should be carefully investigated (considering also other than RHF-type bases), or when configurations from outside of the model space substantially intervene [as, e.g., the configuration $|\Phi_3\rangle = |(\phi_1)^2(\phi_4)^2\rangle$ may in the case of nonplanar model considered below] or, of course, when considering models of lower symmetry (such as the H4 model studied in paper I).

In the case of the P4 model, for example, configurations $|\Phi_1\rangle$ and $|\Phi_2\rangle$ are degenerate and equally contribute to the exact ground state at $\alpha = a$ (square nuclear configuration), although the HOMO and LUMO energies are well separated in view of the symmetry breaking implied by the one electron approximation, as already mentioned (see paper I for details). Thus it is $|\Phi_2\rangle$ that represents the RHF ground state for $\alpha < a$. If we would employ the RHF MO's associated with the ground state for $\alpha < a$, the HOMO and LUMO energies would never become de-

generate. Only when $|\Phi_1\rangle$ is used as an RHF reference, the HOMO and LUMO energies cross one another (see above). In view of the above discussion, the fact that we employ $|\Phi_1\rangle$ as an RHF "ground state" even for $\alpha < a$ (or, equivalently, that the HOMO and LUMO are degenerate or almost degenerate) has no detrimental effect on the performance of the MRCC method, which in fact works best when the reference configurations in the model space are degenerate. In this way, however, we can explore the entire range of the orbital quasidegeneracy effects [48], including nondegenerate cases [cf., e.g., Figs. 5(d) and 5(e)] and vanishing of the HOMO-LUMO gap [cf. Fig. 5(a)]. With the RHF MO's associated with configuration $|\Phi_1\rangle$, we can even study an interesting case of degeneracy of three orbitals ϕ_2, ϕ_3, and ϕ_4, which takes place when $\alpha = 0.7117$ a.u. in the V4 model (cf. Fig. 7). Thus the RHF MO's used throughout this study are those associated with the configuration $|\Phi_1\rangle$.

It is well known that orbital degeneracy alone causes few problems for CC approaches [48]. Even the simplest L-CC methods give accurate correlation energies in such cases (cf., e.g., Refs. [52–54]). Configurational degeneracy [48], on the other hand, is of much greater concern. In this case, the SR L-CC approaches, such as L-CCD or L-CCSD, suffer from singular behavior due to the strong interaction of the ground-state configuration with the low-lying biexcited ones [15,19,55–59], while the L-MRCC methods fail due to the presence of intruder states, which strongly interact with one or more model space configurations [5,10,14]. Inclusion of nonlinear terms removes the L-CC singularities [5,10,14,15,19,55–57] (which can be classified as poles [60]), but new serious problems arise when both types of quasidegeneracies (orbital and configurational) are simultaneously present or when the dimension of the quasidegenerate reference space becomes very large [48]. In these cases it may even happen that the full CCSD or CCSDT (CC with singles, doubles, and triples) approaches suffer from singular behavior [14,56,57,60] due to the appearance of the algebraic branch points [60].

It is thus important to examine the effect of various degeneracies. The nonplanar H_4 models, similarly as their planar counterparts (see paper I), provide us with a useful example in this regard. In order to illustrate this fact, we give in Tables II and III the FCI expansion coefficients of configurations $|\Phi_1\rangle = |(\phi_1)^2(\phi_2)^2\rangle$, $|\Phi_2\rangle = {}^{(1)}G^{33}_{22}(0)|\Phi_1\rangle$, and $|\Phi_3\rangle = {}^{(1)}G^{44}_{22}(0)|\Phi_1\rangle$ for the two lowest totally symmetric singlet states $|\Psi_1\rangle$ and $|\Psi_2\rangle$ for all T4 models studied in this work. We immediately recognize an important role played by the above three configurations, even though there are regions where the ground-state FCI wave function has manifestly a SR character (e.g.,

TABLE II. FCI coefficients associated with configurations $|\Phi_1\rangle=|(\phi_1)^2(\phi_2)^2\rangle$, $|\Phi_2\rangle = |(\phi_1)^2(\phi_3)^2\rangle$, and $|\Phi_3\rangle = |(\phi_1)^2(\phi_4)^2\rangle$ for the ground-state wave function of the MBS T4 model with the H–H internuclear separation $a = 2.0$ a.u. and different values of the intermolecular distance R and angular parameter α. In general, the ground-state wave function is nondegenerate and represents the lowest singlet of $A(D_2)$ symmetry. The only exception is the tetrahedral geometry ($R = \sqrt{2}$ a.u., $\alpha = 0.5$), where the lowest two singlets of $A(D_2)$ symmetry are degenerate and span the two-dimensional irreducible representation $E(T_d)$ (see the text for details).

α	$\|\Phi_1\rangle$	$\|\Phi_2\rangle$	$\|\Phi_3\rangle$	$\|\Phi_1\rangle$	$\|\Phi_2\rangle$	$\|\Phi_3\rangle$	$\|\Phi_1\rangle$	$\|\Phi_2\rangle$	$\|\Phi_3\rangle$
	$R = 1.1428$ a.u.			$R = \sqrt{2}$ a.u.			$R = 2.0$ a.u.		
0.0	-0.072	0.990	-0.047	0.119	-0.981	0.057	0.690	-0.690	0.0
0.1	-0.076	0.989	-0.050	0.127	-0.979	0.060	0.731	-0.645	-0.009
0.2	-0.090	0.985	-0.063	0.154	-0.972	0.072	0.821	-0.519	-0.038
0.3	-0.116	0.977	-0.089	0.210	-0.954	0.094	0.894	-0.372	-0.078
0.4	-0.151	0.956	-0.162	0.325	-0.907	0.136	0.927	-0.258	-0.124
0.5	0.0	0.687	-0.687	0.785	-0.393	-0.393	0.936	-0.180	-0.180
	$R = 3.0$ a.u.			$R = 4.0$ a.u.			$R = 7.0$ a.u.		
0.0	0.961	-0.143	-0.093	0.967	-0.105	-0.095	0.968	-0.088	-0.090
0.1	0.961	-0.141	-0.094	0.967	-0.105	-0.096	0.968	-0.088	-0.090
0.2	0.961	-0.137	-0.097	0.967	-0.104	-0.096	0.968	-0.088	-0.090
0.3	0.962	-0.131	-0.103	0.967	-0.103	-0.098	0.968	-0.089	-0.089
0.4	0.962	-0.124	-0.109	0.967	-0.102	-0.099	0.968	-0.089	-0.089
0.5	0.962	-0.116	-0.116	0.967	-0.101	-0.101	0.968	-0.089	-0.089

TABLE III. Same as Table II for the first excited singlet state of $A(D_2)$ symmetry. For the tetrahedral geometry ($R = \sqrt{2}$ a.u., $\alpha = 0.5$), the lowest two singlets of $A(D_2)$ symmetry are degenerate and span the two-dimensional irreducible representation $E(T_d)$ (see the text for details).

α	$\|\Phi_1\rangle$	$\|\Phi_2\rangle$	$\|\Phi_3\rangle$	$\|\Phi_1\rangle$	$\|\Phi_2\rangle$	$\|\Phi_3\rangle$	$\|\Phi_1\rangle$	$\|\Phi_2\rangle$	$\|\Phi_3\rangle$
	$R = 1.1428$ a.u.			$R = \sqrt{2}$ a.u.			$R = 2.0$ a.u.		
0.0	0.964	0.068	-0.106	0.960	0.114	-0.117	0.678	0.678	-0.169
0.1	0.960	0.072	-0.125	0.956	0.122	-0.130	0.632	0.718	-0.178
0.2	0.941	0.081	-0.194	0.943	0.144	-0.174	0.502	0.803	-0.207
0.3	0.874	0.075	-0.377	0.909	0.182	-0.269	0.341	0.857	-0.266
0.4	0.635	-0.022	-0.713	0.807	0.223	-0.470	0.186	0.833	-0.400
0.5	0.491	-0.591	-0.591	0.0	0.680	-0.680	0.0	0.655	-0.655
	$R = 3.0$ a.u.			$R = 4.0$ a.u.			$R = 7.0$ a.u.		
0.0	0.099	0.840	-0.273	0.024	0.638	-0.384	0.000	0.447	-0.433
0.1	0.096	0.833	-0.284	0.023	0.632	-0.390	0.000	0.446	-0.433
0.2	0.085	0.809	-0.318	0.020	0.615	-0.408	0.000	0.445	-0.434
0.3	0.065	0.764	-0.379	0.014	0.587	-0.436	0.000	0.444	-0.436
0.4	0.036	0.689	-0.471	0.008	0.551	-0.471	0.000	0.442	-0.437
0.5	0.0	0.584	-0.584	0.0	0.511	-0.511	0.0	0.440	-0.440

for all T4 models with large values of R). There are also geometries (near the square conformation) where we observe a strong interaction of only two configurations, namely $|\Phi_1\rangle$ and $|\Phi_2\rangle$.

The T4 model with $R = 1.1428$ a.u. describes a transition from the case of the exact degeneracy of HOMO and LUMO orbitals, ϕ_2 and ϕ_3, respectively [cf. Fig. 5(a)], arising when $\alpha = 0$, to the case of a strong interaction of $|\Phi_1\rangle$, $|\Phi_2\rangle$, and $|\Phi_3\rangle$, taking place when $\alpha \sim 0.5$. Thus, if we employ a two-reference model space $\mathcal{M}_0$ (see Sec. III D)

$$\mathcal{M}_0 = \text{span}\{|\Phi_1\rangle, |\Phi_2\rangle\}\ , \tag{39}$$

we encounter a strong interaction of $\mathcal{M}_0^{\perp}$ states with $\mathcal{M}_0$ in the $\alpha = 0.5$ limit. Actually, strong interaction of the $\mathcal{M}_0$ and $\mathcal{M}_0^{\perp}$ configurations characterizes all V4 models. Another interesting situation is represented by the T4 model with $R = \sqrt{2}$ a.u. In this case, we deal with a transition from a region of relatively strong orbital quasidegeneracy [small HOMO-LUMO gap; cf. Fig. 5(b)] and weak configurational quasidegeneracy to a strongly correlated $\alpha = 0.5$ limit, where we again observe a substantial contribution of all three configurations $|\Phi_1\rangle$, $|\Phi_2\rangle$, and $|\Phi_3\rangle$ in the FCI expansions for $|\Psi_1\rangle$ and $|\Psi_2\rangle$ (cf. Tables II and III). As pointed out above, the $\alpha = 0.5$ limit of the T4 model with $R = \sqrt{2}$ a.u. represents an interesting case of T_d symmetry breaking by the Fock operator. This symmetry breaking will certainly influence the behavior of all MRCC formalisms employing $\mathcal{M}_0$, Eq. (39), as a model space (see Secs. III D and IV).

In the case of the T4 model with $R = 2.0$ a.u., the HOMO-LUMO gap is relatively large [cf. Fig. 5(c)]. Nonetheless, we observe a strong configurational degeneracy involving $|\Phi_1\rangle$ and $|\Phi_2\rangle$ when $\alpha \to 0$. For the perfect square ($\alpha = 0$) geometry, configurations $|\Phi_1\rangle$ and $|\Phi_2\rangle$ become exactly degenerate (cf. paper I). When $\alpha \to 0.5$, the interaction of $|\Phi_1\rangle$ and $|\Phi_2\rangle$ almost disappears and the ground-state wave function $|\Psi_1\rangle$ is relatively well approximated by the single CS configuration $|\Phi_1\rangle$. Simultaneously, we observe an increasingly strong interaction of $|\Phi_2\rangle$ with $|\Phi_3\rangle$. This is particularly evident in the first excited state (cf. Table III). For the remaining T4 models (with $R = 3.0$, 4.0, and 7.0 a.u.), we observe an increasingly nondegenerate character of the ground-state wave function $|\Psi_1\rangle$ and increasingly strong interaction of $|\Phi_2\rangle$ with $|\Phi_3\rangle$ and other biexcited configurations relative to $|\Phi_1\rangle$ [cf. Tables II and III; cf. also Figs. 2(d)–2(f)]. When the intermolecular distance R approaches large values, all configurations of the type ${}^{(1)}G^{\rho\rho}_{\alpha\alpha}(0)|\Phi_1\rangle$, $\alpha = 1, 2$, $\rho = 3, 4$ (cf. Sec. III E), contribute with more or less equal weight in the FCI expansions of $|\Psi_1\rangle$ and $|\Psi_2\rangle$. In the case of the ground-state wave function $|\Psi_1\rangle$, which is reasonably well described by the single CS configuration $|\Phi_1\rangle$, the corresponding FCI expansion coefficients remain small (see Table II). However, in the case of the FCI expansion for $|\Psi_2\rangle$, where $|\Phi_1\rangle$ is almost absent, participation of the biexcited configurations ${}^{(1)}G^{\rho\rho}_{\alpha\alpha}(0)|\Phi_1\rangle$ becomes substantial (cf. Table III). Thus all T4 models with large values of R (in particular, P4 and V4 models with large α) represent SR cases with an increasingly rich biexcited manifold that plays a dominant role in the description of $|\Psi_2\rangle$.

Interesting quasidegeneracy effects arise when P4 and V4 models are considered separately and we allow the intermolecular separation R (which in the case of P4 and V4 models is designated by α) to vary from small to large values. In the case of the MBS P4 model with $a = 2.0$ a.u., it is instructive to vary the intermolecular distance α from $\alpha_0' = 1.1428$ a.u. to ∞ [14]. In this way, we encounter several interesting situations including (i) the exact degeneracy of HOMO and LUMO for $\alpha = 1.1428$ a.u., when the lowest two eigenstates of the Hamiltonian possess a definite SR character; (ii) exact degeneracy of $|\Phi_1\rangle$ and $|\Phi_2\rangle$ for $\alpha = 2.0$ a.u., when the orbital quasidegeneracy is absent; and (iii) various nondegenerate cases for $\alpha > a$, when the first excited state involves a strong interaction of a number of biexcited configurations (cf. Fig. 6 and Tables II and III). Similarly, for the MBS V4 model with $a = 2.0$ a.u., it is instructive to vary the intermolecular separation α from $\alpha_0 = 0.7117$ a.u. to ∞. As explained in Sec. III B, the orbitals ϕ_2, ϕ_3, and ϕ_4 become exactly degenerate when $\alpha = 0.7117$ a.u. In the region $0.7117\,\text{a.u.} < \alpha < \sqrt{2}$ a.u., we deal with a strong mixing of orbital and configurational degeneracies involving a strong interaction of $|\Phi_1\rangle$, $|\Phi_2\rangle$, and $|\Phi_3\rangle$ (see Tables II and III and Fig. 7). For $\alpha = \sqrt{2}$ a.u. we then encounter an interesting case of tetrahedral geometry, when the lowest two eigenstates of the Hamiltonian become exactly degenerate [they span a two-dimensional irreducible representation E of T_d; cf. Fig. 2(b) or 4; cf. also Sec. IV]. Finally, we approach the nondegenerate $\alpha \to \infty$ limit, which is characterized by the maximum size of the HOMO-LUMO gap, and which is practically identical to the $\alpha \to \infty$ limit of the P4 model or any $R \to \infty$ T4 model.

D. Model spaces

The accuracy of various MRCC methods strongly depends on the choice of the model space. From a purely pragmatic viewpoint, it is best to keep the dimension of a model space as small as possible. The larger the model space, the more costly is the practical implementation of the MRCC formalism and the more likely we encounter intruder states. On the other hand, inclusion of only a few configurations in the model space (namely, those that dominate in the quasidegenerate regime) may be insufficient to yield a meaningful description of the low energy states in nondegenerate or strongly correlated cases [14]. In the case of T4 models, there are regions of the nuclear configuration space where the ground-state FCI wave function has a definite SR character (for example, all T4 models with large values of R), but there are also regions where we observe a strong interaction of three or more configurations (cf. Tables II and III).

In the present paper, similarly as in paper I, we explore basic characteristics of the two-reference CCSD formalism employing the CS configurations $|\Phi_1\rangle = |(\phi_1)^2(\phi_2)^2\rangle$ and $|\Phi_2\rangle = |(\phi_1)^2(\phi_3)^2\rangle$ as model configurations. As indicated by the FCI results (see Tables II and III), the model space spanned by $|\Phi_1\rangle$ and $|\Phi_2\rangle$ should be sufficient to yield a reasonable description of the lowest two eigenstates of the Hamiltonian in the vicinity of the square geometry, where $|\Phi_1\rangle$ and $|\Phi_2\rangle$ are nearly degenerate, and for all T4 models with $R \leq 3$ a.u. and $\alpha \leq 0.3$, where either $|\Phi_1\rangle$ or $|\Phi_2\rangle$ dominate in the FCI expansions of $|\Psi_1\rangle$ and $|\Psi_2\rangle$.

We can thus employ the two-reference theory described in Sec. II. The lowest totally symmetric orbital ϕ_1 represents the core orbital and the next two orbitals, ϕ_2 and ϕ_3, the active orbitals. Since ϕ_2 and ϕ_3 belong to different symmetry species of D_2, which is the symmetry common to all T4 (including P4 and V4) models (see Table I), the resulting two-configuration model space $\mathcal{M}_0$, Eq. (39), is complete, assuming that we restrict ourselves to the $A(D_2)$ singlet states. Since we study the MBS T4 models, there is only one virtual orbital ϕ_4.

Three cases require special attention. The first one is the S4 model, in which the hydrogen atoms form a square. It arises when $R = a$ and $\alpha = 0$ in the T4 model. In this case, the active orbitals ϕ_2 and ϕ_3 belong to the same symmetry species of the invariance group of the Hamiltonian (namely, the two-dimensional irreducible representation e_u of D_{4h}), so that the basic assumption of our two-reference formalism seems to be violated. One might thus question the D_{4h} invariance of the two-dimensional model space spanned by $|\Phi_1\rangle$ and $|\Phi_2\rangle$ and, consequently, the D_{4h} invariance of the two-reference CC formalism, since neither $|\Phi_1\rangle$ nor $|\Phi_2\rangle$ is D_{4h} scalar. Interestingly enough, this is not the case. First of all, as shown in paper I, the two-dimensional model space $\mathcal{M}_0$, Eq. (39), breaks down into a direct sum of D_{4h} invariant subspaces,

$$\mathcal{M}_0 = \mathcal{M}_{0,B_{1g}} \oplus \mathcal{M}_{0,A_{1g}}\,, \tag{40}$$

where

$$\mathcal{M}_{0,B_{1g}} = \text{span}\left\{|\tilde{\Phi}_1\rangle\right\}\,, \tag{41}$$

$$\mathcal{M}_{0,A_{1g}} = \text{span}\left\{|\tilde{\Phi}_2\rangle\right\}\,, \tag{42}$$

with

$$|\tilde{\Phi}_1\rangle = (|\Phi_1\rangle - |\Phi_2\rangle)/\sqrt{2}\,, \tag{43}$$

$$|\tilde{\Phi}_2\rangle = (|\Phi_1\rangle + |\Phi_2\rangle)/\sqrt{2}\,, \tag{44}$$

so that $\mathcal{M}_0$ is itself D_{4h} invariant and as such can be regarded as a complete reference space. However, the D_{4h} invariance of $\mathcal{M}_0$ is not sufficient to guarantee the D_{4h} invariance of the resulting MRCC formalism. The active orbitals ϕ_2 and ϕ_3 belong to different symmetry species of D_{2h} (cf. Table I), so that we should rather use D_{2h}, which is the symmetry of the more general P4 model, to classify the resulting states. The S4 model represents, however, a special situation. In spite of the fact that the Fock operator associated with the configuration $|\Phi_1\rangle$, and the individual cluster operators $T^{(p)}$, $p = 1, 2$, break the D_{4h} symmetry of the S4 model (they are only D_{2h} invariants), the corresponding MRCC wave operator U, Eq. (15), and the effective Hamiltonian H^{eff}, Eq. (11), are D_{4h} invariants. This unusual behavior of the MRCC formalism for the S4 model is due to the fact that the RHF MO's (29) for the S4 model are adapted to the chain $D_2 \subset D_{2h} \subset D_{4h}$. Consequently, the reference

configurations $|\Phi_p\rangle$, and the individual cluster operators $T^{(p)}$, $p = 1, 2$, are D_{2h} scalars, while for all the remaining operations $O \in D_{4h} \setminus D_{2h}$ we have that (cf. paper I)

$$O|\Phi_p\rangle = |\Phi_q\rangle\,, \tag{45}$$

$$OT^{(p)}O^{-1} = T^{(q)}\,, \tag{46}$$

where $q = 3 - p$. Thus, although the proper symmetry group to be used for the S4 model is D_{2h}, all groups in the chain $D_2 \subset D_{2h} \subset D_{4h}$ can be used to classify the resulting states $|\Psi_\mu\rangle$ ($\mu = 1, 2$), Eqs. (4), (43), and (44). In other words, the two-reference CC theory employing model space (39) for the S4 model produces two states that are totally symmetric with respect to the symmetry of the Fock operator (D_{2h}), but at the same time belong to different symmetry species [A_{1g} and B_{1g}; cf. Eqs. (40)–(44)] of the invariance group of the Hamiltonian (D_{4h}), in agreement with relations

$$A_{1g}(D_{4h}) \downarrow D_{2h} = B_{1g}(D_{4h}) \downarrow D_{2h} = A_g(D_{2h})\,. \tag{47}$$

Quite a different situation arises when we study the V4 model. In this case the invariance group of the Hamiltonian is D_{2d}, but only the first reference configuration $|\Phi_1\rangle$ is a D_{2d} scalar. The second model space configuration $|\Phi_2\rangle$ is invariant under the transformations belonging to D_2, but for the operations $O \in D_{2d} \setminus D_2$ we obtain that

$$O|\Phi_2\rangle = |\Phi_3\rangle\,. \tag{48}$$

Consequently, the two-reference CC formalism employing model space (39) breaks the D_{2d} symmetry of the V4 model and we have to use D_2, which is the symmetry of all T4 models, to classify the resulting solutions. In contrast to the S4 model, neither the individual cluster operators $T^{(p)}$, $p = 1, 2$, nor the corresponding wave operator U are invariant with respect to the symmetry group of the Hamiltonian when our two-reference CC approach is applied to the V4 model. The question arises how this symmetry breaking influences the MRCC results for the lowest two singlets of $A(D_2)$ symmetry. Examination of the V4 model with various intermolecular distances α gives us an opportunity to answer this question.

To obtain a CC formalism that is D_{2d} invariant, we would either have to employ a one-dimensional model space spanned by $|\Phi_1\rangle$ or consider the enlarged model space

$$\tilde{\mathcal{M}}_0 = \mathrm{span}\{|\Phi_1\rangle, |\Phi_2\rangle, |\Phi_3\rangle\}\,. \tag{49}$$

The first option leads to the well-known SRCC formalism. The use, however, of the space $\tilde{\mathcal{M}}_0$ would require the consideration of three-reference CC theory. In our case, this theory would employ three active orbitals ϕ_2, ϕ_3, and ϕ_4 and three CS-type references $|\Phi_1\rangle$, $|\Phi_2\rangle$, and $|\Phi_3\rangle$. The corresponding orthogonally spin-adapted formalism would produce two energetically lowest singlets of $A_1(D_{2d})$ symmetry, namely,

$$|\Psi_\mu\rangle \equiv U|\tilde{\Phi}_\mu\rangle = U\big(c_{1\mu}|\Phi_1\rangle + c_{2\mu}(|\Phi_2\rangle + |\Phi_3\rangle)\big) \qquad (\mu = 1, 3) \tag{50}$$

and the lowest $B_1(D_{2d})$ singlet

$$|\Psi_2\rangle \equiv U|\tilde{\Phi}_2\rangle = U(|\Phi_2\rangle - |\Phi_3\rangle)/\sqrt{2}\,. \tag{51}$$

This is a consequence of the fact that the three-reference CC wave operator U,

$$U = e^{T^{(1)}}P_1 + e^{T^{(2)}}P_2 + e^{T^{(3)}}P_3\,, \tag{52}$$

is D_{2d} invariant, whereas the model space $\tilde{\mathcal{M}}_0$ breaks down into a direct sum of three D_{2d} invariant subspaces

$$\tilde{\mathcal{M}}_0 = \mathcal{M}'_{0,A_1} \oplus \mathcal{M}''_{0,A_1} \oplus \mathcal{M}_{0,B_1}\,, \tag{53}$$

where

$$\mathcal{M}'_{0,A_1} = \mathrm{span}\{|\Phi_1\rangle\}\,, \tag{54}$$

$$\mathcal{M}''_{0,A_1} = \mathrm{span}\{(|\Phi_2\rangle + |\Phi_3\rangle)/\sqrt{2}\}\,, \tag{55}$$

$$\mathcal{M}_{0,B_1} = \mathrm{span}\{(|\Phi_2\rangle - |\Phi_3\rangle)/\sqrt{2}\}\,. \tag{56}$$

As in the case of the S4 model, the wave operator U, Eq. (52), is invariant with respect to the invariance group of the Hamiltonian, in spite of the fact that the individual cluster operators break this symmetry for the V4 model. Careful inspection of the three-reference case indicates that

$$OT^{(p)}O^{-1} = T^{(p)} \quad (p = 1 - 3) \tag{57}$$

for $O \in D_2$ and

$$OT^{(p)}O^{-1} = \begin{cases} T^{(p)} & \text{if } p = 1 \\ T^{(5-p)} & \text{if } p = 2, 3 \end{cases} \tag{58}$$

for $O \in D_{2d} \setminus D_2$. Since similar relations hold for the projection operators P_p, Eq. (1) [cf. Eq. (48)], the three-reference wave operator U, Eq. (52), must be D_{2d} invariant. Neither the SRCC formalism nor the three-reference theory employing the enlarged space $\tilde{\mathcal{M}}_0$ are subject of the present study. Clearly, the latter approach requires a larger than a MBS model and will be examined in the future.

The third and the last case deserving special attention is the tetrahedral (T_d) T4 model that arises when $R = a/\sqrt{2}$ and $\alpha = \frac{1}{2}$. Tetrahedral geometry also represents a special case of the V4 model when $\alpha = a/\sqrt{2}$, so that most of the above made remarks concerning general V4 models apply in this case as well. First of all, neither $|\Phi_1\rangle$ nor $|\Phi_2\rangle$ is a T_d scalar, so that the two-dimensional model space $\mathcal{M}_0$, Eq. (39), is not T_d invariant. Consequently, the two-reference CC formalism employing $|\Phi_1\rangle$ and $|\Phi_2\rangle$ as model configurations breaks the T_d symmetry of the Hamiltonian. In fact, as pointed out earlier, the two-reference CC theory employing $\mathcal{M}_0$ breaks even D_{2d} symmetry, characterizing all V4 models. We thus have to classify the resulting solutions by the irreducible representations of D_2, which is the symmetry common to all T4 models. The two-reference CC theory employing $\mathcal{M}_0$, Eq. (39), will produce two singlets that are totally symmetric with respect to D_2 but

do not belong to any particular irreducible representation of D_{2d} or T_d. As a result, the two-reference CC formalism will destroy the twofold degeneracy characterizing the exact electronic ground state of the tetrahedral H_4 model [the FCI wave functions $|\Psi_1\rangle$ and $|\Psi_2\rangle$ carry the two-dimensional irreducible representation E of T_d; cf. Fig. 2(b) or 4]. The question thus arises how large an energy gap between $|\Psi_1\rangle$ and $|\Psi_2\rangle$ will result from MRCC calculations.

In order to obtain a T_d invariant MRCC formalism we would have to consider again an enlarged model space (49), including also the configuration $|\Phi_3\rangle$. An analysis of this case shows that the three-reference wave operator U, Eq. (52), is T_d invariant, whereas the model space $\tilde{\mathcal{M}}_0$, Eq. (49), breaks down into a direct sum of two T_d invariant subspaces,

$$\tilde{\mathcal{M}}_0 = \mathcal{M}_{0,E} \oplus \mathcal{M}_{0,A_1} , \tag{59}$$

where

$$\mathcal{M}_{0,E} = \text{span}\left\{|\tilde{\Phi}_1\rangle, |\tilde{\Phi}_2\rangle\right\} , \tag{60}$$

$$\mathcal{M}_{0,A_1} = \text{span}\left\{|\tilde{\Phi}_3\rangle\right\} , \tag{61}$$

with

$$|\tilde{\Phi}_1\rangle = \sqrt{\tfrac{2}{3}}|\Phi_1\rangle - \tfrac{1}{\sqrt{6}}(|\Phi_2\rangle + |\Phi_3\rangle) , \tag{62}$$

$$|\tilde{\Phi}_2\rangle = \tfrac{1}{\sqrt{2}}(|\Phi_2\rangle - |\Phi_3\rangle) , \tag{63}$$

$$|\tilde{\Phi}_3\rangle = \tfrac{1}{\sqrt{3}}(|\Phi_1\rangle + |\Phi_2\rangle + |\Phi_3\rangle) . \tag{64}$$

As a result, the three-reference CC theory, employing $|\Phi_1\rangle$, $|\Phi_2\rangle$, and $|\Phi_3\rangle$ as model configurations, would yield two singlet states of $E(T_d)$ symmetry

$$|\Psi_\mu\rangle = U|\tilde{\Phi}_\mu\rangle \quad (\mu = 1, 2) \tag{65}$$

and the lowest singlet state of $A_1(T_d)$ symmetry

$$|\Psi_3\rangle = U|\tilde{\Phi}_3\rangle , \tag{66}$$

with $|\tilde{\Phi}_\mu\rangle$, $\mu = 1, 2, 3$, given by Eqs. (62)–(64). Thus the three-reference CC formalism would correctly describe the twofold degeneracy of the electronic ground state of the tetrahedral H_4 model. Notice also that the two $E(T_d)$ singlets, defined by Eqs. (62), (63), and (65), transform as $A_1(D_{2d})$ and $B_1(D_{2d})$ states, in agreement with Eqs. (50), with $\mu = 1$, and (51), and the fact that

$$E(T_d) \downarrow D_{2d} = A_1 \oplus B_1 . \tag{67}$$

In particular, the state $|\Psi_1\rangle$ represents the lowest singlet of $A_1(D_{2d})$ symmetry and the totally symmetric singlet state $|\Psi_3\rangle$, Eq. (66), the first excited state of the same symmetry, in agreement with Eq. (50), with $\mu = 3$ [cf. Fig. 2(b)]. Again, the three-reference wave operator U, Eq. (52), is invariant with respect to the symmetry group of the Hamiltonian, in spite of the fact that neither the reference configurations $|\Phi_p\rangle$ nor the corresponding cluster operators $T^{(p)}$, $p = 1 - 3$, are T_d scalars. This is a consequence of the fact that the RHF MO's (29) for the tetrahedral geometry are adapted to the chain $D_2 \subset D_{2d} \subset T_d$, so that T_d symmetry operations leave $|\Phi_p\rangle$ unchanged or simply permute them among themselves.

The above discussion indicates that we must be very careful in selecting reference configurations. Inappropriate choice of the model space may spoil an invariant character of cluster and wave operators, and the resulting CC formalism may produce solutions that do not reflect the symmetry properties of the Hamiltonian. An application of the two-reference CC formalism employing the model space spanned by $|\Phi_1\rangle$ and $|\Phi_2\rangle$ to MBS V4 models gives us an opportunity to study such symmetry breaking. Although an invariant character of the MRCC formalism can always be restored by enlarging the model space, information about the potential usefulness of broken symmetry solutions may prove useful in practical calculations. We also note the similarity between the present study of broken-symmetry CC solutions and an investigation of the applicability of MRCC approaches employing incomplete model spaces (cf., e.g., Ref. [8]). If we examined V4 models using three active orbitals ϕ_2, ϕ_3, and ϕ_4, we could not regard the two-dimensional model space $\mathcal{M}_0$, Eq. (39), as the "complete" subspace of $\tilde{\mathcal{M}}_0$, Eq. (49), since $\mathcal{M}_0$ does not represent a D_{2d} invariant subspace of $\mathcal{H}_N$.

E. CI and CC configuration spaces

To assess the effectiveness of various MRCC approaches we compare them with the exact FCI results. As already mentioned, we restrict ourselves to $A(D_2)$ singlet states. We thus need only eight configurations to describe the corresponding FCI space. The excitation operators generating the required orthogonally spin-adapted configurations $|\Phi_j\rangle$, $j = 2 - 8$, when acting on the reference $|\Phi_1\rangle = |(\phi_1)^2(\phi_2)^2\rangle$, are listed in Table IV.

Notice the absence of mono- and triexcited configurations. They may be ignored, since they belong to a different symmetry species than the model configurations $|\Phi_1\rangle$ and $|\Phi_2\rangle$ [namely, to $B_3(D_2)$]. Thus, for all MBS T4 models (including P4 and V4), the CI method limited to doubly and quadruply excited states and the FCI approach are equivalent.

For the P4 model, whose spatial symmetry is D_{2h}, the $A(D_2)$ singlet states become $A_g(D_{2h})$ singlets, in view of the subduction

$$A_g(D_{2h}) \downarrow D_2 = A . \tag{68}$$

Additional splitting of the $A(D_2)$ or $A_g\,(D_{2h})$ FCI matrix for the S4 model, whose spatial symmetry is D_{4h}, into the $A_{1g}\,(D_{4h})$ and $B_{1g}\,(D_{4h})$ subproblems is not essential here, since the two-reference CC theory considered in this paper yields solutions belonging to different D_{4h} subproblems (see the discussion in Sec. III D). The ground state of the S4 model belongs to the $B_{1g}\,(D_{4h})$ subproblem, whereas the first excited $A(D_2)$ singlet becomes the $A_{1g}\,(D_{4h})$ state. Similarly, we do not split the $A(D_2)$

TABLE IV. Excitation operators ${}^{(1)}G_i$ generating orthogonally spin-adapted configurations $|\Phi_j\rangle = {}^{(1)}G_j|\Phi_1\rangle$ spanning the FCI totally symmetric singlet space for the MBS T4 models. (See Refs. [9] and [32] for definitions of orthogonally spin-adapted configurations and excitation operators.) As usual, D and Q designate double and quadruple excitations, respectively. Mono- and triexcited configurations are not listed since they belong to the $B_3(D_2)$ [or $B_{3u}(D_{2h})$ in the P4 case] subproblem.

Configuration number (j)	Excitation operator ${}^{(1)}G_j$	Type	Excitation order
1	1	REF	0
2	${}^{(1)}G^{33}_{22}(0)$	D	2
3	${}^{(1)}G^{44}_{22}(0)$	D	2
4	${}^{(1)}G^{33}_{11}(0)$	D	2
5	${}^{(1)}G^{44}_{11}(0)$	D	2
6	${}^{(1)}G^{34}_{12}(0)$	D	2
7	${}^{(1)}G^{34}_{12}(1)$	D	2
8	${}^{(1)}G^{3344}_{1122}(0,0,0,0,0) = {}^{(1)}G^{33}_{11}(0){}^{(1)}G^{44}_{22}(0)$	Q	4

FCI matrix for the V4 model into smaller $A_1(D_{2d})$ and $B_1(D_{2d})$ subproblems, since the two-reference CC theory employing the model space $\mathcal{M}_0$, Eq. (39), breaks the D_{2d} symmetry. Let us only mention that for intermolecular distances $\alpha > a/\sqrt{2}$, the exact ground state belongs to the $A_1(D_{2d})$ subproblem and the first excited $A(D_2)$ singlet represents the $B_1(D_{2d})$ state. For $\alpha < a/\sqrt{2}$, this order is reversed (cf. Tables II and III), whereas for tetrahedral geometry of the H_4 molecular cluster ($\alpha = a/\sqrt{2}$), the two states become degenerate and span the two-dimensional irreducible representation $E(T_d)$, in agreement with relation (67).

The orthogonally spin-adapted doubly excited operators ${}^{(p)}G^{\rho\sigma}_{\alpha\beta}(i)$, ($p = 1,2$; $i = 0,1$) that are required in the two-reference CCSD formalism when applied to the MBS T4 models and their special cases P4, S4, and V4, are listed in Table V. Acting on model configurations $|\Phi_1\rangle$ and $|\Phi_2\rangle$, they generate totally symmetric $[A(D_2)]$ singlet configurations in $\mathcal{M}_0^{\perp}$, so that all of them carry at least one nonvalence index (1 or 4). Only biexcited operators are listed, since monoexcitations do not contribute. Due to the high symmetry of T4 models and the MBS employed, monoexcited cluster operators $T_1^{(p)}$, $p = 1,2$, vanish. This means that the MRCCSD and MRCCD methods are equivalent when MBS T4 models are examined (this is not the case when larger basis sets are employed). Vanishing of $T_1^{(p)}$ implies that there is no difference between the MRCCSD-2 and MRCCSD-3 approximations for MBS T4 models (cf. Sec. II). Finally, notice the absence of the biexcitation operators ${}^{(p)}G^{\rho\sigma}_{\alpha\alpha}(0)$, $\rho \neq \sigma$, and ${}^{(p)}G^{\rho\rho}_{\alpha\beta}(0), \alpha \neq \beta$, which also generate the states that are not totally symmetric with respect to the D_2 symmetry, common to all T4 models (cf. Table I).

F. Solution of MRCC equations

Fully quadratic MRCCSD equations (20) represent an energy-independent system of nonlinear algebraic equations of the general form

TABLE V. Biexcitation operators ${}^{(p)}G^{\rho\sigma}_{\alpha\beta}(i)$, ($p = 1,2$; $i = 0,1$) required in the two-reference CCSD formalism when applied to the MBS T4 models. Equation number I labels the equations in system (69).

p	Equation number (I)	${}^{(p)}G^{\rho\sigma}_{\alpha\beta}(i)$
1	1	${}^{(1)}G^{44}_{22}(0)$
	2	${}^{(1)}G^{33}_{11}(0)$
	3	${}^{(1)}G^{44}_{11}(0)$
	4	${}^{(1)}G^{34}_{12}(0)$
	5	${}^{(1)}G^{34}_{12}(1)$
2	6	${}^{(2)}G^{44}_{33}(0)$
	7	${}^{(2)}G^{22}_{11}(0)$
	8	${}^{(2)}G^{44}_{11}(0)$
	9	${}^{(2)}G^{24}_{13}(0)$
	10	${}^{(2)}G^{24}_{13}(1)$

$$a_I + \sum_{J=1}^{N} b_{IJ} t_J + \sum_{J \leq K}^{N} c_{IJK} t_J t_K = 0 \quad (I = 1, 2, \ldots, N), \tag{69}$$

with N designating the number of linearly independent singly and doubly excited cluster coefficients t_I (recall that in the present case t_I represent only biexcited amplitudes; cf. the preceding section).

Since the order of the spin- and symmetry-adapted MRCCSD system of equations for the MBS T4 models is very small ($N = 10$; cf. Table V), we can use the same computational strategy as in paper I. We thus store the coefficients a_I, b_{IJ}, and c_{IJK} and solve the system (69) for the unknown cluster amplitudes t_I using the Newton-Raphson procedure (see, e.g., Appendix B in Ref. [53]), while employing Gaussian elimination to solve the linear system resulting in each iteration. Normally, only a few iterations (at most a dozen or so) are needed to achieve the eight-digit accuracy for cluster amplitudes, or better. This algorithm is very similar to that used in our SRCC calculations [15,19,31,48,52–54,56,57,60–63], except for the presence of the effective Hamiltonian matrix elements $H_{21}^{\rm eff}$ and $H_{12}^{\rm eff}$ in the linear and bilinear coupling terms, entering Eq. (69), which depend on cluster amplitudes and must be recalculated in every Newton-Raphson iteration.

The convergence rate of the Newton-Raphson scheme and the actual solution that we obtain (nonlinear equations possess generally multiple solutions) strongly depend on the initial guess for cluster amplitudes $\mathbf{t}^{(0)} = \| t_I^{(0)} \|_{1 \leq I \leq N}$ (cf. Refs. [5,10,14,60]). Thus an appropriate choice of $\mathbf{t}^{(0)}$ is very crucial. The L-MRCC solutions [obtained by solving system (69) with the nonlinear part neglected $c_{IJK} = 0$] are very often of little help in view of their singular behavior due to the presence of intruder states [5,10,14]. To avoid problems stemming from an inappropriate choice of initial guess for cluster amplitudes, we exploit an "analytic continuation" of solutions from the region of geometries for which a good starting point is easily available. This procedure employs as the first approximation $\mathbf{t}^{(0)}$ the converged solution for a sufficiently close geometry $\mathbf{t}^{(0)}(\alpha + \Delta\alpha) \equiv \mathbf{t}(\alpha)$ while choosing a sufficiently small step $\Delta\alpha$. In this way, we can examine analytic properties of CC solutions and determine the limits of applicability of CC approaches. The method of analytic continuation is particularly helpful in the vicinity of singularities that plague some of the nonlinear MRCCSD solutions (see the following sections), where extremely small steps $\Delta\alpha$ (such as 10^{-6} or smaller) are applied in order to localize the position of the singularity. It is the only procedure that enables us to follow a particular solution of the system (69) while changing the geometry of the model under consideration [5,10,14,15,19,48,56,57,60–63].

The actual MRCC computations were carried out with a set of programs exploiting spin and spatial symmetry common to all (planar as well as nonplanar) H_4 models, which was also employed in paper I. The GAMESS electronic structure package [64] was used for the initial RHF calculations. The one- and two-electron molecular integrals needed to construct the coefficients a_I, b_{IJ}, and c_{IJK} and the effective Hamiltonian matrix were computed using the transformation routines that form a part of the GAMESS CI system.

IV. RESULTS

We now focus on a comparison of MRCCSD energies and FCI data. We first discuss L-MRCCSD results (Sec. IV A) before turning our attention to nonlinear MRCCSD-n results (Sec. IV B).

A. L-MRCCSD results

In the vicinity of the square geometry, where $|\Phi_1\rangle$ and $|\Phi_2\rangle$ are nearly degenerate, and for all T4 models with 1.1428 a.u. $\leq R \leq$ 2.0 a.u. and $\alpha \leq$ 0.3, where either $|\Phi_1\rangle$ or $|\Phi_2\rangle$ is a dominant configuration in FCI expansions for $|\Psi_1\rangle$ and $|\Psi_2\rangle$, the L-MRCCSD formalism provides very good correlation energies. In this region, the differences between the L-MRCCSD and FCI results for the energy of the ground state are usually smaller than 1 mhartree. Except for the highly compressed cases, the differences between the L-MRCCSD and FCI results increase with R, but even for the T4 model with $R = 2.0$ a.u. and $\alpha \leq 0.3$ they do not exceed 2 mhartree. In the case of the first excited state of $^1A(D_2)$ symmetry, the differences between the L-MRCCSD and FCI energies are slightly larger, but again for the majority of geometries belonging to the above region they do not exceed couple of millihartrees. This excellent performance of the L-MRCCSD method is apparent from Figs. 8(a)–8(c), which display the α dependence of the L-MRCCSD and MRCCSD-2,3 energies for T4 models with $R = 1.1428$, $\sqrt{2}$ and 2.0 a.u. The remaining Figs. 8(d)–8(f) display the α dependence of the L-MRCCSD and MRCCSD-2,3 energies for T4 models with larger intermolecular distances, namely, $R = 3.0$, 4.0, and 7.0 a.u.

L-MRCCSD results are meaningful up to $R \sim 2.0$ a.u. and $\alpha \sim 0.3$. Already for $R = 3.0$ a.u., the discrepancies between the L-MRCCSD and FCI results become substantial. The differences between the L-MRCCSD and FCI results for the first excited state of $^1A(D_2)$ symmetry exceed in this case 60 mhartree, even if we restrict ourselves to the well-behaved $\alpha \sim 0$ geometries [cf. Fig. 8(d)]. This can also be seen by considering the R dependence of the L-MRCCSD energies for the T4 model with $\alpha = 0$ or, equivalently, the α dependence of the L-MRCCSD energies for the P4 model (see Fig. 9).

Serious problems with the linear approximation begin to appear for large intermolecular separations R or when $\alpha \rightarrow 0.5$ in the T4 model. In both cases the choice of a two-dimensional (or, actually, of any low-dimensional) model space becomes problematic due to an increasingly strong interaction between the model space configurations and configurations belonging to $\mathcal{M}_0^{\perp}$. Indeed, when the intermolecular separation R approaches large values, their interaction becomes very substantial, so that we find an almost equal participation of

the reference configuration $|\Phi_2\rangle = {}^{(1)}G^{33}_{22}(0)|\Phi_1\rangle$ and of the doubly excited configurations (cf. Table IV) $|\Phi_3\rangle = {}^{(1)}G^{44}_{22}(0)|\Phi_1\rangle$, $|\Phi_4\rangle = {}^{(1)}G^{33}_{11}(0)|\Phi_1\rangle$, $|\Phi_5\rangle = {}^{(1)}G^{44}_{11}(0)|\Phi_1\rangle$, and $|\Phi_7\rangle = {}^{(1)}G^{34}_{12}(1)|\Phi_1\rangle$ in the first excited-state wave function $|\Psi_2\rangle$ (e.g., for $R = 7.0$ a.u., the corresponding FCI expansion coefficients equal about 0.4, −0.4, −0.4, 0.4, and 0.5, respectively, independently of α). At the same time, the reference $|\Phi_1\rangle$, which represents a dominant configuration in the FCI expansion of $|\Psi_1\rangle$, is almost totally absent. For small intermolecular

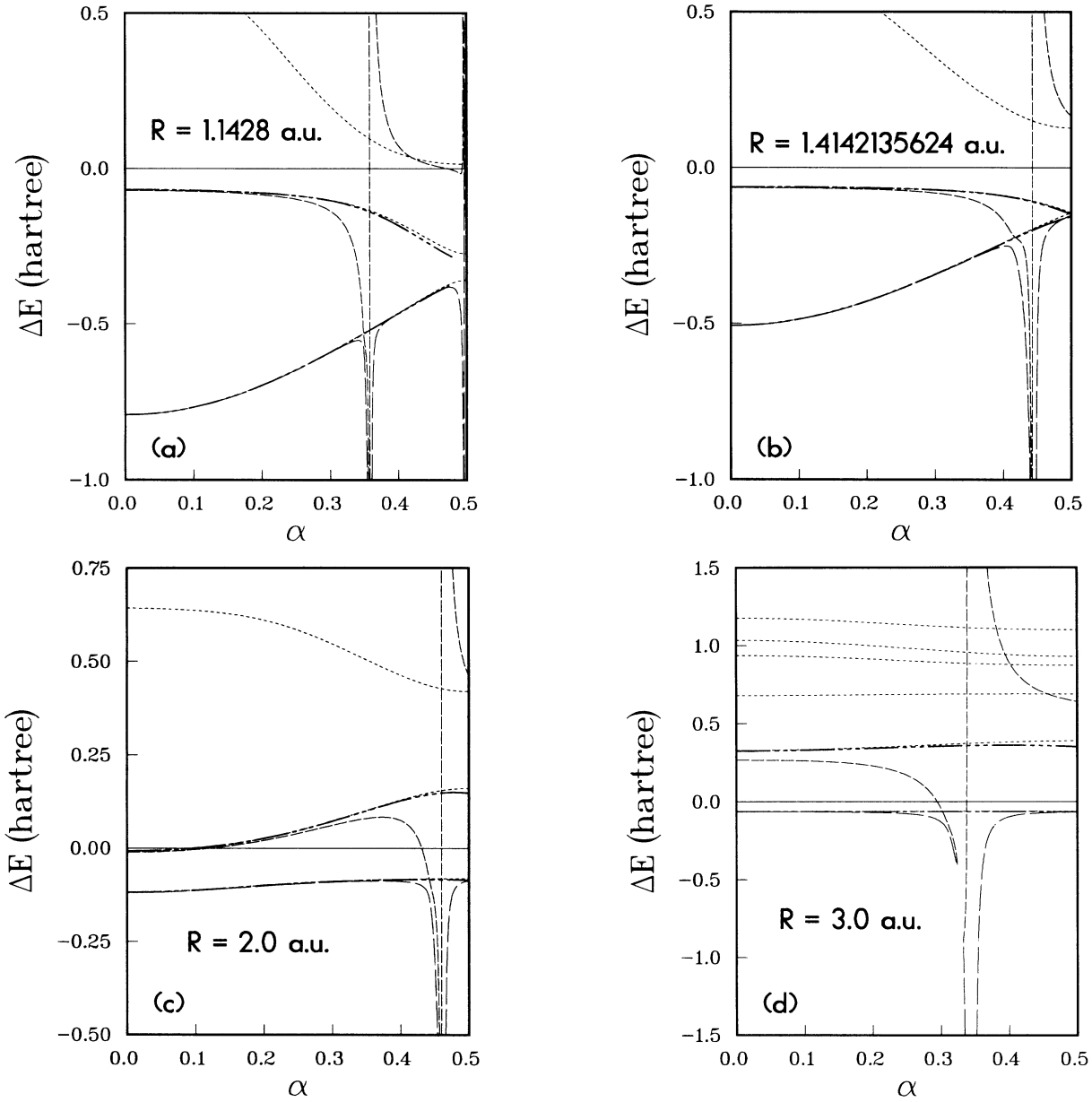

FIG. 8. A comparison of the FCI and various MRCCSD energies ΔE (in hartrees) relative to the energy of the configuration $|\Phi_1\rangle$, $\Delta E = E - H_{11}$, for the low energy singlet states of $A(D_2)$ symmetry for the MBS T4 models with $a = 2.0$ a.u. and $R = 1.1428$ (a), $\sqrt{2}$ (b), 2.0 (c), 3.0 (d), 4.0 (e), and 7.0 (f) a.u., considered over the whole range of the angular parameter α. In all cases we employ the RHF MO's associated with configuration $|\Phi_1\rangle = |(\phi_1)^2(\phi_2)^2\rangle$. The L-MRCCSD energies that are represented by the long- (lower energy root) and short-dashed (higher energy root) lines display a singular behavior around $\alpha \cong 0.358$ and 0.496 for $R = 1.1428$ a.u., $\alpha \cong 0.445$ for $R = \sqrt{2}$ a.u., $\alpha \cong 0.461$ for $R = 2.0$ a.u., and $\alpha \cong 0.343$ for $R = 3.0$ a.u. For $R = 1.1428$, $\sqrt{2}$, 2.0, and 3.0 a.u., there are regions where the L-MRCCSD method yields complex energies. For T4 models with $R = 1.1428$, $\sqrt{2}$, and 2.0 a.u. [Figs. 8(a)–8(c)], they are very narrow, so that we display them in a separate Fig. 11. In the case of the T4 model with $R = 3.0$ a.u., complex L-MRCCSD energies are obtained for $\alpha \in (0.3237, 0.3326)$ [see Fig. 8(d)]. Pairs of energies associated with the MRCCSD-2,3 solution are represented by the thick chain-dashed lines. For the T4 model with $R = 1.1428$ a.u., continuation of the MRCCSD-2,3 solution towards $\alpha = 0.5$ limit becomes impossible due to the appearance of an algebraic branch point at $\alpha \cong 0.4794$. As in Figs. 2–4, the dotted lines represent the successive FCI eigenstates of the ${}^1A(D_2)$ symmetry.

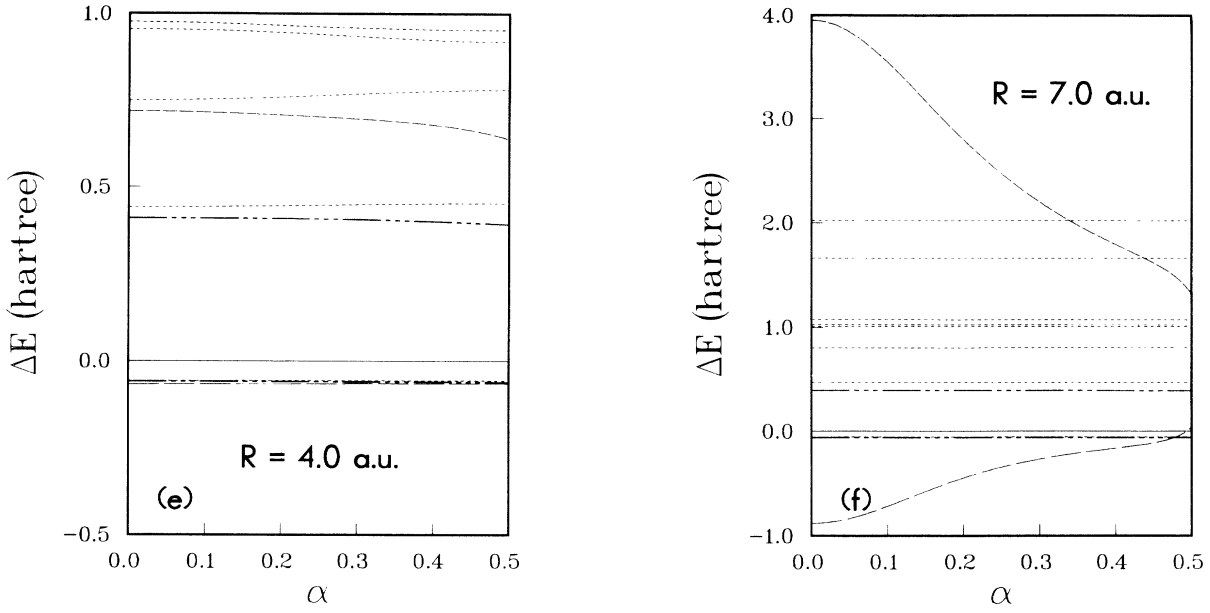

FIG. 8 *(Continued).*

separations R ($R < 2.0$ a.u.) and $\alpha \to 0.5$, we observe a substantial contribution of the $\mathcal{M}_0^{\perp}$ configuration $|\Phi_3\rangle$ in both FCI states $|\Psi_1\rangle$ and $|\Psi_2\rangle$ (cf. Tables II and III).

As shown in paper I (cf. also Refs. [5,10]), a strong interaction of the model space configurations with configurations from $\mathcal{M}_0^{\perp}$ results in singular behavior of the

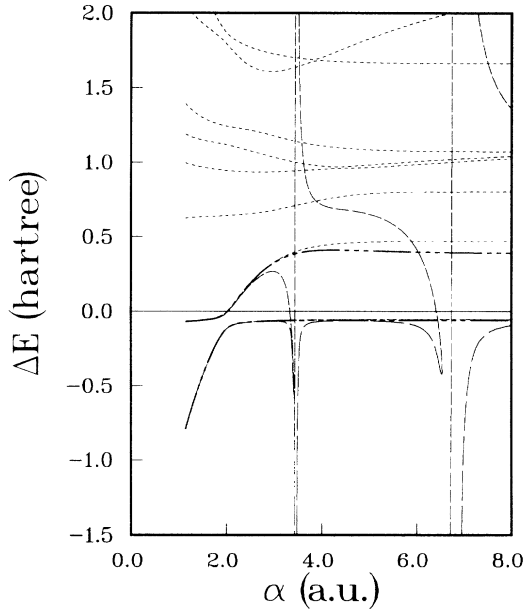

FIG. 9. Same as Fig. 8 for the MBS P4 model with $a =$ 2.0 a.u. and 1.1428 a.u. $\leq \alpha \leq$ 8.0 a.u. Recall that for $\alpha =$ 1.1428 a.u., active orbitals ϕ_2 and ϕ_3 become degenerate and the reference configuration $|\Phi_1\rangle$ represents the ground-state RHF wave function only for $\alpha \geq 2.0$ a.u. The L-MRCCSD method becomes singular for $\alpha \cong 3.46$ a.u. and $\alpha \cong 6.80$ a.u. For $\alpha \in$ (3.41 a.u., 3.43 a.u.) and $\alpha \in$ (6.54 a.u., 6.70 a.u.), the energies resulting from the L-MRCCSD theory become complex.

L-MRCCSD formalism. The nature of these singularities is very similar to those encountered in SR approaches [15,19,35,36,55–60]. Whenever one of the model space configurations becomes degenerate with some low-lying state belonging to $\mathcal{M}_0^{\perp}$, the L-MRCCSD coefficient matrix $\mathbf{b} \equiv \mathbf{b}(\alpha) \equiv \|b_{IJ}(\alpha)\|_{1 \leq I,J \leq N}$ [cf. Eq. (69)] becomes singular and we observe the appearance of one or more poles in the functional dependence of the solution vector $\mathbf{t} \equiv \mathbf{t}(\alpha) = \|t_I(\alpha)\|_{1 \leq I \leq N}$ and the corresponding energies $E_{\mu}^{\text{L-MRCCSD}}(\alpha)$, $\mu = 1, 2$, on the geometry of the nuclear framework. In fact, L-MRCC formalisms are more likely to suffer from singular behavior than SR theories, since the probability to encounter intruder states increases with the dimension of the model space (see the relevant discussion in paper I). This is precisely what happens when the intermolecular distance R becomes large or the angular parameter α approaches its largest possible value 0.5. Let us consider, for example, the T4 model with $R = 1.1428$ a.u. In this case, L-MRCCSD approach has two singularities [see Fig. 8(a)]. The first one appears for $\alpha = 0.358$, corresponding to the region of a very strong interaction between $|\Phi_1\rangle$ and $|\Phi_3\rangle$, whereas the second one appears for $\alpha = 0.496$, where $|\Phi_3\rangle$ strongly interacts with $|\Phi_2\rangle$. We have seen in paper I that we can predict the occurrence of these singularities by examining the dependence of configurational energies, given by the diagonal CI matrix elements $H_{jj} = \langle \Phi_j | H | \Phi_j \rangle$, on the geometry of the nuclear framework, since they will occur in the vicinity of geometries for which the model space configuration energies cross those corresponding to $\mathcal{M}_0^{\perp}$. Thus, for example, when we plot the α dependence of the diagonal CI matrix elements H_{jj} for the T4 model with $R = 1.1428$ a.u. [see Fig. 2(a)], we immediately realize that the L-MRCCSD singularities at $\alpha = 0.358$ and 0.496 correlate reasonably well with crossings of H_{11} with H_{33} at $\alpha \approx 0.39$ and of H_{22} with H_{33} at $\alpha = 0.5$.

In the case of the T4 model with $R = \sqrt{2}$ a.u., the L-MRCCSD approach has only one singularity [see Fig.

8(b)]. It appears at $\alpha = 0.445$, which is the region of strong interaction between $|\Phi_1\rangle$, $|\Phi_2\rangle$, and $|\Phi_3\rangle$. The occurrence of only one singularity in this case seems to correlate with the fact that there is only one geometry for which H_{11} and H_{22} intersect with H_{33}, namely, $\alpha = 0.5$ [see Fig. 2(b)]. Singularities for T4 models with $R = 2.0$ and 3.0 a.u. [see Figs. 8(c) and 8(d), respectively] seem to correlate with the interaction between $|\Phi_2\rangle$ and $|\Phi_3\rangle$ [note the crossing of H_{22} and H_{33} at $\alpha = 0.5$, Figs. 2(c) and 2(d)]. For the T4 model with $R = 2.0$ a.u., the L-MRCCSD method becomes singular at $\alpha = 0.461$, while for $R = 3.0$ a.u., the singularity is shifted towards the $\alpha = 0$ limit and appears at $\alpha = 0.343$. This is very likely due to the increasing proximity between the H_{22} and H_{33} energies that occurs in a much broader region of α values than only in the immediate vicinity of the $\alpha = 0.5$ limit when R becomes large [cf. Fig. 2(d)].

All L-MRCCSD singularities for T4 models with intermediate or small values of R are invariably associated with a strong interaction between $|\Phi_1\rangle$ and $|\Phi_3\rangle$ or $|\Phi_2\rangle$ and $|\Phi_3\rangle$. Thus inclusion of $|\Phi_3\rangle$ in the model space should eliminate the singular behavior of the two-reference L-CCSD formalism for small values of R (just as the inclusion of $|\Phi_2\rangle$ removes singularities arising in the SR L-CC approach). The situation gets more complicated for $R \to \infty$ when the interaction between the reference configuration $|\Phi_2\rangle$ and other configurations $|\Phi_j\rangle$ from $\mathcal{M}_0^{\perp}$ strongly increases [cf. Figs. 2(e) and 2(f)]. As a consequence, we find quite a few L-MRCCSD singularities for T4 models with large values of R, which can hardly be eliminated by incorporating $|\Phi_3\rangle$ in the model space. In fact, it becomes rather difficult to detect these singularities when examining T4 models with a large but fixed intermolecular separation R since they are practically isotropic [cf. Figs. 8(e) and 8(f)]. It is thus more revealing to examine the dependence of the L-MRCCSD energies on the intermolecular distance R. The most important are the cross sections of the L-MRCCSD potential-energy surfaces for the P4 and V4 models, shown together with the MRCCSD-2,3 and FCI energies in Figs. 9 and 10. In the case of the P4 model, we find two singularities at $\alpha = 3.46$ and 6.80 a.u. As explained in paper I, they are associated with a strong interaction between the reference configuration $|\Phi_2\rangle$ and doubly excited configurations $|\Phi_3\rangle$, $|\Phi_4,\rangle$, $|\Phi_5\rangle$, and $|\Phi_7\rangle$ (cf. Table IV), as may be seen from Fig. 3, which shows an increasing degeneracy of $|\Phi_2\rangle$, $|\Phi_3\rangle$, $|\Phi_4\rangle$, and $|\Phi_5\rangle$ for $\alpha \to \infty$ and the crossing of H_{22} with H_{77} at $\alpha \approx 5.6$ a.u.

Even more complicated situation arises in the V4 model, where $|\Phi_2\rangle$ and $|\Phi_3\rangle$ are degenerate and a strong interaction between $|\Phi_2\rangle$, $|\Phi_3\rangle$, $|\Phi_4\rangle$, $|\Phi_5\rangle$, and $|\Phi_7\rangle$ sets in for larger values of α (see Fig. 4). Matrix elements $H_{22} = H_{33}$ cross H_{77} at $\alpha \approx 5.0$ a.u and for $\alpha \to \infty$ we have that $H_{22} = H_{33} = H_{44} = H_{55}$. In addition, for $\alpha = \sqrt{2}$ a.u., $H_{11} = H_{22} = H_{33}$. Strong interaction between $|\Phi_1\rangle$, $|\Phi_2\rangle$, and $|\Phi_3\rangle$ in the vicinity of the tetrahedral geometry correlates well with the appearance of a singularity at $\alpha = 1.28$ a.u. This singularity is very steep and is shown in greater detail in Fig. 10(b). Other singularities appearing in this region are also associated with the degeneracy between $|\Phi_2\rangle$ and $|\Phi_3\rangle$, but can-

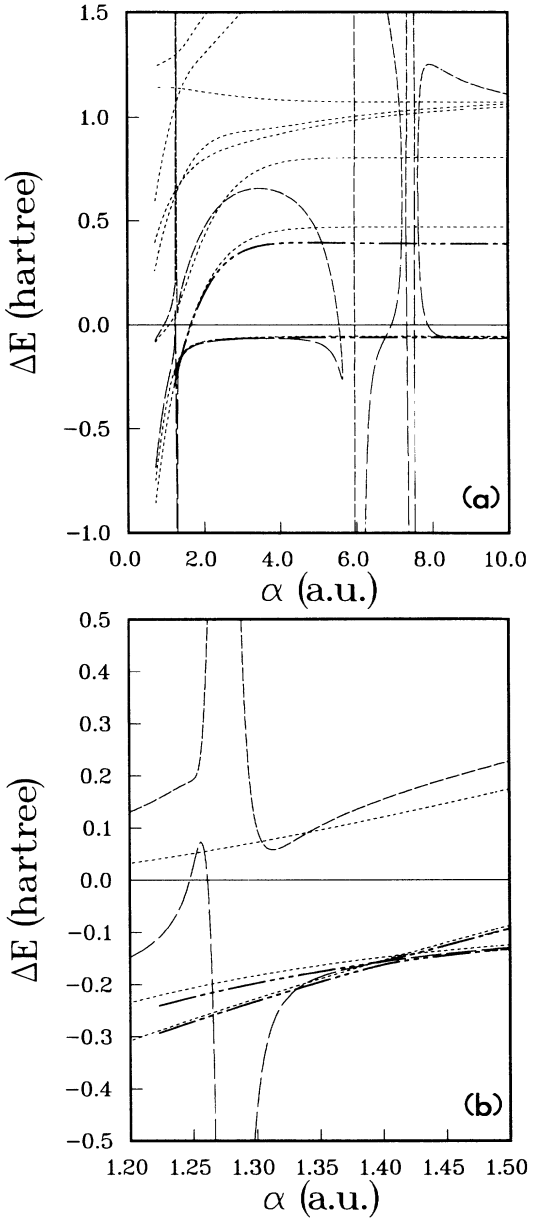

FIG. 10. Same as Figs. 8 and 9 for the MBS V4 model with $a = 2.0$ a.u. and 0.7117 a.u. $\leq \alpha \leq 10.0$ a.u. Recall that for $\alpha = 0.7117$ a.u., active orbitals ϕ_2 and ϕ_3 and virtual orbital ϕ_4 become degenerate and that the reference configuration $|\Phi_1\rangle$ represents the ground-state RHF solution only for $\alpha \geq \sqrt{2}$ a.u. The L-MRCCSD method becomes singular for $\alpha \cong 1.28$, 6.03, and 7.45 a.u. For $\alpha \in$ (5.64 a.u.,5.93 a.u.), (7.21 a.u.,7.32 a.u.), and (7.55 a.u.,7.63 a.u.), the energies resulting from the L-MRCCSD theory become complex. The region of the singular behavior of the MRCCSD-2,3 approach (MRCCSD-2,3 solution cannot be continued beyond $\alpha \cong 1.2226$ a.u.) and the steepest L-MRCCSD singularity (appearing at $\alpha \cong 1.28$ a.u.) is displayed in detail in (b). Recall that the two-reference CCSD formalism breaks the D_{2d} symmetry of the V4 model. As a consequence, the broken-symmetry MRCCSD-2,3 solution destroys the twofold degeneracy of the ground state for $\alpha = \sqrt{2}$ a.u. Notice, however, that MRCCSD-2,3 solution correctly approximates the shape of the FCI energy curves by minimizing the gap between the two roots of the effective Hamiltonian for $\alpha \approx 1.40$ a.u.

not be seen here, since they are shifted away from the $\alpha = 0.5$ geometry of the T4 model (cf. the above discussion). It is rather improbable that the two singularities appearing in the long-range region of the V4 model [at $\alpha = 6.03$ and 7.45 a.u.; cf. Fig.10(a)] are associated with this degeneracy. They seem to result from the proximity of $H_{22} = H_{33}$ and $H_{44} = H_{55}$ and a strong interaction between $|\Phi_2\rangle$, $|\Phi_3\rangle$, and $|\Phi_7\rangle$ for $\alpha \sim 5.0$ a.u. It is, in fact, remarkable that configurations $|\Phi_2\rangle$ and $|\Phi_3\rangle$ are degenerate for all intermolecular distances α, whereas the number of L-MRCCSD singularities in the V4 model is relatively small. We must not forget, however, that the above analysis has only an approximate character. We must also remember that MRCC amplitudes $t_I(\alpha)$ are algebraic functions of α (due to the algebraic nature of MRCC equations), so that the solution vector $\mathbf{t}(\alpha)$ is defined for all complex α with the possible exception of a finite number of isolated poles and algebraic branch points. The appearance of algebraic branch points at the linear level of approximation is rather unlikely (cf. Ref. [60]). Thus the number of L-MRCCSD singularities cannot become very large, especially when we realize that we employ very small configuration space.

Recall that whenever we pass a singular region, the second root of the effective Hamiltonian approximates successively higher and higher excited states, even though the lowest root of $H^{\rm eff}$ invariably describes the ground state [14]. In fact, only for T4 models with $R \leq 3.0$ a.u. and α not exceeding 0.3–0.4, where the L-MRCCSD approach remains nonsingular, the L-MRCCSD energies approximate the first two $A(D_2)$ singlets. Once we pass the singularities in the $\alpha \sim 0.4$–0.5 region, the second root of $H^{\rm eff}$ approximates the third $^1A(D_2)$ state. For $R \to \infty$, i.e., when all singularities have been passed, the second L-MRCCSD root approximates a group of the fourth, fifth, and sixth $^1A(D_2)$ states, which are degenerate for $R \to \infty$ (see Figs. 8–10). This interesting behavior of the L-MRCCSD formalism is related to an increasingly large participation of the model configurations $|\Phi_1\rangle$ or $|\Phi_2\rangle$ in the FCI expansions of consecutive $A(D_2)$ singlets and an increasingly strong interaction between the $\mathcal{M}_0$ and $\mathcal{M}_0^{\perp}$ configurations for $\alpha \to 0.5$ and $R \to \infty$ (cf. paper I). Let us consider, for example, the behavior of the L-MRCCSD formalism for the T4 model with $R = 1.1428$ a.u. [cf. Fig. 8(a)]. For $\alpha < 0.358$, the model space configurations $|\Phi_1\rangle$ and $|\Phi_2\rangle$ represent dominant configurations in the FCI expansions of $|\Psi_2\rangle$ and $|\Psi_1\rangle$. In this region, references $|\Phi_1\rangle$ and $|\Phi_2\rangle$ do not significantly interact with configurations belonging to $\mathcal{M}_0^{\perp}$ so that the FCI energies E_1 and E_2 differ little from the diagonal CI matrix elements H_{22} and H_{11} [see Fig. 2(a)]. It is thus not surprising that the L-MRCCSD approximation describes the lowest two $A(D_2)$ singlets. However, once we pass the singular region ($\alpha \approx 0.358$), which is characterized by a strong interaction between $|\Phi_1\rangle$ and $|\Phi_3\rangle$, we observe an increasingly large participation of the reference $|\Phi_1\rangle$ in the FCI expansion of the third $A(D_2)$ singlet and a smaller and smaller role of $|\Phi_1\rangle$ in the FCI expansion of $|\Psi_2\rangle$. For $\alpha = 0.4$, $|\Phi_1\rangle$, and $|\Phi_3\rangle$ are almost degenerate and the absolute values of corresponding FCI expansion coefficients for each of the lowest three states of $^1A(D_2)$ symmetry are almost equal in this region (they equal 0.151 and 0.162 for $|\Psi_1\rangle$, 0.635 and 0.713 for $|\Psi_2\rangle$, and 0.703 and 0.627 for $|\Psi_3\rangle$, respectively). Once we pass the singular region ($\alpha \sim 0.3$–0.4), the reference $|\Phi_1\rangle$ begins to play the dominant role in the FCI expansion of $|\Psi_3\rangle$ (for $\alpha = 0.5$, the corresponding FCI expansion coefficient equals 0.821), compared to relatively small role of $|\Phi_1\rangle$ in the FCI expansion of $|\Psi_2\rangle$. In the vicinity of the $\alpha = 0.5$ limit, we can hardly distinguish between the CI matrix element H_{11} and the FCI energy of $|\Psi_3\rangle$ [cf. Fig. 2(a)]. As a result, the second root of the L-MRCCSD effective Hamiltonian begins to approximate the third $A(D_2)$ singlet rather than the second $^1A(D_2)$ state [cf. Fig. 8(a)]. A similar analysis can be carried out for the remaining cases. Notice again the usefulness of Figs. 2–4 in this regard.

As pointed out in paper I, the off-diagonal matrix elements of $H^{\rm eff}$ and the non-Hermiticity of the effective Hamiltonian, as measured by the difference $H_{12}^{\rm eff} - H_{21}^{\rm eff}$, assume large values in the vicinity of L-MRCCSD singularities. It may thus happen that the discriminant of the secular equation (12),

$$\Delta = \left(H_{22}^{\rm eff} - H_{11}^{\rm eff}\right)^2 + 4H_{12}^{\rm eff}H_{21}^{\rm eff}, \tag{70}$$

becomes negative, so that the L-MRCCSD formalism fails to provide real energies for $\alpha \in \Omega_\alpha = (\alpha_1, \alpha_2)$ near the singularity. For the models studied in this paper, this type of breakdown of the L-MRCCSD theory occurs several times. We observe such a behavior for both P4 and V4 geometries and for the T4 models with $R = 1.1428, \sqrt{2}, 2.0$, and 3.0 a.u. In the case of the T4 models, the regions Ω_α are usually very narrow. For example, for the T4 model with $R = 1.1428$ a.u., complex L-MRCCSD energies are obtained only for $0.3567 < \alpha < 0.3573$ and $0.4967 < \alpha < 0.4970$. The corresponding regions Ω_α are so narrow that they must be displayed separately in Figs. 11(a) and 11(b). These regions could be easily overlooked if the dependence on the angular parameter α were not carefully examined. In the case of the T4 model with $R = \sqrt{2}$ a.u., there is only one L-MRCCSD singularity and, correspondingly, only one region $\Omega_\alpha = (0.4408, 0.4414)$, which is shown in Fig. 11(c). Similarly, there is only one narrow region Ω_α for the T4 model with $R = 2.0$ a.u. In this case, the L-MRCCSD method produces complex energies when $0.4574 < \alpha < 0.4589$ [see Fig. 11(d)]. For the T4 model with $R = 3.0$ a.u., and for the P4 and V4 models, the situation is slightly different. In this case, regions of nonexistence of real L-MRCCSD energies become considerably larger. For example, for the T4 model with $R = 3.0$ a.u., the L-MRCCSD method fails to provide real energies for $\alpha \in (0.3237, 0.3326)$ [see Fig. 8(d)]. For the P4 model, there are two regions Ω_α. In this case, the L-MRCCSD energies become complex for 3.41 a.u. $< \alpha <$ 3.43 a.u. and 6.54 a.u. $< \alpha <$ 6.70 a.u. (cf. paper I and Fig. 9). For the V4 model (see Fig. 10), there are three such regions, namely, (5.64 a.u.,5.93 a.u.), (7.21 a.u.,7.32 a.u.), and (7.55 a.u.,7.63 a.u.). We thus see that the size of the interval Ω_α increases with R. Notice that at the terminal points of every interval

Ω_α, i.e., at $\alpha = \alpha_1$ and $\alpha = \alpha_2$, the L-MRCCSD energies $E_1^{\text{L-MRCCSD}}$ and $E_2^{\text{L-MRCCSD}}$ are identical [cf. Figs. 8(d) and 9–11]. This becomes clear when we realize that $\Delta < 0$ for $\alpha_1 < \alpha < \alpha_2$ and $\Delta > 0$ for $\alpha < \alpha_1$ and $\alpha > \alpha_2$, so that for $\alpha = \alpha_1$ and $\alpha = \alpha_2$ we must have $\Delta = 0$ and

$$E_1^{\text{L-MRCCSD}} = E_2^{\text{L-MRCCSD}} = \tfrac{1}{2}\left(H_{11}^{\text{eff}} + H_{22}^{\text{eff}}\right) . \quad (71)$$

As a final remark, we should recall that the above type of breakdown of the L-MRCCSD approximation (namely, the existence of regions Ω_α, where L-MRCCSD energies are complex) distinguishes the MR L-CC theories from the SR ones, which may become singular, but can never yield complex energies (cf. paper I).

B. Nonlinear MRCCSD results

Just as in the SR case [15,19], singular behavior of the linear approximation can be eliminated by a proper ac-

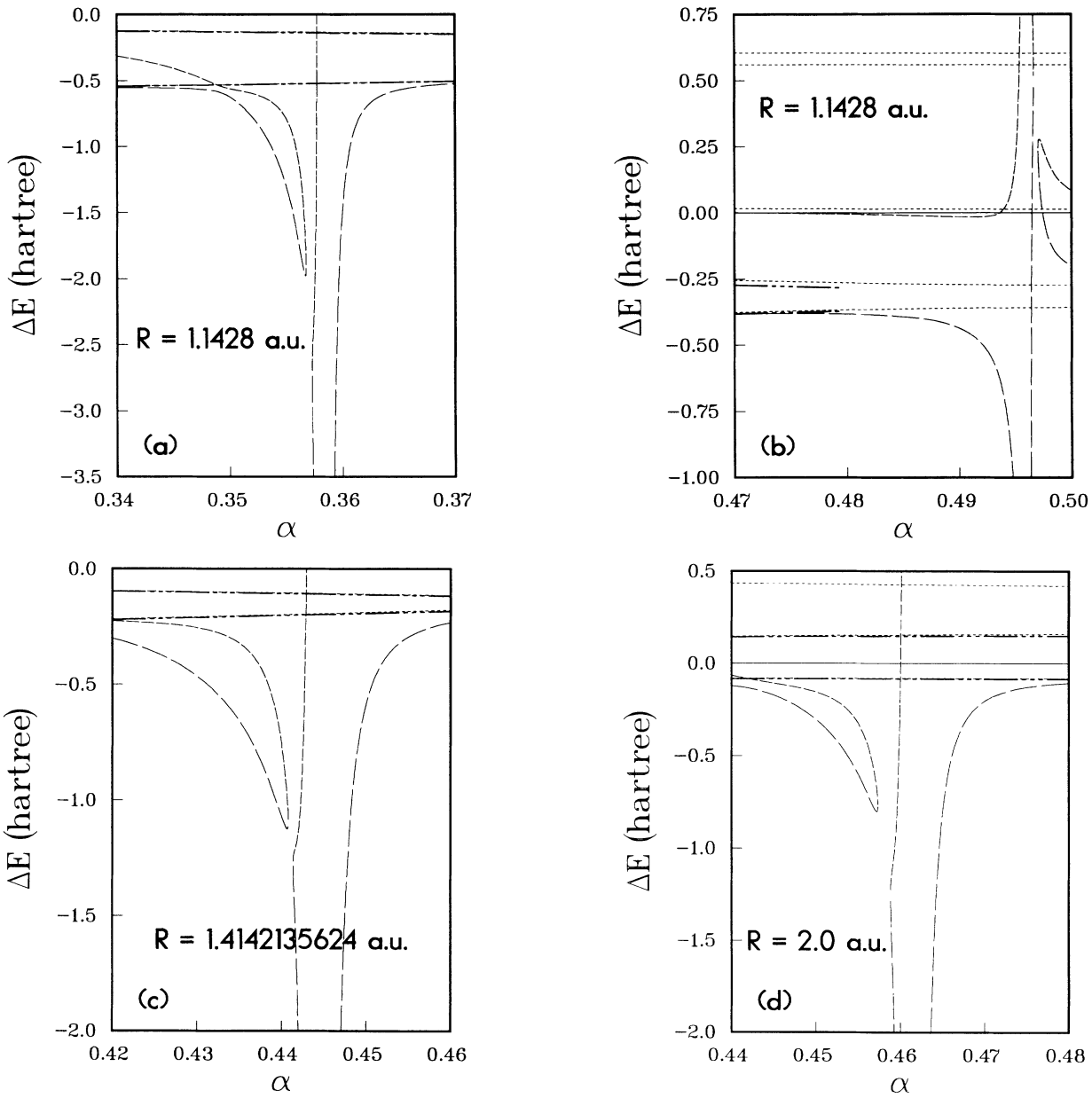

FIG. 11. A comparison of the FCI and MRCCSD energies ΔE (in hartrees) relative to the energy of the configuration $|\Phi_1\rangle$ for the low energy singlet states of $A(D_2)$ symmetry for the MBS T4 models with $a = 2.0$ a.u. and $R = 1.1428$ a.u. [(a) and (b)], $\sqrt{2}$ a.u. (c), and 2.0 a.u. (d) in the vicinity of the regions $\Omega_\alpha = (\alpha_1, \alpha_2)$, where the L-MRCCSD formalism fails to yield real energies. For $R = 1.1428$ a.u. [(a) and (b)], the L-MRCCSD method gives complex energies for $\alpha \in (0.3567, 0.3573)$ and $\alpha \in (0.4967, 0.4970)$. For $R = \sqrt{2}$ a.u. (c), complex L-MRCCSD energies are obtained for $\alpha \in (0.4408, 0.4414)$, whereas for $R = 2.0$ a.u., $\Omega_\alpha = (0.4574, 0.4589)$. Notice that at the terminal points of every interval Ω_α, i.e., at $\alpha = \alpha_1$ and $\alpha = \alpha_2$, the L-MRCCSD energies $E_1^{\text{L-MRCCSD}}$ and $E_2^{\text{L-MRCCSD}}$ are identical.

count of nonlinear terms. This is illustrated graphically in Figs. 8–10 and in greater detail in Tables VI–IX, where three different nonlinear approximations, designated as MRCCSD-n, n = 1,2,3 (see Sec. II), are compared with the FCI results. All MRCCSD solutions were obtained by an analytic continuation procedure described in Sec. III F. Even in the vicinity of the square geometry, where the L-MRCCSD method represents an excellent approxima-

TABLE VI. Comparison of the FCI and MRCCSD-n (n=1,2,3) energies, relative to the electronic energy of the configuration $|\Phi_1\rangle$, $\Delta E = E - H_{11}$ (in mhartrees), for the two lowest singlet states of $A(D_2)$ symmetry of the MBS T4 model with a = 2.0 a.u. and R = 1.1428; $\sqrt{2}$ and 2.0 a.u. RHF MO's associated with the configuration $|\Phi_1\rangle$ are employed throughout. For R = 1.1428 a.u. and α = 0, active orbitals ϕ_2 and ϕ_3 are degenerate. For α = 0.5, ϕ_3 and ϕ_4 are degenerate for all intermolecular distances R employed. NC(↓) designates no convergence when continued towards the α = 0.5 limit. For the T4 model with R = 1.1428 a.u., the critical α values for the MRCCSD-1 and MRCCSD-2,3 solutions are 0.4824 and 0.4794, respectively.

			FCI		MRCCSD-1		MRCCSD-2,3	
	α	H_{11}	ΔE_1	ΔE_2	ΔE_1	ΔE_2	ΔE_1	ΔE_2
R = 1.1428 a.u.	0.000	-4701.263	-791.128	-67.990	-791.152	-67.794	-791.113	-67.790
	0.100	-4684.804	-766.579	-70.081	-766.621	-69.904	-766.567	-69.899
	0.200	-4646.461	-696.389	-78.132	-696.527	-78.155	-696.407	-78.148
	0.250	-4625.603	-647.208	-86.483	-647.470	-86.883	-647.281	-86.880
	0.300	-4606.528	-590.903	-101.072	-591.437	-102.458	-591.130	-102.471
	0.350	-4590.653	-529.266	-127.897	-530.453	-131.805	-529.946	-131.842
	0.400	-4578.857	-464.208	-173.392	-466.916	-182.092	-466.171	-182.084
	0.450	-4571.629	-399.328	-232.471	-404.421	-247.349	-403.774	-247.087
	0.500	-4569.198	-358.014	-273.111	NC(↓)	NC(↓)	NC(↓)	NC(↓)
$R = \sqrt{2}$ a.u.	0.000	-4683.700	-507.653	-62.335	-507.675	-62.205	-507.626	-62.197
	0.100	-4674.077	-487.032	-62.862	-487.073	-62.760	-487.011	-62.750
	0.200	-4650.493	-428.825	-65.039	-428.954	-65.054	-428.849	-65.040
	0.250	-4636.978	-388.386	-67.286	-388.622	-67.429	-388.477	-67.414
	0.300	-4624.199	-342.290	-70.977	-342.736	-71.338	-342.537	-71.326
	0.350	-4613.257	-292.179	-77.319	-293.070	-78.057	-292.800	-78.064
	0.400	-4604.946	-240.082	-88.810	-242.031	-90.237	-241.688	-90.290
	0.450	-4599.774	-188.993	-109.706	-193.707	-112.327	-193.366	-112.441
	0.500	-4598.021	-143.668	-143.668	-155.710	-147.524	-155.639	-147.564
R = 2.0 a.u.	0.000	-4565.348	-117.621	-7.268	-117.686	-7.263	-117.575	-7.266
	0.100	-4561.751	-111.672	0.495	-111.797	0.499	-111.672	0.495
	0.200	-4552.580	-98.907	26.518	-99.249	26.500	-99.082	26.499
	0.250	-4547.083	-92.911	47.392	-93.443	47.312	-93.240	47.311
	0.300	-4541.710	-88.109	72.839	-88.909	72.582	-88.652	72.575
	0.350	-4536.965	-84.601	101.112	-85.793	100.381	-85.453	100.353
	0.400	-4533.267	-82.262	129.069	-84.081	127.069	-83.602	126.993
	0.450	-4530.923	-80.934	151.292	-83.857	145.920	-83.138	145.783
	0.500	-4530.120	-80.504	160.158	-85.444	147.143	-84.307	147.050

tion, this procedure required fewer iterations than when starting from the L-MRCCSD solution. We thus used the L-MRCCSD solution as an initial guess only for one of the geometries near the square conformation. The resulting solution of nonlinear MRCCSD equations was then continued towards the $\alpha = 0$ and $\alpha \to \infty$ limits of the P4 model, then towards the $\alpha = 0.5$ limit of the T4 model with fixed intermolecular separation R, and, finally, towards the $\alpha = 0$ and $\alpha \to \infty$ limits of the V4 model. Convergence of the Newton-Raphson scheme was usually very fast. Exceptions were the vicinity of the $\alpha = 0.5$ limit of every T4 model and T4 models with larger intermolecular separations R (designated as α in P4 and V4 models). Serious convergence problems began to appear for $R < \sqrt{2}$ and $\alpha \sim 0.5$ (cf. the later part of this

TABLE VII. Same as Table VI for $R = 3.0$, 4.0, and 7.0 a.u.

			FCI		MRCCSD-1		MRCCSD-2,3	
	α	H_{11}	ΔE_1	ΔE_2	ΔE_1	ΔE_2	ΔE_1	ΔE_2
$R = 3.0$ a.u.	0.000	-4306.127	-63.061	327.960	-64.154	324.820	-63.600	324.720
	0.100	-4305.146	-62.919	333.039	-64.128	329.364	-63.521	329.252
	0.200	-4302.597	-62.552	346.901	-64.157	341.243	-63.369	341.090
	0.250	-4301.034	-62.329	355.941	-64.288	348.374	-63.336	348.186
	0.300	-4299.481	-62.109	365.410	-64.575	354.965	-63.387	354.732
	0.350	-4298.088	-61.912	374.382	-65.098	359.734	-63.573	359.443
	0.400	-4296.987	-61.757	381.838	-65.948	361.343	-63.954	360.989
	0.450	-4296.283	-61.659	386.804	-67.214	358.736	-64.587	358.313
	0.500	-4296.041	-61.625	388.551	-68.958	351.530	-65.517	351.035
$R = 4.0$ a.u.	0.000	-4083.972	-57.269	441.613	-62.072	410.376	-59.529	409.908
	0.100	-4083.631	-57.216	442.639	-62.223	410.160	-59.570	409.670
	0.200	-4082.741	-57.077	445.331	-62.714	409.137	-59.718	408.579
	0.250	-4082.192	-56.992	446.999	-63.114	408.049	-59.852	407.437
	0.300	-4081.645	-56.907	448.669	-63.636	406.411	-60.041	405.729
	0.350	-4081.153	-56.831	450.178	-64.290	404.122	-60.294	403.354
	0.400	-4080.763	-56.770	451.377	-65.084	401.124	-60.618	400.252
	0.450	-4080.513	-56.732	452.148	-66.020	397.416	-61.017	396.420
	0.500	-4080.427	-56.718	452.414	-67.089	393.057	-61.492	391.919
$R = 7.0$ a.u.	0.000	-3711.257	-54.701	469.618	-67.143	395.450	-59.856	393.807
	0.100	-3711.230	-54.697	469.620	-67.184	395.305	-59.872	393.653
	0.200	-3711.157	-54.689	469.626	-67.304	394.885	-59.919	393.208
	0.250	-3711.111	-54.683	469.629	-67.392	394.584	-59.954	392.890
	0.300	-3711.066	-54.678	469.632	-67.495	394.233	-59.996	392.517
	0.350	-3711.026	-54.673	469.635	-67.613	393.840	-60.045	392.099
	0.400	-3710.993	-54.669	469.637	-67.742	393.414	-60.099	391.647
	0.450	-3710.973	-54.667	469.639	-67.881	392.967	-60.158	391.172
	0.500	-3710.966	-54.666	469.639	-68.026	392.509	-60.221	390.684

section).

Our calculations imply that the inclusion of direct $(T_2^{(p)})^2$ terms already provides a nonsingular formalism yielding reasonably good results. It is, however, the MRCCSD-2,3 formalism that renders the best description of the ground state. For small values of R, the difference between the MRCCSD-1 and MRCCSD-2,3 approximations is very small. Thus, for $R \leq 2.0$ a.u., the differences between the MRCCSD-1 and MRCCSD-2,3 energies do not exceed 1 mhartree (cf. Table VI). For large values of R, however, the nonlinear coupling term $B_{22}^{(p)}(G_i^\dagger)$ plays a substantial role. Differences between the MRCCSD-1 and MRCCSD-2,3 results for the ground-state energy of the T4 model with $R = 4.0$ a.u. range from 2.5 mhartree for $\alpha = 0$ to almost 5.6 mhartree for $\alpha = 0.5$. For $R = 7.0$ a.u., the difference between the MRCCSD-1 and MRCCSD-2,3 ground-state energies equals about 8 mhartree, independently of the α value (cf. Tables VII; see also Tables VIII and IX).

A different situation arises when considering the first excited singlet state $|\Psi_2\rangle$. For 1.1428 a.u. $\leq R \leq 2.0$ a.u., the difference between MRCCSD-1 and MRCCSD-2,3 results is usually smaller than 0.1 mhartree, and even for the T4 model with $R = 7.0$ a.u. it does not exceed 2 mhartree. In the latter case, however, none of the MRCCSD-n approximations provides good results. For $R = 4.0$ a.u., the difference between the MRCCSD-n and FCI results for the energy of $|\Psi_2\rangle$ ranges from

TABLE VIII. Same as Tables VI and VII for the MBS P4 model with $a = 2.0$ a.u. In this case, the $A(D_2)$ singlet states become $A_g(D_{2h})$ singlets. For $\alpha = 1.1428$ a.u., active orbitals ϕ_2 and ϕ_3 become degenerate.

		FCI		MRCCSD-1		MRCCSD-2,3	
α	H_{11}	ΔE_1	ΔE_2	ΔE_1	ΔE_2	ΔE_1	ΔE_2
1.1428	-4701.263	-791.128	-67.990	-791.152	-67.794	-791.113	-67.790
1.145	-4701.293	-788.553	-67.953	-788.577	-67.757	-788.538	-67.753
1.15	-4701.347	-782.719	-67.867	-782.742	-67.673	-782.704	-67.668
1.20	-4700.974	-725.733	-66.978	-725.756	-66.795	-725.716	-66.790
1.30	-4695.734	-618.873	-65.001	-618.896	-64.842	-618.852	-64.836
1.40	-4685.498	-520.896	-62.696	-520.918	-62.563	-520.870	-62.555
1.60	-4654.017	-349.331	-56.397	-349.349	-56.318	-349.290	-56.307
1.80	-4612.684	-210.047	-44.008	-210.065	-43.982	-209.988	-43.974
1.90	-4589.587	-155.978	-30.868	-156.010	-30.859	-155.917	-30.857
1.95	-4577.592	-134.584	-20.648	-134.629	-20.643	-134.527	-20.644
1.98	-4570.273	-123.867	-13.009	-123.924	-13.004	-123.816	-13.007
1.99	-4567.815	-120.655	-10.202	-120.716	-10.197	-120.606	-10.201
2.00	-4565.348	-117.621	-7.268	-117.686	-7.263	-117.575	-7.266
2.01	-4562.872	-114.760	-4.209	-114.830	-4.203	-114.717	-4.207
2.02	-4560.388	-112.069	-1.030	-112.143	-1.024	-112.029	-1.028
2.05	-4552.889	-104.949	9.171	-105.038	9.178	-104.920	9.174
2.10	-4540.247	-95.815	27.951	-95.930	27.959	-95.806	27.956
2.20	-4514.525	-84.443	68.960	-84.613	68.959	-84.475	68.958
2.50	-4435.563	-70.873	187.247	-71.256	187.012	-71.039	187.000
3.00	-4306.127	-63.061	327.960	-64.154	324.820	-63.600	324.720
4.00	-4083.972	-57.269	441.613	-62.072	410.376	-59.529	409.908
5.00	-3919.365	-55.391	464.667	-64.236	407.406	-59.283	406.416
7.00	-3711.257	-54.701	469.618	-67.143	395.450	-59.856	393.807
10.00	-3547.071	-54.650	469.740	-67.914	391.961	-60.078	390.161

about 32 mhartree for $\alpha = 0$ to about 60 mhartree for $\alpha = 0.5$. For T4 models with $R \geq 7.0$ a.u., the difference between the MRCCSD-n and FCI energies of the first excited singlet is about 75–80 mhartree, independently of the value of the angular parameter α (see Table VII; cf. also Tables VIII and IX and Figs. 8–10). Larger discrepancies between the MRCCSD-n and FCI results for $\alpha \sim 0.5$ are observed already for $R = 2.0$ a.u. In this case, the MRCCSD-n error in the first excited state energy increases from a few microhartrees for $\alpha \sim 0$ to about 13 mhartree for $\alpha = 0.5$ (cf. Table VI). This indicates an increasing importance of configurations from $\mathcal{M}_0^{\perp}$ for $R \to \infty$ and $\alpha \to 0.5$. They are not necessarily dominant configurations, but, as already pointed out, their contribution to low-lying eigenstates of the Hamiltonian is substantial (cf. Secs. III C and IV A). This is especially the case for excited states. In the case of $|\Psi_2\rangle$, we observe a large and almost equal participation of all biexcitations ${}^{(1)}G^{\rho\rho}_{\alpha\alpha}(0)|\Phi_1\rangle$, and even larger contribution of ${}^{(1)}G^{34}_{12}(1)|\Phi_1\rangle$, while $|\Phi_1\rangle$ is almost totally absent (cf. the third paragraph in Sec. IV A). Clearly, the model space $\mathcal{M}_0$, Eq. (39), is not large enough to describe such a situation. Notice that an increasingly substantial role of $\mathcal{M}_0^{\perp}$ configurations correlates with the decreasing energy gap between the orbital energies of the active orbital ϕ_3 and the virtual orbital ϕ_4 (cf. Figs. 5–7).

Another indication of an increasing importance of configurations from $\mathcal{M}_0^{\perp}$ for large values of R and $\alpha \to 0.5$ is the increasing role of quadruply excited clusters $T_4^{(p)}$ that

TABLE IX. Same as Tables VI–VIII for the MBS V4 model with $a = 2.0$ a.u. In this case, the $A(D_2)$ FCI singlet states are either ${}^1A_1(D_{2d})$ or ${}^1B_1(D_{2d})$ states. We do not distinguish between the $A_1(D_{2d})$ and $B_1(D_{2d})$ FCI subproblems, since all MRCCSD-n formalisms break the D_{2d} symmetry of the V4 model. For all values of α, the active orbital ϕ_3 and the virtual orbital ϕ_4 are degenerate. NC(↑) designates no convergence when continued towards the $\alpha = 0$ limit. The critical α values for the MRCCSD-1 and MRCCSD-2,3 solutions are 1.2112 and 1.2226 a.u., respectively.

		FCI		MRCCSD-1		MRCCSD-2,3	
α	H_{11}	ΔE_1	ΔE_2	ΔE_1	ΔE_2	ΔE_1	ΔE_2
1.20	-4580.420	-307.736	-234.724	NC(↑)	NC(↑)	NC(↑)	NC(↑)
1.25	-4587.733	-266.173	-206.370	-271.038	-224.401	-271.063	-224.258
1.30	-4592.948	-226.692	-182.695	-231.991	-197.509	-232.016	-197.440
1.35	-4596.262	-189.167	-163.288	-195.107	-175.252	-195.128	-175.220
1.40	-4597.858	-153.488	-147.559	-162.187	-155.126	-162.151	-155.140
$\sqrt{2}$	-4598.021	-143.668	-143.668	-155.710	-147.524	-155.639	-147.564
1.45	-4597.900	-134.858	-119.554	-144.525	-125.021	-144.415	-125.067
1.50	-4596.535	-124.572	-87.274	-132.745	-93.522	-132.570	-93.567
1.60	-4590.117	-109.257	-27.347	-115.769	-34.752	-115.422	-34.801
1.70	-4579.546	-98.617	26.881	-104.267	18.288	-103.728	18.232
1.80	-4565.605	-90.890	75.917	-96.092	66.009	-95.356	65.944
1.90	-4548.946	-85.055	120.210	-90.050	108.831	-89.115	108.753
2.00	-4530.120	-80.504	160.158	-85.444	147.143	-84.307	147.050
2.10	-4509.589	-76.861	196.127	-81.848	181.303	-80.506	181.191
2.20	-4487.742	-73.883	228.452	-78.992	211.647	-77.439	211.511
2.30	-4464.910	-71.407	257.440	-76.694	238.488	-74.923	238.325
2.40	-4441.369	-69.320	283.377	-74.828	262.124	-72.833	261.928
2.50	-4417.355	-67.542	306.529	-73.305	282.838	-71.079	282.605
3.00	-4296.041	-61.625	388.551	-68.958	351.530	-65.517	351.035
3.50	-4181.836	-58.480	431.446	-67.459	381.805	-62.844	380.978
4.00	-4080.427	-56.718	452.414	-67.089	393.057	-61.492	391.919
5.00	-3917.979	-55.183	466.480	-67.349	396.043	-60.460	394.487
7.00	-3710.966	-54.666	469.639	-68.026	392.509	-60.221	390.684
10.00	-3547.019	-54.646	469.735	-68.120	391.303	-60.179	389.463

are neglected in the MRCCSD formalism (triply excited clusters $T_3^{(p)}$ are also neglected, but for the MBS T4 models they do not appear for symmetry reasons). To provide a better insight, we have carried out a detailed cluster analysis of the two energetically lowest FCI eigenstates of $^1A(D_2)$ symmetry, using our reference space $\mathcal{M}_0$ and the cluster ansatz of Eq. (15) (for details, see Sec. VII and the Appendix in paper I), obtaining exact values of the orthogonally spin-adapted cluster amplitudes defining the operators $T_i^{(p)}$, $i = 2,4, p = 1,2$ (recall that $T_1^{(p)} = 0$). Thanks to the small dimension of MBS configuration spaces, there are only two quadruply excited cluster amplitudes, namely, $\langle t_4^{(1)} \rangle \equiv \langle 3344|t_4^{(1)}|1122\rangle_{0,0,0,0,0}$ and $\langle t_4^{(2)} \rangle \equiv \langle 2244|t_4^{(2)}|1133\rangle_{0,0,0,0,0}$. They are associated with quadruple excitations ${}^{(1)}G^{3344}_{1122}(0,0,0,0,0)$ and ${}^{(2)}G^{2244}_{1133}(0,0,0,0,0)$, respectively (cf. Table IV). Their exact values for the MBS T4 model and several values of R and α are given in Table X. In the following we concentrate on the region $R \geq 2.0$ a.u. Let us first notice that the absolute values of both tetraexcited cluster coefficients increase with R and α. Exception is the short-range ($R < 2.0$ a.u.) region, which we shall discuss later on. An especially rapid increase (by a few orders of magnitude) is observed when we vary the intermolecular distance R for $\alpha \sim 0$, or when R is fixed and equal to 2.0–3.0 a.u. while α changes from 0 to 0.5. Much smaller changes are found when we vary R for $\alpha \sim 0.5$, but we must keep in mind that in this region the tetraexcited coefficients $\langle t_4^{(1)} \rangle$ and $\langle t_4^{(2)} \rangle$ approach their maximum values, independently of the intermolecular separation R (cf. Table X). While the amplitude $\langle t_4^{(1)} \rangle$ remains small for $R \geq 2.0$ a.u., the amplitude $\langle t_4^{(2)} \rangle$ assumes large values when $R \to \infty$. Consider, as an example, the T4 model with $R = 7.0$ a.u. In this case, the absolute value of $\langle t_4^{(2)} \rangle$ equals to about 0.63–0.65, whereas the total weight of pair clusters in the many-body expansion of $T^{(2)}$, defined as (cf. Table V) $(\sum_{I=6}^{10} t_I^2)^{\frac{1}{2}}$, is only three times larger and equals 1.77–1.80. Large values of $\langle t_4^{(2)} \rangle$ are also observed for the T4 models with $R \sim 2.0$–3.0 a.u. and $\alpha \approx 0.5$. For the T4 model with

TABLE X. Exact values of the orthogonally spin-adapted quadruply excited cluster amplitudes associated with reference states $|\Phi_1\rangle = |(\phi_1)^2(\phi_2)^2\rangle$ and $|\Phi_2\rangle = |(\phi_1)^2(\phi_3)^2\rangle$ for the MBS T4 model with the H–H internuclear distance $a = 2.0$ a.u. and different values of the intermolecular separation R and angular parameter α, as obtained by the cluster analysis of two energetically lowest FCI eigenstates of $^1A(D_2)$ symmetry. The quadruply excited cluster amplitudes $\langle t_4^{(1)} \rangle \equiv \langle 3344|t_4^{(1)}|1122\rangle_{0,0,0,0,0} = \langle {}^{(1)}G^{3344}_{1122}(0,0,0,0,0)\Phi_1|T_4^{(1)}|\Phi_1\rangle$ and $\langle t_4^{(2)} \rangle \equiv \langle 2244|t_4^{(2)}|1133\rangle_{0,0,0,0,0} = \langle {}^{(2)}G^{2244}_{1133}(0,0,0,0,0)\Phi_2|T_4^{(2)}|\Phi_2\rangle$ are designated as t_{11} and t_{12}, respectively [for definition of quadruple excitations ${}^{(1)}G^{3344}_{1122}(0,0,0,0,0)$ and ${}^{(2)}G^{2244}_{1133}(0,0,0,0,0)$, see Table IV]. Triexcited clusters are not listed, since they vanish due to symmetry (see the text for details).

α	t_{11}	t_{12}	t_{11}	t_{12}	t_{11}	t_{12}
	$R = 1.1428$ a.u.		$R = \sqrt{2}$ a.u.		$R = 2.0$ a.u.	
0.0	0.003112	0.000146	0.002376	0.000276	0.000398	0.000398
0.1	0.002774	0.000031	0.001946	0.000134	-0.000027	0.000016
0.2	-0.000268	-0.000447	-0.000091	-0.000467	-0.001442	-0.001590
0.3	-0.015910	-0.002104	-0.006107	-0.002403	-0.004239	-0.006694
0.4	-0.091250	-0.010467	-0.023136	-0.010741	-0.009392	-0.025984
0.5	-0.237800	-0.049799	-0.065858	-0.065858	-0.019794	-0.119471
	$R = 3.0$ a.u.		$R = 4.0$ a.u.		$R = 7.0$ a.u.	
0.0	-0.004544	-0.027128	-0.011740	-0.212660	-0.020794	-0.625927
0.1	-0.004954	-0.031111	-0.012088	-0.221581	-0.020846	-0.626956
0.2	-0.006227	-0.045274	-0.013121	-0.248853	-0.020997	-0.629933
0.3	-0.008497	-0.077589	-0.014795	-0.295587	-0.021231	-0.634550
0.4	-0.011994	-0.145298	-0.017016	-0.362315	-0.021525	-0.640338
0.5	-0.016890	-0.274609	-0.019628	-0.447324	-0.021850	-0.646729

$R = 3.0$ a.u., the absolute value of $\langle t_4^{(2)} \rangle$ equals about 0.27, whereas $(\sum_{I=6}^{10} t_I^2)^{\frac{1}{2}}$ is only 1.32, so that the ratio $\langle t_4^{(2)} \rangle / (\sum_{I=6}^{10} t_I^2)^{\frac{1}{2}}$ equals 0.2. A similar ratio for the reference $|\Phi_1\rangle$, namely, $\langle t_4^{(1)} \rangle / (\sum_{I=1}^{5} t_I^2)^{\frac{1}{2}}$, is four times smaller. In view of these facts, it is not surprising that our two-reference CCSD formalism provides a poor description of the first excited state when $R \to \infty$ and $\alpha \to 0.5$. It is also not surprising that in this region, the description of the first excited state is much worse than the description of the ground state. To obtain a correct description of the first excited state, to which $|\Phi_1\rangle$ hardly contributes, we must either account for the $T_4^{(2)}$ cluster component or increase the dimension of $\mathcal{M}_0$. The connected cluster components $T_4^{(1)}$ are far less important here so that there is no need to include them to achieve a relatively good description of the ground-state wave function, even though increasingly poor description of the first excited state affects the MRCCSD results for the ground state. Despite the fact that the two-dimensional model space (39) seems to be well suited for both quasidegenerate and nondegenerate regimes (cf. Table II), for large values of R the error in the MRCCSD-2,3 results for the ground state reaches almost 6 mhartree (MRCCSD-1 method gives $\sim$ 13 mhartree error). This is another indication of an increasingly large role of the coupling terms. These terms couple the ground state with the first excited state, so that the poor description of the latter state must result in a poorer description of the ground state.

Clearly, when approaching the $R \to \infty$ limit, where the ground-state FCI wave function has a definitely nondegenerate character (cf. Table II), a preferred solution would be to switch to the well-known SRCCSD formalism (cf. Refs. [15] and [19]). To illustrate this, we have performed a series of SRCCSD calculations for T4 models with $R \geq 2.0$ a.u. The results are given in Table XI. They clearly reveal a well-known fact that SRCCSD formalism is well suited to describe nondegenerate situations. For $R = 2.0$ a.u. and $\alpha \sim 0.5$ and $R \geq 3.0$ a.u., the SRCCSD method gives invariably better description of the ground state compared to all MRCCSD methods investigated in this paper. For $R = 4.0$ a.u., the difference between SRCCSD and FCI results does not exceed ~ 10 μhartree and for $R = 7.0$ a.u. one can hardly distinguish between SRCCSD and FCI energies. The situation changes when we approach the highly degenerate region near the square geometry ($R \sim 2.0$ a.u., $\alpha < 0.3$). In this case, MRCCSD-2,3 method gives better results. The difference between ground-state energies obtained with the MRCCSD-2,3 and FCI approaches does not exceed 0.2 mhartree, compared to nearly 3 mhartree obtained with the SRCCSD method for $R = 2.0$ a.u. and $\alpha \sim 0$ (cf. Table XI). The SRCCSD method is clearly less reliable in this region. It is also more difficult to converge the SRCCSD solution. On the other hand, even for the

TABLE XI. Comparison of the MRCCSD-2,3 ground-state energies (in mhartrees), relative to the electronic energy of the configuration $|\Phi_1\rangle$ (represented by the matrix element H_{11}), with the exact (FCI) data and SRCCSD results employing $|\Phi_1\rangle$ as a reference for the MBS T4 models with $a = 2.0$ a.u. and $R = 2.0$, 3.0, 4.0, and 7.0 a.u. For $R \geq a$, $|\Phi_1\rangle$ represents the ground-state RHF solution, so that FCI, SRCCSD, and MRCCSD-2,3 results listed here are the ground-state correlation energies (see the text for details).

α	H_{11}	FCI	SRCCSD	MRCCSD-2,3	H_{11}	FCI	SRCCSD	MRCCSD-2,3
	$R = 2.0$ a.u.				$R = 3.0$ a.u.			
0.000	-4565.348	-117.621	-120.455	-117.575	-4306.127	-63.061	-63.034	-63.600
0.100	-4561.751	-111.672	-114.054	-111.672	-4305.146	-62.919	-62.895	-63.521
0.200	-4552.580	-98.907	-100.223	-99.082	-4302.597	-62.552	-62.535	-63.369
0.300	-4541.710	-88.109	-88.556	-88.652	-4299.481	-62.109	-62.100	-63.387
0.400	-4533.267	-82.262	-82.328	-83.602	-4296.987	-61.757	-61.756	-63.954
0.500	-4530.120	-80.504	-80.474	-84.307	-4296.041	-61.625	-61.626	-65.517
	$R = 4.0$ a.u.				$R = 7.0$ a.u.			
0.000	-4083.972	-57.269	-57.258	-59.529	-3711.257	-54.701	-54.701	-59.856
0.100	-4083.631	-57.216	-57.206	-59.570	-3711.230	-54.697	-54.697	-59.872
0.200	-4082.741	-57.077	-57.071	-59.718	-3711.157	-54.689	-54.689	-59.919
0.300	-4081.645	-56.907	-56.905	-60.041	-3711.066	-54.678	-54.678	-59.996
0.400	-4080.763	-56.770	-56.771	-60.618	-3710.993	-54.669	-54.670	-60.099
0.500	-4080.427	-56.718	-56.720	-61.492	-3710.966	-54.666	-54.666	-60.221

$R = 2.0$ a.u. model, the performance of the SRCCSD method improves with increasing α while the opposite is the case for the MRCCSD. Indeed, for $R = 2.0$ a.u. and $\alpha = 0.5$, the difference between the SRCCSD and FCI energies is only 30 μhartree, while the corresponding difference for the MRCCSD case is almost 4 mhartree. Thus it is very remarkable that the simple SR theory is capable of describing highly degenerate ground state so accurately. This must be related to the fact that two quasidegenerate model-space configurations $|\Phi_1\rangle$ and $|\Phi_2\rangle$ differ only by a double excitation and no other configurations play an essential role in the ground-state wave function for $R \geq 2.0$ a.u.

Although SRCCSD method yields highly accurate description of the ground state over the broad range of T4 geometries, it has a clear disadvantage compared to MRCCSD methods, namely, it does not provide us with any information about the excited states. The two-reference CCSD formalism gives us automatically such an information, even though results for the first excited state become rather poor when R becomes large. Perhaps a better solution would be to employ the three-reference model space $\tilde{\mathcal{M}}_0$, Eq. (49) (cf. the discussion in Secs. III C and III D and later in this section), which should provide us with a much better overall description of the first excited state, while yielding additional information about the second excited $A(D_2)$ singlet. An especially large improvement could be expected for the V4 model. The wave functions provided by our two-reference method violate the D_{2d} symmetry of this model, whereas the wave functions resulting from the three-reference theory can be adapted to this symmetry (cf. Sec. III D).

A poor description of the first excited state by the two-reference CCSD formalism, for large values of R, does not imply that the two-reference theory is completely useless in this region. It should be noted that our two-reference CCSD method yields a qualitatively correct shape of the potential energy surface for the first excited $^1A(D_2)$ state [see Figs. 9 and 10(a)]. For large intermolecular separations, the FCI and MRCCSD-n energies saturate and do not change with further increase in R, even though the MRCCSD-n results are off by about 80 mhartree due to the small dimension of the reference space employed.

As already mentioned, in the vicinity of the square geometry, where $|\Phi_1\rangle$ and $|\Phi_2\rangle$ are nearly degenerate, and for all T4 models with 1.1428 a.u. $\leq R \leq 2.0$ a.u. and $\alpha \leq 0.3$, where $|\Phi_1\rangle$ and $|\Phi_2\rangle$ are dominant configurations in the FCI expansions of $|\Psi_1\rangle$ and $|\Psi_2\rangle$, all MRCCSD-n methods provide very good results. In this region, the difference between the FCI and MRCCSD-n energies for both $|\Psi_1\rangle$ and $|\Psi_2\rangle$ does not exceed 1 mhartree and is often smaller than 0.1–0.2 mhartree. This excellent behavior of nonlinear MRCCSD-n formalisms is largely due to the fact that the configurations from $\mathcal{M}_0^{\perp}$ contribute little to both FCI states $|\Psi_1\rangle$ and $|\Psi_2\rangle$ (notice, however, an important role of $|\Phi_3\rangle$ for $\alpha \sim 0.3$) and due to a relatively large energy gap between the active orbital ϕ_3 and the virtual orbital ϕ_4 in this entire region. Consequently, the connected tetraexcited cluster components $T_4^{(1)}$ and $T_4^{(2)}$ are very small (see Table X). In this regard it would be desirable to examine other choices of molecular orbital bases (such as MCSCF orbitals, triplet orbitals, etc. [20]), as well as, of course, the effect of basis size [6,23]. This problem was already addressed in the context of the MR MBPT study of the P4 model, where it was shown that various shifting techniques of the orbital energy levels can accelerate the convergence of perturbation theory series and thus extend the range of applicability of MR theories [20].

In the quasidegenerate region ($R \sim 2.0$ a.u. and $\alpha \leq 0.3$), we get better results for the first excited state rather than for the ground state (see Table VI). The opposite is true in regions of nondegenerate ground state ($R \ll 2.0$ a.u. and $\alpha \sim 0$, $R \sim 2.0$ a.u. and $\alpha \sim 0.5$, $R \gg 2.0$ a.u.), independently of the character (degenerate or nondegenerate) of the first excited state (see Tables VI–IX and Figs. 8–10). Better results for the ground state are also obtained in strongly correlated cases characterized by a heavy mixing of orbital and configurational quasidegeneracies ($R \ll 2.0$ a.u. and $\alpha \sim 0.5$), provided that the MRCCSD-n results are available [cf. Tables VI and IX; see also Figs. 8(a), 8(b), and 10(b)].

In general, the nonlinear MRCCSD results are available as long as reference configurations significantly contribute to at least one of the FCI states $|\Psi_1\rangle$ or $|\Psi_2\rangle$. The results for T4 models with large R indicate that the weight of reference configurations in one of the two FCI states can be relatively small in order to obtain a convergent MRCCSD solution, although the rate of convergence of the Newton-Raphson scheme deteriorates and the MRCCSD results for one of the two states become rather poor. The situation changes when the weight of reference configurations in the FCI expansions of both $|\Psi_1\rangle$ and $|\Psi_2\rangle$ becomes too small. In this case the MRCCSD energies begin to deviate from the FCI results and the nonlinear MRCCSD method may even become singular. This is precisely what happens for the T4 models with $R \ll 2.0$ a.u. and $\alpha \approx 0.5$, or for the V4 model with $\alpha < \sqrt{2}$ a.u. In this region, configurations from $\mathcal{M}_0^{\perp}$ significantly contribute to both $|\Psi_1\rangle$ and $|\Psi_2\rangle$, and we observe an increasingly strong quasidegeneracy of the orbital ϕ_2 with orbitals ϕ_3 and ϕ_4 [cf. Tables II and III and Figs. 5(a) and 7]. Recall that for the V4 model with $\alpha = 0.7117$ a.u., orbitals ϕ_2, ϕ_3, and ϕ_4 become exactly degenerate (cf. Sec. III B and Fig. 7). It is thus inappropriate to use our $\mathcal{M}_0$ as a reference space in this region. This is why for the T4 model with $R = 1.1428$ a.u. we were unable to continue the MRCCSD-1 solution beyond $\alpha_c = 0.4824$ and the MRCCSD-2,3 solution beyond $\alpha_c = 0.4794$ [see Table VI and Fig. 8(a)]. The MRCCSD-1 and MRCCSD-2,3 solutions for the V4 model cannot be continued beyond the intermolecular distances $\alpha_c = 1.2112$ and 1.2226 a.u., respectively (cf. Table X and Fig. 10). In the vicinity of the above geometries, the MRCCSD-n energies begin to deviate from the FCI results, the rate of convergence of the Newton-Raphson procedure dramatically deteriorates, and the critical point where no convergent solution can be obtained is soon reached, even when we carefully "analytically continue" a given solution, allowing only very small changes in the geometry (such as 10^{-6} or smaller; see Sec. III F).

This behavior is very much reminiscent of that found in the strongly correlated limit of cyclic polyene models, where no real solution of SRCC (CCD, CCSD, CCSDT-1, or ACPTQ [60]) equations, which is continuous as a function of the resonance integral β from the weakly correlated side, can be found beyond a certain critical value β_c (see Refs. [56,57,60]). In this case we were able to prove that this critical value $\beta = \beta_c$ represents an algebraic branch point of the first order, so that the SRCC energy bifurcates into the two complex solutions that have no physical meaning. It seems that the critical geometries α_c of the V4 or T4 model with $R = 1.1428$, beyond which further continuation of the MRCCSD-n solutions is not possible, also represent algebraic branch points. The critical values α_c do not represent poles, since none of the cluster components $t_J(\alpha)$ tends to infinity as $\alpha \to \alpha_c$. Just as in the SR case [56,57,60], the Jacobian of MRCCSD-n system (69) vanishes for $\alpha = \alpha_c$. This invalidates the Newton-Raphson procedure and causes its failure in the immediate vicinity of α_c in the same way as in the SRCC approach to cyclic polyenes [56,57,60]. Recall that similar behavior of nonlinear MRCCSD-n formalisms was found for the S4 model. It was also found for other planar geometries when we examined multiple solutions of MRCCSD-n equations describing higher than the first-excited state (see paper I).

In order to avoid a singular behavior of the nonlinear MRCCSD formalism for T4 models with $R \ll 2.0$ a.u. and $\alpha \approx 0.5$, we must employ a larger model space. It is very likely that such a model space can be obtained by including the reference $|\Phi_3\rangle$ in $\mathcal{M}_0$. Alternatively, we must go beyond the CCSD approximation. The cluster analysis of the exact wave functions $|\Psi_1\rangle$ and $|\Psi_2\rangle$ [assuming the cluster *Ansatz* of Eq. (15)] for the T4 model with $R = 1.1428$ a.u. and different values of α indicates a rapid increase in the importance of $T_4^{(1)}$ and $T_4^{(2)}$ clusters with increasing α (by two orders of magnitude when α changes from 0 to 0.5; see Table X). These clusters remain negligible up to $\alpha \approx 0.2$. Then, a rapid increase sets in. For $\alpha = 0.5$, the ratio of the connected tetraexcited components $T_4^{(p)}$ to their disconnected counterparts $\frac{1}{2}(T_2^{(p)})^2$, $p = 1, 2$, defined as

$$k^{(p)} = |\langle t_4^{(p)}\rangle / \langle t_4^{(p)}\rangle_D| , \tag{72}$$

where

$$\langle t_4^{(1)}\rangle_D = \langle {}^{(1)}G^{3344}_{1122}(0,0,0,0,0,0)\Phi_1 | \tfrac{1}{2}(T_2^{(1)})^2 | \Phi_1\rangle \tag{73}$$

and

$$\langle t_4^{(2)}\rangle_D = \langle {}^{(2)}G^{2244}_{1133}(0,0,0,0,0,0)\Phi_2 | \tfrac{1}{2}(T_2^{(2)})^2 | \Phi_2\rangle \tag{74}$$

become as large as 0.470 516 for $p = 1$ and 0.339 409 for $p = 2$, in spite of the fact that the absolute value of $\langle t_4^{(2)}\rangle$ remains relatively small in this region. These values of $k^{(p)}$, $p = 1, 2$, should be compared to 0.097 028 and 0.019 285, respectively, obtained for $\alpha = 0$. This indicates that neither $T_4^{(1)}$ nor $T_4^{(2)}$ is negligible in comparison with coupled-pair cluster components $\frac{1}{2}(T_2^{(p)})^2$ when $R \ll 2.0$ a.u. and $\alpha \approx 0.5$. It is thus not surprising that in this region the two-reference CCSD formalism, employing model space (39), fails.

In the case of the V4 model, the ratio of connected tetraexcited components $T_4^{(p)}$ and their disconnected counterparts $\frac{1}{2}(T_2^{(p)})^2$ remains large for all values of α. In the nonsingular ($\alpha > 1.21$ a.u.) region, the coefficient $k^{(1)}$ varies between 0.25 and 0.44 (the maximum value of 0.44 is reached for $\alpha \approx 1.21$ a.u.), whereas the coefficient $k^{(2)}$ is never smaller than 0.34. FCI values of the quadruply excited cluster coefficients $\langle t_4^{(p)}\rangle$ become large as well. Except for $\alpha \approx \sqrt{2}$ a.u., one of the two coefficients $\langle t_4^{(p)}\rangle$ is always larger (in absolute value) than 0.1 (cf. Table X). Large values of connected tetraexcited components $T_4^{(p)}$ indicate that the two-dimensional model space $\mathcal{M}_0$, Eq. (39), is not rich enough to describe low-lying eigenstates of the V4 model. Similar conclusion can be drawn by looking at the FCI expansion coefficients for $|\Psi_1\rangle$ and $|\Psi_2\rangle$ (see Tables II and III; cf. also Sec. III C). For example, in the immediate vicinity of the MRCCSD-n singularities we observe a large and almost equal participation of reference configurations $|\Phi_1\rangle$ and $|\Phi_2\rangle$, and $\mathcal{M}_0^{\perp}$ configuration $|\Phi_3\rangle$, in the first excited state (for $\alpha = 1.20$ a.u., the corresponding FCI expansion coefficients equal 0.561, -0.556, and -0.556, respectively). Actually, the model space $\mathcal{M}_0$ is not even invariant with respect to the D_{2d} symmetry of the V4 model. In consequence, the two-reference CCSD formalism yields broken symmetry solutions. The resulting wave functions do not belong to any particular symmetry species of D_{2d}. As in the case of all T4 models, they classify as $A(D_2)$ singlets (cf. Sec. III C).

In view of the above discussion, we should expect rather poor performance of all MRCCSD-n methods for the V4 model. Remarkably enough, this is not the case. For a wide range of V4 geometries, results are quite reasonable (cf. Table IX and Fig. 10). The difference between the MRCCSD-2,3 and FCI results for the ground state is usually smaller than 5 mhartree (only in the vicinity of the T_d geometry it exceeds 10 mhartree), and all MRCCSD-n approaches provide us with a qualitatively correct shape of the potential energy surface for the first excited state. The broken-symmetry MRCCSD-n solutions destroy the exact twofold degeneracy of the FCI states $|\Psi_1^{\mathrm{FCI}}\rangle$ and $|\Psi_2^{\mathrm{FCI}}\rangle$ that occurs for $\alpha = \sqrt{2}$ a.u. (cf. Secs. III C–III E). Instead of the crossing of $E_1^{\mathrm{FCI}}(\alpha)$ and $E_2^{\mathrm{FCI}}(\alpha)$ at $\alpha = \sqrt{2}$ a.u., we observe the two roots of the MRCCSD-n effective Hamiltonian avoiding one another [see Fig. 10(b)]. It is interesting to observe how MRCCSD-n methods try to recover the correct shape of the FCI energy curves in the vicinity of $\alpha = \sqrt{2}$ a.u. geometry. In this region, the gap between the MRCCSD-n energy curves $E_1^{\text{MRCCSD-}n}(\alpha)$ and $E_2^{\text{MRCCSD-}n}(\alpha)$ reaches its minimum value of about 7 mhartree for $\alpha \approx 1.40$ a.u. As explained in Sec. III D, we would have to include the third reference configuration $|\Phi_3\rangle$ in the model space to achieve a correct description of the twofold degeneracy of the ground state for the tetrahedral V4 model. In general, the inclusion of $|\Phi_3\rangle$ in $\mathcal{M}_0$ should lead to a D_{2d} invariant MRCCSD formalism and to a substantial improvement of MRCCSD results (perhaps even to overcoming of the singular be-

havior at $\alpha \approx 1.2$ a.u.), even though other configurations $|\Phi_j\rangle$ may still be required to obtain a quantitatively good description of the first excited state in the $\alpha \to \infty$ limit. It is, however, remarkable that a much simpler two-reference CCSD formalism is capable of providing us with the most essential information about the low-lying eigenstates of the Hamiltonian, in spite of the fact that the two-reference theory breaks the symmetry of the Hamiltonian. This indicates that the Hilbert-space MRCC methods have a much larger potential than one might expect solely on the basis of cluster analysis of FCI results and symmetry considerations.

So far, we have compared the MRCCSD results with FCI data. Our results clearly indicate that Hilbert-space MRCCSD methods provide us with a very good description of the configurational quasidegeneracy (or nondynamic correlation) effects. Another indication of the potential of the state-universal CC formalism is its ability to describe dynamic correlation effects for multiconfigurational states. We must, of course, emphasize that the distinction between the dynamic and nondynamic correlation effects is based on intuitive concepts, which may not be very useful in quasidegenerate situations where one can hardly distinguish between them. For example, SRCCSD method yields, in principle, only dynamic correlation, since it assumes a nondegenerate reference. However, for the completely degenerate T4 model with $R = 2.0$ a.u. and $\alpha = 0$, it yields almost all the correlation energy, including dynamic as well as nondynamic effects (cf. the above discussion). Nonetheless, we can estimate the importance of dynamic vs nondynamic correlation effects by diagonalizing the effective Hamiltonian truncated at the first MR MBPT order [39],

$$
\begin{aligned}
{}^{(0+1)}H^{\text{eff}} \equiv PH^{(0)}P + PVU^{(0)} &= PH^{(0)}P + PVP \\
&= PHP,
\end{aligned}
\tag{75}
$$

in the model space (39), and by comparing the resulting roots $E_\mu^{(0+1)}$ with the exact (FCI) energies $E_\mu \equiv E_\mu^{\text{FCI}}$ ($\mu = 1, 2$). Notice that ${}^{(0+1)}H^{\text{eff}}$ is simply a 2×2 CI matrix $\|H_{pq}\|_{p,q=1,2} \equiv \|\langle\Phi_p|H|\Phi_q\rangle\|_{p,q=1,2}$. The energies $E_\mu^{(0+1)}$, $\mu = 1, 2$ (or, rather, their counterparts $\Delta E_\mu^{(0+1)}$ calculated relative to H_{11}), for T4 models with

TABLE XII. Matrix elements of the effective Hamiltonian truncated at the first order of the perturbation, ${}^{(0+1)}H^{\text{eff}} \equiv PHP$ and its roots $\Delta E_\mu^{(0+1)} = E_\mu^{(0+1)} - H_{11}$ ($\mu = 1, 2$) calculated relative to the energy of the configuration $|\Phi_1\rangle$ for the MBS T4 models with $\alpha = 2.0$ a.u. and $R = 1.1428$, $\sqrt{2}$, 2.0, 3.0, 4.0, and 7.0 a.u. Clearly, we have ${}^{(0+1)}H_{pq}^{\text{eff}} = H_{pq}$, $p, q = 1, 2$ (cf. Sec. V).

α	H_{11}	H_{22}	$H_{12} = H_{21}$	$\Delta E_1^{(0+1)}$	$\Delta E_2^{(0+1)}$	H_{11}	H_{22}	$H_{12} = H_{21}$	$\Delta E_1^{(0+1)}$	$\Delta E_2^{(0+1)}$
	$R = 1.1428$ a.u.					$R = \sqrt{2}$ a.u.				
0.000	-4701.263	-5461.676	51.289	-763.856	3.444	-4683.700	-5149.566	52.914	-471.801	5.935
0.100	-4684.804	-5419.584	53.187	-738.610	3.830	-4674.077	-5117.721	54.406	-450.219	6.575
0.200	-4646.461	-5306.913	58.305	-665.559	5.108	-4650.493	-5030.263	58.584	-388.602	8.832
0.300	-4606.528	-5152.639	65.477	-553.852	7.741	-4624.199	-4905.225	64.783	-295.240	14.215
0.400	-4578.857	-4981.169	73.758	-415.408	13.096	-4604.946	-4758.872	72.371	-182.608	28.682
0.500	-4569.198	-4802.149	82.654	-259.298	26.347	-4598.021	-4598.021	80.949	-80.949	80.949
	$R = 2.0$ a.u.					$R = 3.0$ a.u.				
0.000	-4565.348	-4565.348	56.970	-56.970	56.970	-4306.127	-3833.710	63.894	-8.489	480.906
0.100	-4561.751	-4545.979	58.051	-50.698	66.471	-4305.146	-3823.545	64.637	-8.524	490.125
0.200	-4552.580	-4490.814	61.186	-37.655	99.421	-4302.597	-3793.960	66.811	-8.629	517.267
0.300	-4541.710	-4406.846	66.104	-26.997	161.861	-4299.481	-3747.354	70.270	-8.803	560.930
0.400	-4533.267	-4301.151	72.488	-20.778	252.894	-4296.987	-3686.911	74.789	-9.034	619.111
0.500	-4530.120	-4177.664	80.052	-17.330	369.786	-4296.041	-3616.082	80.075	-9.303	689.262
	$R = 4.0$ a.u.					$R = 7.0$ a.u.				
0.000	-4083.972	-3357.672	68.857	-6.470	732.770	-3711.257	-2715.242	73.604	-5.410	1001.425
0.100	-4083.631	-3352.089	69.360	-6.518	738.060	-3711.230	-2714.575	73.721	-5.424	1002.078
0.200	-4082.741	-3335.842	70.824	-6.657	753.556	-3711.157	-2712.652	74.061	-5.463	1003.968
0.300	-4081.645	-3310.343	73.129	-6.872	778.175	-3711.066	-2709.699	74.588	-5.525	1006.892
0.400	-4080.763	-3277.713	76.082	-7.144	810.195	-3710.993	-2706.049	75.252	-5.604	1010.549
0.500	-4080.427	-3240.586	79.429	-7.446	847.287	-3710.966	-2702.088	75.987	-5.691	1014.568

$R = 1.1428$, $\sqrt{2}$, 2.0, 3.0, 4.0, and 7.0 a.u. are given in Table XII.

It is seen that for $R < 2.0$ a.u. and $\alpha < 0.3$, the correlation effects have mostly nondynamic character. Indeed, in this region the difference between $E_1^{(0+1)}$ and FCI ground-state energy does not exceed 40 mhartree, whereas the corresponding difference between $E_2^{(0+1)}$ and the energy of the first excited state is smaller than 75 mhartree. As a result, for $R < 2.0$ a.u. and $\alpha < 0.3$, the MRCCSD-2,3 method yields very accurate results for both states considered (with the accuracy of less than ~ 0.1 mhartree for $|\Psi_1\rangle$ and less than ~ 0.4 mhartree for $|\Psi_2\rangle$). This corresponds to our earlier observation that in this region either $|\Phi_1\rangle$ or $|\Phi_2\rangle$ dominate in the FCI expansion of the lowest two $A(D_2)$ singlets. For large values of R and $\alpha \sim 0.5$, the situation is entirely different. In this region, the MR dynamic correlation effects, as measured by the difference $E_\mu^{\mathrm{FCI}} - E_\mu^{(0+1)}$ ($\mu = 1, 2$), represent a dominant contribution to the correlation energy of the first ($\mu = 2$) excited state. For example, for $R = 7.0$ a.u., the difference between $E_2^{(0+1)}$ and E_2^{FCI} becomes as large as ~ 550 mhartree, which is a clear indication of the large role of $\mathcal{M}_0^\perp$ configurations, or, equivalently, $T_4^{(2)}$ cluster components, in describing the first excited $A(D_2)$ singlet. The presence of extremely large dynamic correlation effects for the first excited state affects the performance of the MRCCSD formalism and leads to 75–80 mhartree error in the resulting energy. On the other hand, it is quite remarkable that simple two-reference CCSD theory is capable of reducing the ~ 550 mhartree error obtained by diagonalizing ${}^{(0+1)}H^{\mathrm{eff}}$ to about 75–80 mhartree and, in this way, of recovering a large portion of dynamic correlation effects for the first excited state, despite the fact that the model space $\mathcal{M}_0$, Eq. (39), is not large enough to reasonably approximate $|\Psi_2\rangle$ and despite the fact that the CCSD approximation is not accurate enough to account for important high-order cluster components.

In this regard, it is also instructive to compare the separation (or excitation) energy between the two singlet states considered as given by the zero and first order energies, i.e., by $\Delta H \equiv |H_{22} - H_{11}|$ and $\Delta E^{(0+1)} = E_2^{(0+1)} - E_1^{(0+1)}$, and by the MRCCSD-2,3 and FCI methods, i.e., $\Delta E^{\mathrm{MRCCSD}} \equiv E_2^{\mathrm{MRCCSD\text{-}2,3}} - E_1^{\mathrm{MRCCSD\text{-}2,3}} = \Delta E_2^{\mathrm{MRCCSD\text{-}2,3}} - \Delta E_1^{\mathrm{MRCCSD\text{-}2,3}}$ and $\Delta E^{\mathrm{FCI}} = E_2^{\mathrm{FCI}} - E_1^{\mathrm{FCI}} = \Delta E_2^{\mathrm{FCI}} - \Delta E_1^{\mathrm{FCI}}$. For very short internuclear separations ($R < 2$ a.u.), the rough estimates provided by ΔH and $\Delta E^{(0+1)}$ are quite reasonable. The differences between ΔH and corresponding FCI separation energies for $R = 1.1428$ a.u. range between 40 and 150 mhartree, and for $\Delta E^{(0+1)}$ between 45 and 200 mhartree; for $R = \sqrt{2}$ a.u., these differences range between, respectively, 0 and 20 mhartree and 30 and 162 mhartree. Corresponding differences for the MRCCSD-2,3 excitation energies range between 0.2 and 7 mhartree for $R = 1.1428$ a.u. (although no solution can be found for $\alpha = 0.5$) and between 0.1 and 8 mhartree for $R = \sqrt{2}$ a.u. For $R = 2$ a.u. and $\alpha = 0$, we have that $\Delta H = 0$, $\Delta E^{(0+1)} = 113.94$, and $\Delta E^{\mathrm{MRCCSD}} = 110.309$ mhartree, while $\Delta E^{\mathrm{FCI}} = 110.353$ mhartree. Thus the first-order result gives a very good separation energy in this case. Note, however, that in a seemingly analogous case when $H_{11} = H_{22}$, which arises when $R = \sqrt{2}$ a.u. and $\alpha = 0.5$, we get $\Delta H = 0$, $\Delta E^{(0+1)} = 161.898$, $\Delta E^{\mathrm{MRCCSD}} = 8.075$, and $\Delta E^{\mathrm{FCI}} = 0$ (all in millihartrees). For $R = 2$ a.u., the first-order description also rapidly deteriorates as α increases, so that for $R = 2.0$ a.u. and $\alpha = 0.5$ we have already that (all in millihartrees) $\Delta H = 352.456$, $\Delta E^{(0+1)} = 387.116$, $\Delta E^{\mathrm{MRCCSD}} = 231.357$, and $\Delta E^{\mathrm{FCI}} = 240.662$. The same holds when R increases, as may be expected on the basis of the excited state behavior described above. Thus, for $R = 7.0$ a.u. and $\alpha \in [0, 0.5]$, we have that (all in millihartrees) $\Delta H \approx 1000$, $\Delta E^{(0+1)} \approx 1013$, $\Delta E^{\mathrm{MRCCSD}} \approx 452$, and $\Delta E^{\mathrm{FCI}} \approx 524$.

V. SUMMARY

In this paper we applied several different variants of the Hilbert-space MRCCSD formalism to a simple MBS four-electron model system consisting of two interacting hydrogen molecules in various geometrical arrangements. We examined nonplanar geometries, generally referred to as T4 models, and their special cases designated as P4 and V4 models. They correspond to different cross sections of the H_4 potential-energy hypersurface, involving the dissociation or simultaneous stretching of two H—H bonds. They comprise various quasidegeneracy types, including orbital and configurational degeneracies, a twofold degeneracy of the ground electronic state and interesting cases of symmetry breaking at both HF and CC levels. Since all MO's employed belong to different symmetry species of the spatial symmetry, common to all T4 models, we were able to exploit our orthogonally spin-adapted formulation of the Hilbert-space MRCC theory, which requires different spatial symmetry of active orbitals [2,5,9].

One of the aims of the present study was to assess the importance of bilinear $(T_2^{(p)})^2$ terms, in particular, the role of the $(T_2^{(p)})^2$ coupling term $B_{22}^{(p)}(G_i^\dagger)$, Eq. (25). Thus, in addition to the L-MRCCSD approximation, in which all nonlinear terms are neglected, we examined three nonlinear MRCCSD theories, which represent different approximations to the fully quadratic MRCCSD-3 approach.

The linear approximation was shown to be reliable as long as the two lowest eigenstates of the Hamiltonian contain a significant contribution from reference configurations. This includes quasidegenerate situations, characterized by a strong interaction of model states, as well as nondegenerate cases, where either the first or the second reference contribute significantly to both low energy eigenstates. There are, however, cases of a nondegenerate ground state, which require several configurations to describe the first excited state. They appear when we break two H—H bonds. In these situations, or in cases of heavy mixing of orbital and configurational degeneracies, the L-MRCCSD formalism suffers from singular behavior. These singularities appear whenever the

low-lying excited configurations become quasidegenerate with reference configurations. The simple diagnostics for the occurrence of L-MRCCSD singularities, based on the behavior of diagonal CI matrix elements and introduced in paper I, was shown to be extremely useful. As in the case of planar models, we found regions where the L-MRCCSD theory fails to yield real energies. These regions appear near the singularities. Their existence is related to a large non-Hermiticity of the L-MRCCSD effective Hamiltonian in the vicinity of each singularity.

Singular behavior of the linear approximation is circumvented by accounting for nonlinear terms. As in the case of planar geometries, it is sufficient to include $(T_2^{(p)})^2$ clusters in the direct term in order to obtain a nonsingular and highly accurate formalism. Inclusion of $(T_2^{(p)})^2$ clusters in the coupling term usually improves the results. In the case of the ground state, this improvement may be substantial. The first excited state is much less sensitive to the presence of bilinear coupling terms.

All nonlinear MRCCSD methods provide excellent results when the two lowest eigenstates of the Hamiltonian contain a significant contribution from reference configurations. However, contrary to the linear formalism, nonlinear two-reference CCSD approaches are capable of yielding a realistic description of both potential-energy surfaces even when the weight of reference configurations in one of the two FCI states is relatively small. When the model space is adequate for the ground state, but is not rich enough to approximate the first excited state, only results for the latter become poor. For our models, this happens in nondegenerate cases involving a dissociation or simultaneous stretching of two chemical bonds. Remarkably enough, even in these cases we obtain a valuable information about the approximate shape of the potential-energy surface for the first excited eigenstate of the Hamiltonian. Excellent description of the first excited state for the T4 model with $a = 2.0$ a.u., $R < \sqrt{2}$ a.u., and $\alpha \approx 0.3$ indicates that the two-reference CCSD formalism may give a highly accurate result even in the region where the role of configurations from $\mathcal{M}_0^+$ is substantial. The larger the gap between the active and virtual orbitals and the smaller the gap between different active orbitals, the better MRCCSD results can be expected. It would thus be instructive to examine different types of MO bases. This would correspond to the exploitation of various shifting techniques of one-electron levels in MR MBPT calculations, which can extend the range of applicability of the MR MBPT formalism for nondegenerate situations [20] (cf. paper I).

The situation changes when the weight of model state configurations in the FCI expansions of the lowest two eigenstates of the Hamiltonian becomes very small. In this case we usually deal with a heavy mixing of orbital and configurational degeneracies and a strong interaction between several configurations. We should thus increase the dimension of the model space to obtain reasonable results. Otherwise, the MRCCSD energies begin to deviate from the FCI results and it may even happen that the nonlinear MRCCSD method becomes singular. We can preserve a small dimension of the model space, but then we must go beyond the CCSD approximation. This was confirmed by performing a cluster analysis of FCI wave functions which shows a rapid increase in the importance of connected tetraexcited clusters in strongly correlated situations. Cluster analysis of FCI wave functions shows that the inclusion of connected quadruply excited clusters (particularly those associated with the second reference) should essentially improve the MRCC results in nondegenerate situations. In particular, we should obtain a much better description of the potential energy surface for the first excited state. Recall that similar behavior of the MRCCSD formalism was observed in paper I. It would thus be worthwhile to investigate the possibility of extending the approximate methods of accounting for connected quadruply excited clusters (such as the ACPQ [65], ACP-D45 [15,53,54], or ACCD [66]), or similar methods that proved to be useful in SR situations (e.g., ACP-D14 [61]), to the MR case [67]. We also hope to address the role of semi-internal tri- and tetraexcited configurations that are singly or doubly excited with respect to the other reference [2]. Another possibility is to employ the three-reference CCSD formalism exploiting the model space spanned by three CS-type reference configurations and using three active orbitals of different symmetry. Implementation of such an approach should not be much more involved than the implementation of the two-reference theory studied in this paper, but we should obtain better description of the low-lying eigenstates for nonplanar H_4 models.

We showed that the two-reference CCSD formalism is capable of providing essential information about the low-lying eigenstates of the Hamiltonian, even when the two-reference theory breaks the symmetry of the Hamiltonian. We examined an interesting case of the tetrahedral geometry, where broken-symmetry MRCCSD-n solutions destroy the twofold degeneracy of the ground state due to a wrong choice of the model space. It was truly impressive to observe how these broken-symmetry solutions recover the correct shape of FCI energy curves by minimizing the gap between the two roots of the effective Hamiltonian in the vicinity of the tetrahedral geometry, where the exact energy curves cross one another.

Results of the present study, together with the results obtained in paper I, indicate that the Hilbert-space MRCC formalism represents a powerful computational method that is capable of describing many-electron correlation effects in systems with varying degree of quasidegeneracy. It will be useful to extend these studies and perform similar computations with larger basis sets, such as the DZP basis of Ref. [19] (preliminary calculations have already been performed; cf. Refs. [6] and [23]).

ACKNOWLEDGMENTS

Continued support by NSERC (J.P.) is gratefully acknowledged. One of us (P.P.) would like to express his sincere gratitude to Professor J. Paldus for his hospitality, thoughtfulness, and numerous helpful discussions during his stay in the Department of Applied Mathematics of the University of Waterloo.

[1] B. Jeziorski and H.J. Monkhorst, Phys. Rev. A **24**, 1668 (1981).
[2] B. Jeziorski and J. Paldus, J. Chem. Phys. **88**, 5673 (1988).
[3] L. Meissner, Ph.D. thesis, Nicholas Copernicus University, Toruń, Poland, 1987 (in Polish); L. Meissner, K. Jankowski, and J. Wasilewski, Int. J. Quantum Chem. **34**, 535 (1988).
[4] L. Meissner, S.A. Kucharski, and R.J. Bartlett, J. Chem. Phys. **91**, 6187 (1989); S.A. Kucharski and R.J. Bartlett, *ibid.* **95**, 8227 (1991).
[5] J. Paldus, L. Pylypow, and B. Jeziorski, in *Many-Body Methods in Quantum Chemistry*, edited by U. Kaldor, Lecture Notes in Chemistry Vol. 52 (Springer, Berlin, 1989), pp. 151–170.
[6] A. Balková, S.A. Kucharski, L. Meissner, and R.J. Bartlett, Theor. Chim. Acta **80**, 335 (1991).
[7] A. Balková, S.A. Kucharski, and R.J. Bartlett, Chem. Phys. Lett. **182**, 511 (1991).
[8] A. Balková, S.A. Kucharski, L. Meissner, and R.J. Bartlett, J. Chem. Phys. **95**, 4311 (1991).
[9] P. Piecuch and J. Paldus, Theor. Chim. Acta **83**, 69 (1992).
[10] J. Paldus, P. Piecuch, B. Jeziorski, and L. Pylypow, in *Recent Progress in Many-Body Theories*, edited by T.L. Ainsworth, C.E. Campbell, B.E. Clements, and E. Krotscheck (Plenum, New York, 1992), Vol. 3, pp. 287–303.
[11] J. Paldus, in *Methods in Computational Molecular Physics*, Vol. 293 of *NATO Advanced Study Institute, Series B: Physics*, edited by S. Wilson and G.H.F. Diercksen (Plenum, New York, 1992), pp. 99–194.
[12] J. Paldus, in *Relativistic and Electron Correlation Effects in Molecules and Solids*, Vol. 318 of *NATO Advanced Study Institute, Series B: Physics*, edited by G.L. Malli (Plenum, New York, 1994), pp. 207–282.
[13] D. Mukherjee and S. Pal, Adv. Quantum Chem. **20**, 291 (1989).
[14] J. Paldus, P. Piecuch, L. Pylypow, and B. Jeziorski, Phys. Rev. A **47**, 2738 (1993) (referred to as paper I).
[15] K. Jankowski and J. Paldus, Int. J. Quantum Chem. **18**, 1243 (1980).
[16] U. Kaldor, Int. J. Quantum Chem. **28**, 103 (1985).
[17] S. Wilson, K. Jankowski, and J. Paldus, Int. J. Quantum Chem. **23**, 1781 (1983); **28**, 525 (1985).
[18] N. Iijima and A. Saika, Int. J. Quantum Chem. **27**, 481 (1985).
[19] J. Paldus, P.E.S. Wormer, and M. Bénard, Coll. Czech. Chem. Commun. **53**, 1919 (1988).
[20] S. Zarrabian and J. Paldus, Int. J. Quantum Chem. **38**, 761 (1990).
[21] K. Jankowski, J. Paldus, and J. Wasilewski, J. Chem. Phys. **95**, 3549 (1991).
[22] S.A. Kucharski, A. Balková, and R.J. Bartlett, Theor. Chim. Acta **80**, 321 (1991).
[23] J. Paldus and L. Pylypow (unpublished).
[24] A. Banerjee and J. Simons, J. Chem. Phys. **76**, 4548 (1982); M.R. Hoffmann and J. Simons, *ibid.* **88**, 993 (1988); **90**, 3671 (1989).
[25] C.L. Janssen and H.F. Schaefer III, Theor. Chim. Acta **79**, 1 (1991).
[26] J. Paldus and X. Li, in *Symmetries in Science VI: From the Rotation Group to Quantum Algebras*, edited by B. Gruber (Plenum, New York, 1993), pp. 573–591; X. Li and J. Paldus (unpublished).
[27] P. Jankowski, B. Jeziorski, and J. Paldus (unpublished).
[28] L. Meissner and R.J. Bartlett, J. Chem. Phys. **92**, 561 (1990).
[29] C. Bloch, Nucl. Phys. **6**, 329 (1958).
[30] J. Čížek, J. Chem. Phys. **45**, 4256 (1966); Adv. Chem. Phys. **14**, 35 (1969); J. Čížek and J. Paldus, Int. J. Quantum Chem. **5**, 359 (1971).
[31] J. Paldus, J. Čížek, and I. Shavitt, Phys. Rev. A **5**, 50 (1972).
[32] J. Paldus, J. Chem. Phys. **67**, 303 (1977); B.G. Adams and J. Paldus, Phys. Rev. A **20**, 1 (1979).
[33] J. Paldus, J. Čížek, and B. Jeziorski, J. Chem. Phys. **90**, 4356 (1989).
[34] R.J. Bartlett, Annu. Rev. Phys. Chem. **32**, 359 (1981).
[35] J. Paldus, *Diagrammatic Methods for Many-Fermion Systems* (University of Nijmegen, Holland, 1981).
[36] J. Paldus, in *New Horizons of Quantum Chemistry*, edited by P.-O. Löwdin and B. Pullman (Reidel, Dordrecht, 1983), pp. 31–60.
[37] R.J. Bartlett, C.E. Dykstra, and J. Paldus, in *Advanced Theories and Computational Approaches to the Electronic Structure of Molecules*, edited by C.E. Dykstra (Reidel, Dordrecht, 1984), pp. 127–159.
[38] R.J. Bartlett, J. Phys. Chem. **93**, 1697 (1989).
[39] I. Lindgren and J. Morrison, *Atomic Many-Body Theory* (Springer, Berlin, 1982).
[40] I. Lindgren, Int. J. Quantum Chem. Symp. **12**, 33 (1978); J. Phys. B **24**, 1143 (1991); I. Lindgren and D. Mukherjee, Phys. Rep. **151**, 93 (1987).
[41] I. Lindgren, J. Phys. B **7**, 2441 (1974).
[42] V. Kvasnička, Czech. J. Phys. B **24**, 605 (1974); **27**, 599 (1977); Adv. Chem. Phys. **36**, 345 (1977).
43] B. Jeziorski and J. Paldus, J. Chem. Phys. **90**, 2714 (1989).
[44] W.D. Laidig and R.J. Bartlett, Chem. Phys. Lett. **104**, 424 (1984); W.D. Laidig, P. Saxe, and R.J. Bartlett, J. Chem. Phys. **86**, 887 (1987).
[45] P. Piecuch and J. Paldus, Int. J. Quantum Chem. **36**, 429 (1989).
[46] J. Paldus and B. Jeziorski, Theor. Chim. Acta **73**, 81 (1988).
[47] J. Paldus, B.G. Adams, and J. Čížek, Int. J. Quantum Chem. **11**, 813 (1977).
[48] J. Paldus, M. Takahashi, and B.W.H. Cho, Int. J. Quantum Chem. Symp. **18**, 237 (1984).
[49] S. Huzinaga, J. Chem. Phys. **42**, 1293 (1965).
[50] H. Fukutome, Prog. Theor. Phys. **47**, 1156 (1972).
[51] H. Fukutome, M. Takahashi, and T. Takabe, Prog. Theor. Phys. **53**, 1580 (1975).
[52] B.G. Adams, K. Jankowski, and J. Paldus, Chem. Phys. Lett. **67**, 144 (1979).
[53] B.G. Adams, K. Jankowski, and J. Paldus, Phys. Rev. A **24**, 2316 (1981).
[54] B.G. Adams, K. Jankowski, and J. Paldus, Phys. Rev. A **24**, 2330 (1981).
[55] K. Jankowski, L. Meissner, and J. Wasilewski, Int. J. Quantum Chem. **28**, 931 (1985).
[56] J. Paldus, M. Takahashi, and R.W.H. Cho, Phys. Rev. B **30**, 4267 (1984).
[57] M. Takahashi and J. Paldus, Phys. Rev. B **31**, 5121 (1985).
[58] J. Paldus, P.E.S. Wormer, F. Visser, and A. van der Avoird, J. Chem. Phys. **76**, 2458 (1982).

[59] K. Jankowski, J. Paldus, and P. Piecuch, Theor. Chim. Acta **80**, 223 (1991).
[60] P. Piecuch, S. Zarrabian, J. Paldus, and J. Čížek, Phys. Rev. B **42**, 3351 (1990).
[61] P. Piecuch and J. Paldus, Int. J. Quantum Chem. Symp. **25**, 9 (1991).
[62] J. Paldus and P. Piecuch, Int. J. Quantum Chem. **41**, 135 (1992); P. Piecuch, J. Čížek, and J. Paldus, *ibid.* **41**, 165 (1992).
[63] M. Takahashi and J. Paldus, Int. J. Quantum Chem. **28**, 459 (1985).
[64] The GAMESS system of programs by M. Dupuis, D. Spangler, and J.J. Wendoloski, National Resource for Computations in Chemistry, Software Catalog, University of California, Berkeley, CA, 1980, Program QG01; M.W. Schmidt, K.K. Baldridge, J.A. Boatz, J.H. Jensen, S. Koseki, M.S. Gordon, K.A. Nguyen, T.L. Windus, and S.T. Elbert, Quantum Chem. Prog. Exch. Bull. **10**, 52 (1990).
[65] J. Paldus, J. Čížek, and M. Takahashi, Phys. Rev. A **30**, 2193 (1984).
[66] R.A. Chiles and C.E. Dykstra, Chem. Phys. Lett. **80**, 69 (1981); S.M. Bachrach, R.A. Chiles, and C.E. Dykstra, J. Chem. Phys. **75**, 2270 (1981); C. E. Dykstra, S.-Y. Liu, M. F. Daskalakis, J. P. Lucia, and M. Takahashi, Chem. Phys. Lett. **137**, 266 (1987).
[67] P. Piecuch, R. Toboła, and J. Paldus, Chem. Phys. Lett. **210**, 243 (1993).